

Solar-Grade Silicon: Techno-economic Assessment, COMSOL Modeling, and Electrolysis

An Major Qualifying Project
submitted to the Faculty of
WORCESTER POLYTECHNIC INSTITUTE
in partial fulfilment of the requirements for the
degree of Bachelor of Science

By
Jacob Hazerjian
Vicky Luu
Ariana Ly

Date:
May 6, 2021

Report Submitted to:

Professor Adam C. Powell
Associate Professor
Mechanical Engineering, WPI

Professor N. Aaron Deskins
Associate Professor
Chemical Engineering, WPI

This report represents the work of WPI undergraduate students submitted to the faculty as evidence of completion of a degree requirement. WPI routinely publishes these reports on its website without editorial or peer review. For more information about the projects program at WPI, please see <http://www.wpi.edu/academics/ugradstudies/project-learning.html>

Abstract

A current issue in the solar industry is producing solar panels cost-effectively. One of the major contributors to the high cost of solar panels is the costs of the production and purification processes of silicon that is at least 99.9999%, or solar-grade. Therefore, our research team developed a techno-economic cost model for a start-up solar-grade silicon plant that uses molten salt electrolysis and a novel bath composition of $\text{MgF}_2\text{-CaF}_2\text{-YF}_3\text{-CaO-SiO}_2$. Through 2-dimensional and 3-dimensional COMSOL modeling, our research team also assessed the distribution of current density, electrical potential, temperature, and velocity in the electrolysis system. Moreover, spectroscopy and microscopy, EDS and SEM respectively, techniques were used in analyzing the silicon wafer samples from the electrolysis experiments.

Acknowledgments

We would like to thank Professor Adam Powell for leading and co-advising our research project. We appreciate everything you taught us and for inspiring us to think about an eco-friendly future. Most importantly, thank you for the opportunity to work on this project.

Thank you to Professor Aaron Deskins for co-advising our project and giving constructive feedback. We appreciate your time and effort that guided us throughout the duration of our research.

We would also like to thank Mohammad Asadikiya, Aditya Moudgal, and Adriana Hera for working with us on various parts of this project. We appreciate all the input and suggestions, which have definitely improved the quality of our work.

Thank you to Mohammad Asadikiya (Materials Science and Engineering, Ph.D.) for leading, guiding, and teaching us in the development of the techno-economic assessment.

Thank you to Aditya Moudgal (Mechanical Engineering, M.S.) for leading the electrolysis experiments and SEM-EDS analysis.

Thank you to Adriana Hera (Mechanical Engineering, Ph.D.) for the support and guidance in developing our COMSOL models.

Executive Summary

Solar-grade silicon is used to make the cells inside of solar panels. However, solar-grade silicon is expensive to produce through current and traditional methods. Using molten salt electrolysis and a novel bath composed of $\text{MgF}_2\text{-CaF}_2\text{-YF}_3\text{-CaO-SiO}_2$, solar-grade silicon may be produced more cost-effectively. Therefore, the purpose of our research is to investigate the feasibility of this pathway and to provide useful tools for analyzing the electrolysis system. To accomplish these goals, our team came up with three objectives.

Objectives and Methods

1. Construct a techno-economic cost model of a start-up plant that uses molten salt electrolysis and the novel bath composition to produce solar-grade silicon.
2. Model our system in COMSOL to see the distribution of current density, electric potential, temperature, and velocity.
3. Perform electrolysis experiments to help establish a baseline for producing solar-grade silicon using the novel bath solution. In addition to performing the experiments, we will analyze these samples from the experiments via microscopy and spectroscopy to determine if there are any silicon deposits.

To accomplish the first objective a Microsoft Excel sheet will be utilized for its ability to input equations as well as being able to reference cells. These two features will allow for the final results to update automatically when changes are made to inputs such as the cost or composition of the salt bath used.

To accomplish the second objective we used COMSOL to model and simulate different physics to get the property distribution throughout the model. The physics that will be used are electric current, laminar flow and heat transfer in solids and fluids. These three physics will then be coupled to each other through the use of multiphysics.

To accomplish the third objective we ran an electrolysis in a molten salt bath inside a furnace. A silicon wafer was attached to the cathode and a yttria-stabilized zirconia shell was placed over the anode. A voltage was run through the electrodes until the electrolysis was done. The silicon wafer was recovered once cooled and polished to make the surface clearly viewable

under a microscope. The sample was then looked at under an electron microscope and analyzed using X-ray spectroscopy.

Table of Contents

Abstract	2
Acknowledgments	3
Executive Summary	4
Table of Contents	6
List of Figures	8
List of Tables	11
Chapter 1: Introduction	12
Chapter 2: Background	14
Section 2.1: The Solar Industry	14
Section 2.2: The Purification of Silicon Methods	17
Section 2.3: Molten Salt Electrolysis and Important Components	20
Section 2.4 Scanning Electron Microscopy (SEM)	23
Section 2.5 Energy Dispersive Spectroscopy (EDS)	25
Chapter 3: Methodology	27
Section 3.1: Techno-economic Cost Model	28
Section 3.2: Modeling our Electrolysis System using COMSOL	29
Section 3.3: Experimentation	33
Chapter 4: Results and Discussion	44
Section 4.1: Techno-economic Cost Model	44
Material Balance	44
Total Capital Investment Summary (CAPEX-Si)	45
Operating Expense/Income Summary	49
Overall Cost Analysis (Cost Analysis Ref. Model)	50
User Friendly Interfaces within our Techno-economic Model	54
Section 4.2: COMSOL Modeling	57
Current Density	57
Electric Potential	58
Temperature	59
Velocity	60
Section 4.3: Electrolysis Experiments and Sample Analysis	62
Experiments 1-6	62
Experiment 7	62
Experiment 8	63

	7
Experiment 9	64
Chapter 5: Conclusions	65
Chapter 6: References	67
Appendix A: Techno-Economic Cost Model	70
Appendix B: COMSOL Simulation Results	73
Calculating Diffusivity and the Peclet Number	77
Appendix C: Electrolysis Experiments and Analysis	78

List of Figures

Figure 1: Electricity Production Via Solar Panel Diagram (Laubach, 2018)	14
Figure 2: A schematic of how quartz rock is used to produce industrial grade silicon with 99.8% purity (Sokolich, 2019)	15
Figure 3: Schematic of a Siemens reactor on the left, and a fluidized bed reactor on the right. Trichlorosilane is produced in the Siemens reactor, and can be fed into the fluidized bed reactor and silicon is ultimately produced (Fisher, et al., 2012).	17
Figure 4: Schematic of the Czochralski Process (Müeller, 2005)	18
Figure 5: Simplified Electrolysis Schematic	20
Figure 6: SOM Electrolysis for Solar-grade Silicon (Buasai, et al., 2020).	21
Figure 7: This schematic shows the different components of a scanning electron microscope (NanoScience, 2020).	22
Figure 8. A schematic of how the electrons interact with the sample producing various kinds of signals depending on the sample (NanoScience, 2020).	23
Figure 9: EDS electron getting excited and jumping up in energy level (Chem.libretexts, 2021).	24
Figure 10: EDS Setup (Colpan, 2018).	25
Figure 11: EDS Results Example (Corbari, 2008).	25
Figure 12: Stinn-Allanore Equation	27
Figure 13: 2-Dimensional Schematic of Molten-Salt Electrolysis System	29
Figure 14: Salt Bath Material Properties	30
Figure 15: Salt Bath Density Analytic Function Input	31

Figure 16: A schematic of the Mellen Furnace including the positions of the table ledge, supplemental insulation, 310 stainless steel tube, frame, and wheels. The supplemental insulation used was styrofoam (Moudgal, Powell, 2019).	33
Figure 17: A schematic which shows the set-up of connecting the argon gas cylinder to the 310 stainless steel tube high-temperature chamber (Moudgal, Powell, 2019).	35
Figure 18. Photograph of electrolysis cage set up (Espinosa, Rutherford, Wallace, Powell, 2020).	38
Figure 19: A table taken from Buehler’s Guide on how to mount and polish silicon using a 5-step procedure. Note that it is suggested to use EpoThin for mounting, but we used a similar epoxy called Epoxicure 2 for this process (Buehler SumMet, 2007).	40
Figure 20: A photograph of pieces of the silicon wafer mounted using Epoxicure 2 and a metal stand to hold the wafer upright.	41
Figure 21: System Block Diagram	44
Figure 22: Cost per Plant vs Annual Production Capacity Graph	45
Figure 23: USD per Cell vs Number of Cells Graph	46
Figure 24: USD per Ton vs Number of Cells Graph	47
Figure 25: Annual Operating Cost vs Production Capacity Graph	49
Figure 26: Operating Cost Sensitivity to Inputs Graph	50
Figure 27: Annual Operating Costs Breakdown	51
Figure 28: Annual Fixed Costs Breakdown	51
Figure 29: Annual Variable Costs Breakdown	52
Figure 30: Annual Raw Material Costs Breakdown	52

Figure 31: Mass Balance Error Checker	53
Figure 32: Composition Sheet	54
Figure 33: Mass Balance Error Checker	55
Figure 34: 3D Current Density COMSOL Graph	56
Figure 35: 3D Electric Potential COMSOL Graph	57
Figure 36: 3D Temperature COMSOL Graph	58
Figure 37: 3D Velocity COMSOL Graph	59
Figure 38: COMSOL graph with red arrows indicating the velocity field and direction.	60
Figure 39: SEM-EDS Images From Experiment 7	62

List of Tables

Table 1: Variables within Stinn-Allanore Equation	28
Table 2: Dimensions of electrolysis equipment used in modeling the system in COMSOL	30
Table 3: Weighted amount of compounds needed for each experimental run	37

Chapter 1: Introduction

Solar energy, along with several other forms of renewable energy are an eco-friendly alternative to fossil fuels. While these alternative energy sources reduce exposure to harmful and damaging emissions, many homes continue to reject the installation of these forms, especially when it comes to solar energy. Finding methods to capture solar energy and converting it to a more usable form is not only tricky but also expensive. There are many factors that contribute to the high cost of solar energy. For this project we focused on the cost of producing solar-grade silicon. For its semiconducting properties and overall abundance, silicon is the preferred material used in the development of solar cells. However, due to energy intensive processes, solar-grade silicon is expensive to produce and purify. Analyzing the current purification process in use, the Siemens process, the amount of energy consumed to produce solar-grade silicon is rather excessive and costly.

As part of our project we planned to investigate an alternative method to produce economical silicon such as electrolysis. Through solid oxide membrane (SOM) electrolysis using yttria-stabilized zirconia as the anode and a silicon cathode, experiments will be conducted to test and improve the purity of the silicon product. As for the bath being tested, the bath composition was developed by a Boston University group under Uday Pal and consists of $\text{MgF}_2\text{-CaF}_2\text{-YF}_3\text{-CaO-SiO}_2$. This bath composition was found to give better silicon deposition than other baths that usually contain aluminum chloride, lithium chloride and other alkali metal chlorides.

To understand what was happening inside the electrolysis system, COMSOL was used to model the system. This modeling used physics and multiphysics to visualize different properties and their characteristics as they interact with each other in both 3-dimensions and 2-dimensions. The characteristics that were looked at were temperature, velocity, current density and electric potential. These properties were chosen as current will be flowing through the system, so an understanding of how it interacts with the silicon and bath was needed. The system runs at over $1100\text{ }^\circ\text{C}$, but there can be slight variations due to the conductivity of the different parts of the system. This variation is what gives rise to the velocity, as the salt bath has melted and is a viscous fluid and slight temperature changes change the density in small areas inside the bath.

It is important to note that previous work has already been done to further progress this project. A previous research team from Worcester Polytechnic Institute analyzed the material and

energy balances for this system. This research team also conducted a preliminary cost of the proposed silicon plant by using data from an interview with Century Aluminum. Moreover, over summer break, our team worked on finalizing the material balance for this system and assisted in creating a cost model for this plant using a capital cost equation created by researchers from the Massachusetts Institute of Technology. This cost model was then redesigned to allow for costs to be updated when inputs are changed. This allows for a more user-friendly experience when analyzing the cost to invest in a plant for silicon electrolysis.

Therefore, the goals for this project are: (1) construct a techno-economic cost model of a start-up plant that uses molten salt electrolysis and the novel bath composition to produce solar-grade silicon, (2) model the system in COMSOL to see the distribution of current density, electric potential, velocity and temperature and how they interact with each, (3) to perform electrolysis experiments and then analyze the collected samples via microscopy and spectroscopy to create a baseline model for the electrolysis of silicon in a molten salt bath.

Chapter 2: Background

In this chapter we discuss the solar industry and current issues facing the industry. We also describe some of the traditional methods used to purify silicon and the current electrolysis process we are considering to use.

Section 2.1: The Solar Industry

Solar power is a clean form of energy generation that uses the power of the sun to generate electricity. It is a massive industry that has grown by almost 50% in the last decade. The massive industry growth has allowed for 85 gigawatts to be produced in the United States alone, enough to power 16 million houses (SEIA, 2020). This has in large part been due to policies by the federal government such as the Federal Tax Credit for Solar PV. The tax credit gives an incentive for having solar panels generate electricity for both residential and commercial buildings and sites (Energy Department, 2020). One example is that the tax break gives companies and residents the ability to reduce the taxes they will pay based on how much they spend on solar panels. The tax break allows for the government to take the burden of the cost of solar panels off of the buyer and places it on the taxpayers as a whole. This has allowed for more sales of solar panels, allowing for further development of solar technology. Some developments in solar technology are looking into reducing the cost of making the solar panels as well as making them more efficient, which are the two biggest problems facing the solar industry.

How Solar Panels Work

Solar panels work by turning sunlight into electricity, similar to how plants turn sunlight into energy. Inside the panel there are cells made of silicon. Silicon is a semiconductor which allows it to have a conductivity in between that of a metal, which conducts electricity easily, and glass, which has a very tough time conducting electricity. An overview of how solar energy is converted to electricity for homes is shown in Figure 1.

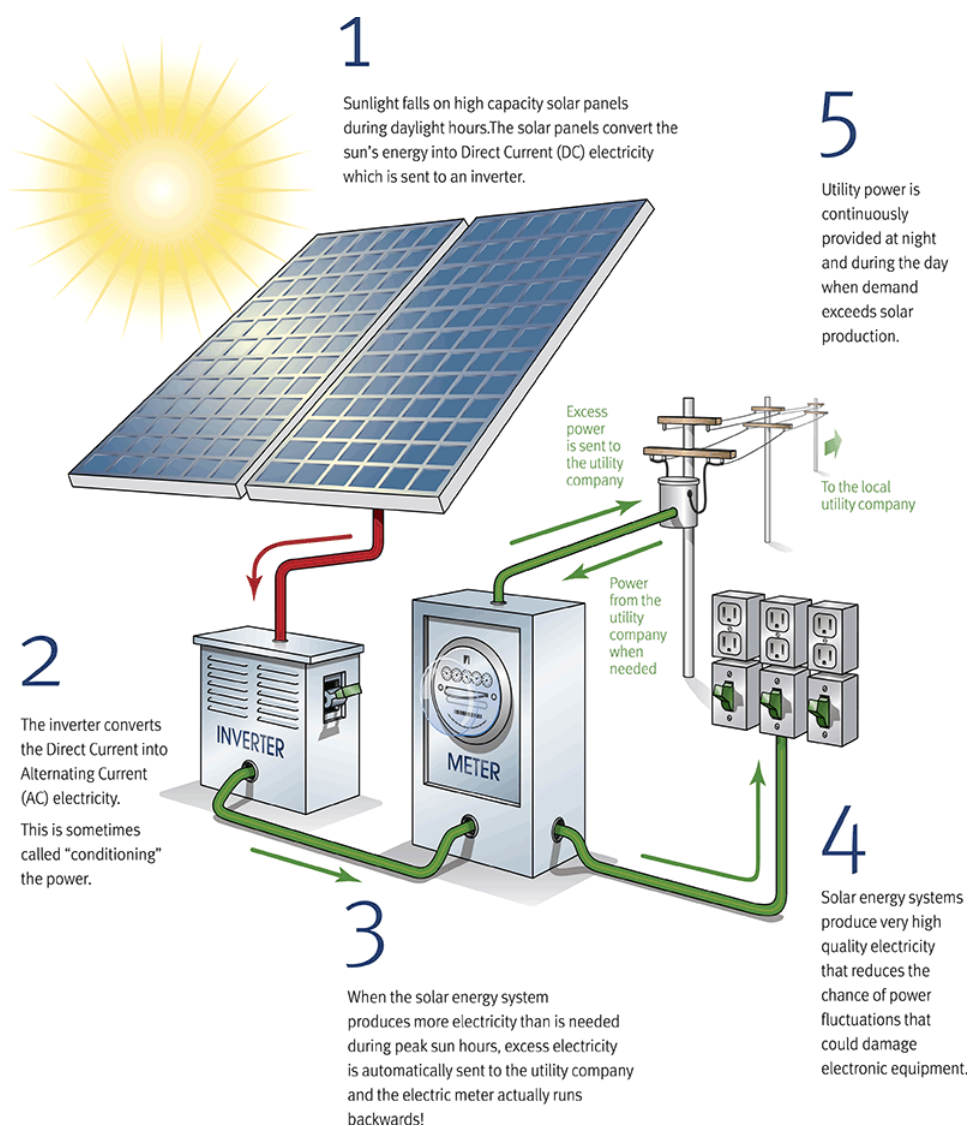


Figure 1: Electricity Production Via Solar Panel Diagram (Laubach, 2018).

Through a process known as doping, the silicon becomes more like a metal in conducting electricity. In the doping process, impurities are added into the silicon in a specific way to get the properties needed. When the sun hits the silicon cells an electron is "knocked off" into the wiring in the cell. It is then combined with all the other cells in the panel (Richardson, 2020). It cannot be used by a house yet as the electricity is in direct current (DC) while in the US, alternating current (AC) is used. Inside the solar panel there is an invert which converts the electricity from DC to AC, allowing it to now be used.

Solar Energy Problems

The biggest problem facing the industry is the cost of producing the solar panels. This is due to the high cost of producing the silicon. The silicon must be purified and then doped, which requires a lot of energy to do. The raw silicon comes in the form of silicon dioxide (SiO_2) and can be found in quartz rock. These rocks are put in an electrode arc furnace with coal and charcoal and heated to $1500\text{ }^\circ\text{C}$ ($2732\text{ }^\circ\text{F}$). Figure 2 shows a good example of how quartz rock is converted to 99.8% pure silicon.

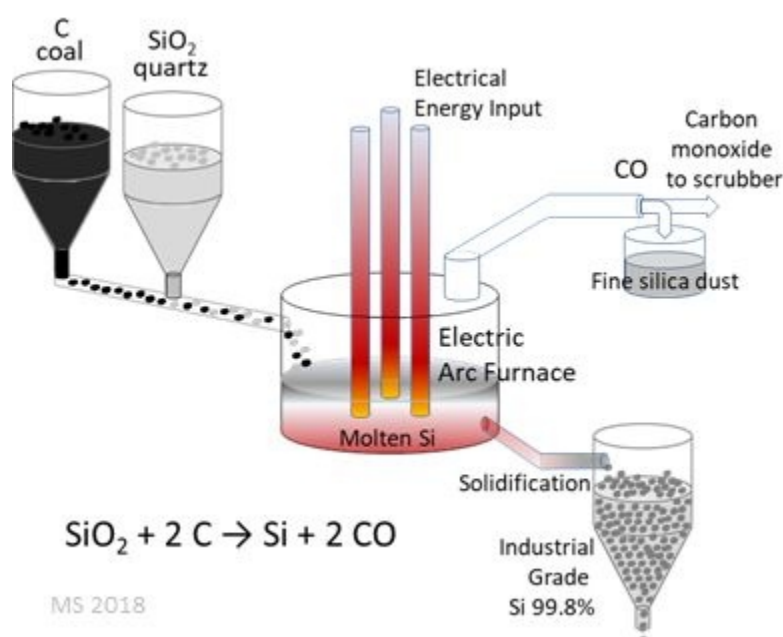


Figure 2: A schematic of how quartz rock is used to produce industrial grade silicon with 99.8% purity (Sokolich, 2019)

The silicon is now metallurgical silicon which is just silicon and magnesium. To get silicon for electronics, the silicon is added to a hydrogen chloride bed at $300\text{ }^\circ\text{C}$ ($572\text{ }^\circ\text{F}$). This reactor needs to be a vacuum as the oxygen in the air can cause the silicon to oxidize and be unusable in electronics (Hasannezhad, 2019).

The other big hurdle for solar panels is their efficiency. The weather strongly dictates how much power they will produce, if it is cloudy the solar panel will produce very little energy compared to when it is sunny. The best places for solar panels are in areas with little cloud cover,

small amount of precipitation and no snow fall. Overall, the best places for solar panels are in deserts where there is little to no rainfall and few clouds to obscure the sun's rays. However, in the desert, sand will often cover the solar panels and reduce their effectiveness.

Deserts aren't the only place where dirt and grime can cover a solar panel and reduce its efficiency. There is dust and dirt everywhere on the planet, however, the dirt and sand are easy to clean off the solar panels. There is other debris that can accumulate on the solar panel and that happens to be from the pollutants in the air that settle on the ground. Some of these pollutants include sulfate aerosols and heavy metals. These pollutants are most present in urban areas which can result in up to a 30% drop in efficiency (Kirpichnikova, 2020). Hence why the efficiency and the production are the main focuses for improving solar panels.

The cost of producing the silicon is an issue for creating solar panels that are more affordable. The cost of production for both the arc furnace and then the hydrogen chloride bath are extremely high. Moreover, this is due to the high temperature of the arc furnace as well as the need to make the hydrogen chloride reactor a vacuum. Therefore, reducing the expenses of producing through different means solar-grade silicon is an important issue.

Section 2.2: The Purification of Silicon Methods

Silicon has several desirable qualities making it the best material to use in the solar industry. One of these qualities is its overall abundance on Earth. While the metalloid is far from rare, the process taken to produce and purify is not only costly but energy intensive. While no major discoveries have been made to improve the cost efficiency of the process, several experiments and studies have been and are still being conducted, some with promising results.

Siemens Process: Polycrystalline Silicon

The Siemens process is used in the purification of silicon in both the photovoltaic and semiconductor-industry. The process is known for its production of high-purity polycrystalline silicon. This process begins with the production of trichlorosilane (TCS). Hydrochlorination of metallurgical silicon in a fluidized bed reactor forms TCS. The TCS found in the reaction product stream undergoes crude distillation, separation, and purification processes. The typical system designs are highly influenced by the impurities found in the raw material. Depending on the composition of the impurities, the conditions and requirements of the system may differ.

Overall, the separation of TCS and its subsequent impurities are driven by the differences in boiling points, performance, and molecular polarity. After distilling all impurities out of TCS, chemicals with similar boiling points may remain in the stream, prohibiting TCS from being completely pure. To attain a better separation, alterations can be made to the impurities that affect the boiling points thus calling for an easier separation. To help visualize this process, see Figure 3 below.

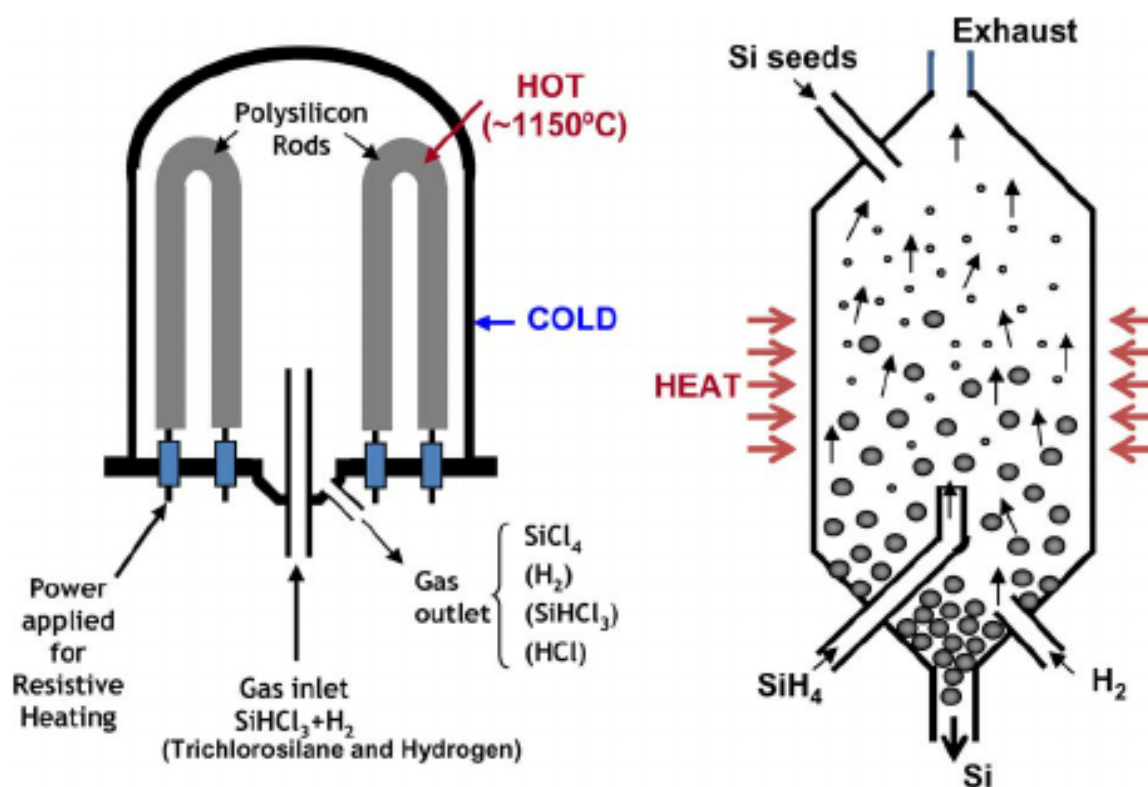


Figure 3: Schematic of a Siemens reactor on the left, and a fluidized bed reactor on the right. Trichlorosilane is produced in the Siemens reactor, and can be fed into the fluidized bed reactor and silicon is ultimately produced (Fisher, et al., 2012).

The Siemens process takes place within a bell reactor where thin rods of silicon are heated up using a power supply. The rods are arranged vertically in the electrodes with a horizontal bridge attaching every two rods forming a U-shape. In the reactor, hydrogen gas will react with a silicon-containing component such as TCS to form high purity silicon deposits on the rods. This chemical vapor deposition (CVD) step forms a high purity polysilicon, however

the overall energy consumed is significant reaching anywhere from 45-80 kWh/kg (Ramos, et al, 2015). Such high energy consumption is used to create and maintain a constant temperature difference between the rods and reactor walls. This large temperature difference between the heated rods and cooled reactor walls is crucial to obtain high purity silicon. While there are several studies and experiments being conducted to improve the Siemens process, the application of these experimental processes does reduce the energy consumption. However, these experimental processes also raise other concerns such as lower yield, environmental impacts, etc (Pal, 2020). Such a large amount of energy used does result in a polysilicon purity of 99.999999% however to fit photovoltaic cell requirements, such purity reading is rather excessive (Ramos, et al, 2015). As the Siemen process was initially developed to produce electronic-grade silicon, the demand for higher product purity is required for EI-Si but not needed for solar cells. Solar-grade silicon is typically 99.99% pure.

Czochralski Process: Monocrystalline Silicon

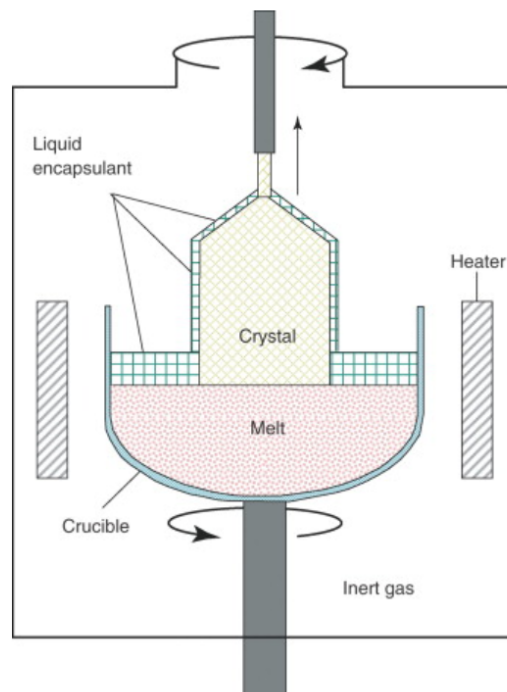


Figure 4: Schematic of the Czochralski Process (Müller, 2005)

Although the Siemens process is the technique currently practiced in the production of solar-grade silicon, there are other notable methods like the Czochralski process. Unlike the Siemens process, the Czochralski method produces monocrystalline silicon which happens to provide for a more efficient photovoltaic cell than those constructed from polycrystalline structures.

The process begins with the insertion of a rotating monocrystalline silicon seed crystal into the melt within the double crucible. The melt consists of polysilicon that enters through the feeder into the outer layer of the crucible known as the outer feed layer. The seed is then pulled upwards from the crucible, allowing the melt to cool and freeze forming a silicon ingot. The diameter of the ingot can be controlled by regulating the speed at which the seed is being pulled, speed at which the seed is rotating, and the heat power (Müller, 2005). For a more simplified look into the Czochralski process setup, please see Figure 4 above. The ingot composed of monocrystalline silicon is now cut into thin wafers. While this process is easy to control, however this method poses some inefficiencies. For one, the prolonged use of the system will cause build up of impurities within the bath melt. The inner crucible composed of quartz will degrade as part of it will dissolve into the bath melt.

Section 2.3: Molten Salt Electrolysis and Important Components

Compared to traditional practices of producing solar-grade silicon, electrolysis may be a less expensive and promising alternative. Electrolysis is the process that occurs when electrical current is passed through a substance and results in a chemical change. The chemical change is a result of a substance losing or gaining an electron. When a substance loses an electron, it is known as an oxidation reaction. If the substance gains an electron, it is a reduction reaction. Electrolysis is carried out in an electrolytic cell, in which there are positive and negative electrodes separated by some distance and in contact with the bath solution (Encyclopaedia Britannica, 2020). Therefore, design choices for the electrodes, bath composition, temperature, and current in electrolysis experiments are important in optimizing the purity of a solar-grade silicon product.

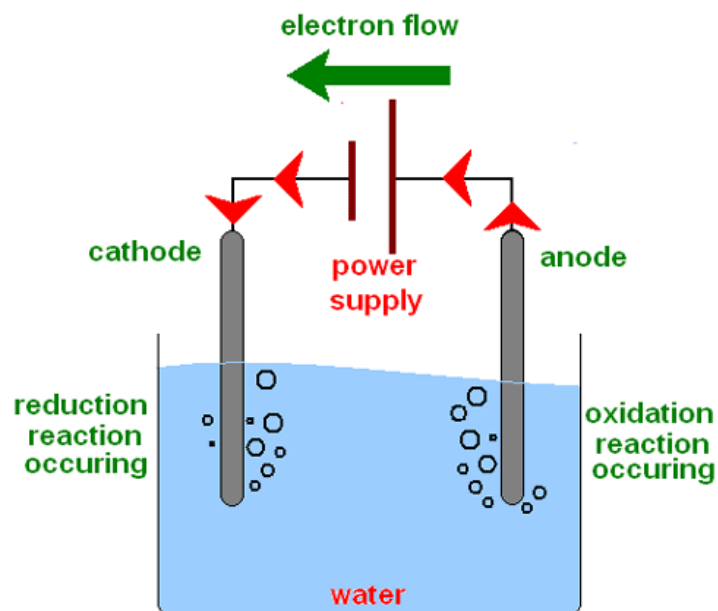


Figure 5: Simplified Electrolysis Schematic; A typical set-up of an electrolysis experiment. Here, the direction of the electron flow is shown. Oxidation occurs at the anode and reduction occurs at the cathode to produce a desired product. Water is used as the bath in the image, but the bath can contain molten salts or any solution of electrolytes (OpenEI, 2010).

YSZ SOM Electrolysis

It is important to note that there are different types of electrolysis processes, and therefore it is important to choose the type of process to produce solar-grade silicon. One example is solid oxide membrane (SOM) electrolysis that uses an oxygen-ion conducting membrane made out of yttria-stabilized zirconia (YSZ). A schematic of an electrolysis set-up using a YSZ SOM anode is shown below in Figure 5. When comparing solid oxide membrane (SOM) electrolysis to the Siemens process, we see the SOM electrolysis process has many advantages including lower feed material and pre-treatment costs and no by-product creation of perfluorocarbons or perfluorocarbons from anode effects (Guan, et al., 2016).

A recent study shows that SOM electrolysis, using an oxygen-ion-conducting membrane made out of yttria-stabilized zirconia, can directly electrolyze metal oxides (Guan, et al., 2016). The membrane separates the inert anode from a molten bath and a cathode. During SOM electrolysis, the metal is attracted to the cathode where it is reduced and oxygen ions are attracted to the anode where they travel across the SOM and are oxidized to create byproduct

oxygen gas (Guan, et al., 2016). As shown in Figure 6, silicon is produced at the cathode while pure oxygen gas develops at the anode.

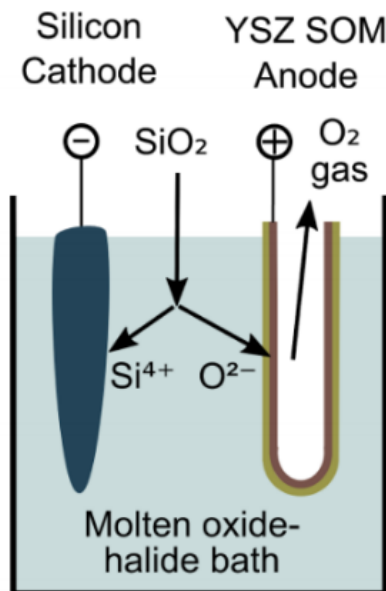


Figure 6: SOM Electrolysis for Solar-grade Silicon (Buasai, et al., 2020).

In the case of producing solar-grade silicon, the cathode material is made out of silicon. The anode is typically constructed using an inert material, with a solid oxide membrane constructed out of yttria-stabilized zirconia. It is also important to determine the bath composition used for electrolysis. For producing solar-grade silicon, one promising composition is a novel bath composed of $\text{MgF}_2\text{-CaF}_2\text{-YF}_3\text{-CaO-SiO}_2$ developed by Professor Uday Pal and his research group at Boston University. According to last year's research team, this bath has low viscosity, low volatility, high ionic conductivity, and SiO_2 solubility (Buasai, et al., 2020). These factors are important to consider for bath composition, as a low viscosity allows for effective heat transfer. Furthermore, a low volatility is also preferred, since in some cases the electrolysis system needs to be heated by a furnace. The high ionic conductivity of the novel bath enables efficient flow of current supplied to the system, and the SiO_2 solubility is good for allowing raw silicon to mix well in the solution and lead to better reaction rates.

Section 2.4 Scanning Electron Microscopy (SEM)

A scanning electron microscope (SEM) is used to produce useful images for sample analysis. The technique is especially useful for creating images of samples from electrolysis experiments. These images are produced from the focused beams of electrons that hit the surface of the sample which can then be used to understand the surface topography and chemical composition (NanoScience, 2020). Since electrons have shorter wavelengths, the images are produced with higher resolution and allow us to see structures on the sample more clearly (NanoScience, 2020). Figure 7 indicates the important features inside of a scanning electron microscope.

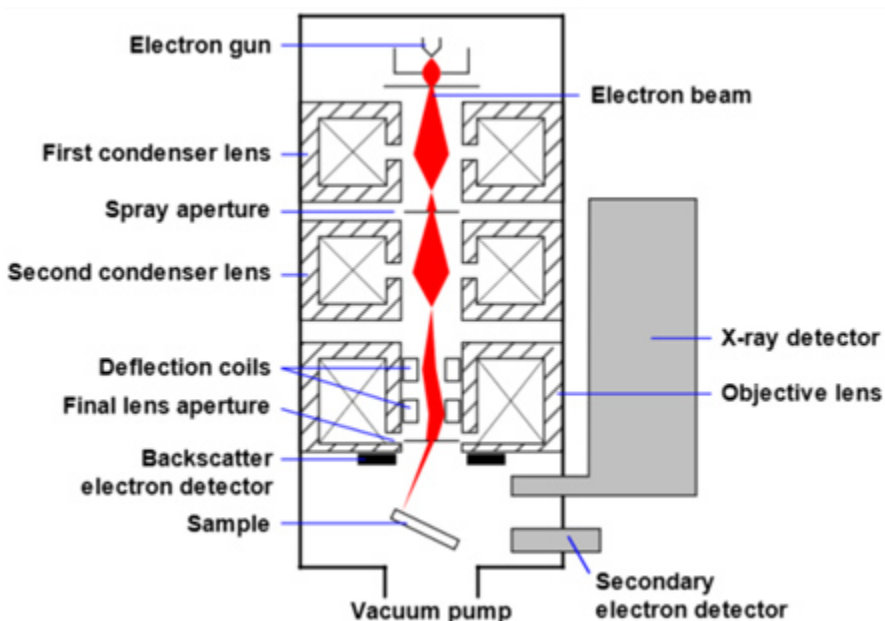


Figure 7: This schematic shows the different components of a scanning electron microscope (NanoScience, 2020).

One important component of a scanning electron microscope is the electron gun, as this is where electrons are produced. The electrons are released by the gun and travel down a pathway of different lenses and apertures. This causes the electrons to be focused in a beam-like fashion and reaches the surface of the sample (NanoScience, 2020). The location that the electron beam reaches the sample is directed by deflection coils, and so the coils can direct the beam to scan the surface of the sample (NanoScience, 2020). Once the beam reaches the sample, an

electron-sample interaction occurs which produces different signals detected by the various detectors (NanoScience, 2020). More details on the electron-sample interactions can be seen in Figure 8.

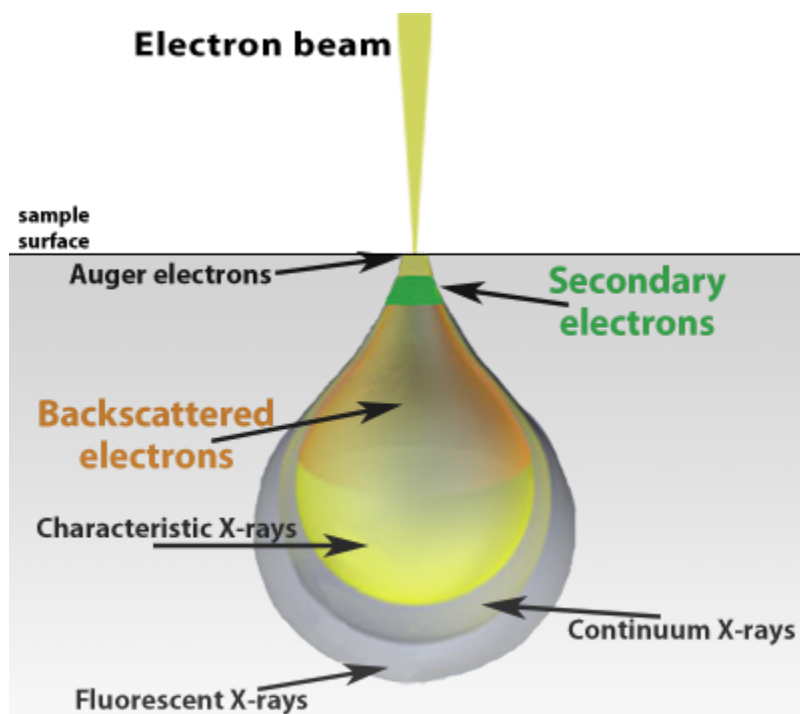


Figure 8. A schematic of how the electrons interact with the sample producing various kinds of signals depending on the sample (NanoScience, 2020).

The various signals that can result from the electron-sample interactions include producing secondary electrons, backscattered electrons, and X-rays (NanoScience, 2020). As seen in the schematic, the electron beam penetrates the sample with depths ranging in the microns. The depth the electrons reach depends on the potential difference that causes voltage acceleration and the material density of the sample (NanoScience, 2020). Furthermore, the SEM analysis can be used in conjunction with energy dispersive spectroscopy to determine the elements on the surface of samples.

Section 2.5 Energy Dispersive Spectroscopy (EDS)

Energy dispersive spectroscopy (EDS) is a technique used to analyze the composition of a material. Electrons are focused onto a sample which in turn causes electrons in to get excited and jump up an energy level. The electron for the atom gets hit by the beam of electrons from the EDS machine causing it to gain energy. This newly gained energy causes the electron to get kicked out of the ring system of the atom which can be seen in Figure 9.

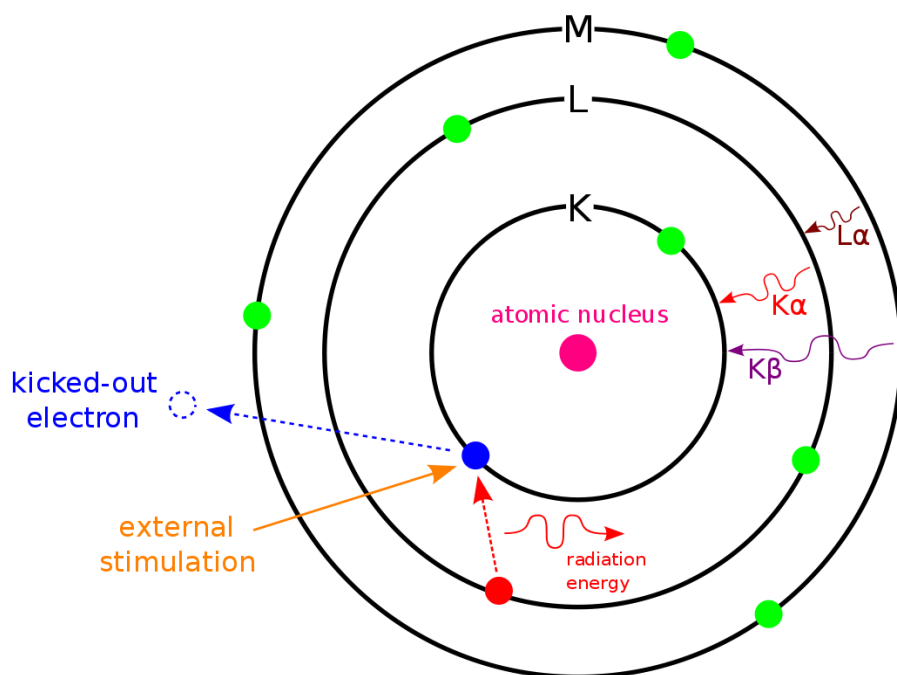


Figure 9: EDS electron getting excited and jumping up in energy level (Chem.libretexts, 2021).

This electron will then return to its original state due to the stability that comes with being in said position. When this electron returns to its ground state, energy is released in the form of X-rays. Figure 10 shows a typical setup of an EDS experiment.

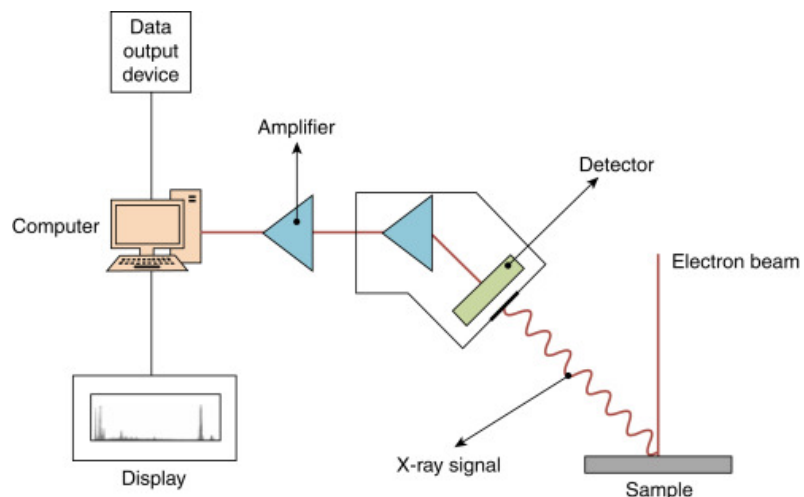


Figure 10: EDS setup (Colpan, 2018).

The amount and intensity of the X-rays is determined by the atomic structure of the atom. As all elements have unique atomic structures, the elements inside the sample can be determined by the reflected X-rays (Ngo, 1999). In Figure 11 below, an example of what the results of EDS give. The different peaks represent the elements found on the sample and their abundance. As seen in the figure, the height of the peaks indicates how much of the element was found on the sample.

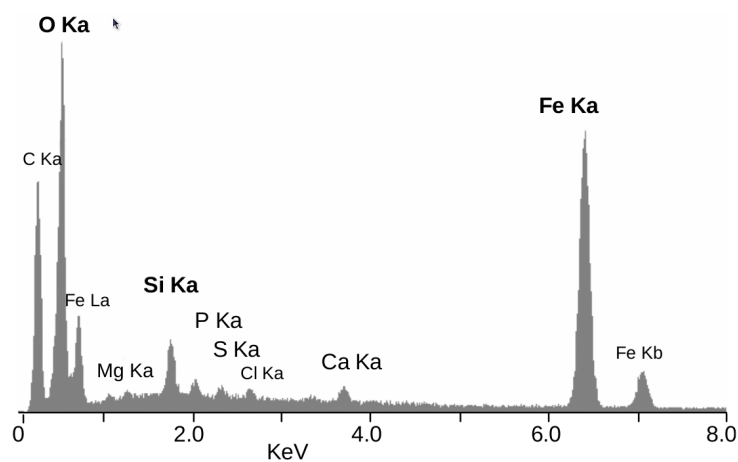


Figure 11: EDS results example (Corbari, 2008).

Chapter 3: Methodology

The purpose of our research is to investigate the feasibility of using molten salt electrolysis and a novel bath containing $\text{MgF}_2\text{-CaF}_2\text{-YF}_3\text{-CaO-SiO}_2$ to produce silicon with high purity that is at least 99.99%. Additionally, our team wants to create useful tools for analyzing the cost of a start-up plant and the electrolysis system. To accomplish these goals, our team came up with three objectives:

1. Construct a techno-economic cost model of a start-up plant that uses molten salt electrolysis and the novel bath composition to produce solar-grade silicon.
2. Model our system in COMSOL to see the distribution of current density, electric potential, temperature, and velocity.
3. Perform electrolysis experiments to help establish a baseline for producing solar-grade silicon using the novel bath solution. In addition to performing the experiments, we will analyze these samples from the experiments via microscopy and spectroscopy to determine if there are any silicon deposits.

To elaborate, the objectives for this research project are to further improve the preexisting techno-economic cost model of a proposed solar-grade silicon production plant and to achieve a baseline through a series of experimentation. To achieve the first objective, our team focused our efforts in constructing a more comprehensive material balance of the proposed process as this will guide all subsequent experiments in the right direction. The next step is to further expand the cost model by providing a more thorough cost analysis of all aspects of a solar-grade silicon production plant. The overall techno-economic cost model is based on a cost equation developed by researchers from the Massachusetts Institute of Technology and for more details please refer to Section 3.1.

Establishing a baseline for the molten salt electrolysis of solar-grade silicon requires weekly experimentation conducted at the Foundry in Washburn Shops on campus. Time must be allotted to assembling the bath, heating the furnace, melting the salt composition, and cooling down the furnace prior to running the electrolysis process. The post-electrolysis steps center around analyzing the metallography of the sample for silicon deposits. In order to understand the underlying physics of our system, the experiment is modeled using COMSOL to reveal the

behavior and activity of the bath during electrolysis. This model can provide an accurate insight and information our team is unable to attain through physical experimentation.

Section 3.1: Techno-economic Cost Model

Our team developed a techno-economic cost model using built-in functions developed by the ARPA-E-METALS program within Microsoft Excel. The ARPA-E-METALS program is a program that works to find economical and energy-efficient manufacturing techniques to process and recycle metals. We built on previous work to improve the material balance and utilized an equation (Figure 12) developed by researchers from the Massachusetts Institute of Technology to develop our cost analysis. This analysis would model the cost of creating and running a start-up plant to produce solar-grade silicon using molten-salt electrolysis and a novel bath composition consisting of $\text{MgF}_2\text{-CaF}_2\text{-YF}_3\text{-CaO-SiO}_2$.

$$C = \frac{51010}{1 + e^{-3.823 \cdot 10^{-3} \cdot (T-631)}} P^{0.8} + \frac{5634000}{1 + e^{-7.813 \cdot 10^{-3} \cdot (T-349)}} \left(\frac{p \cdot F}{j A \varepsilon M} \right)^{0.9} + 750000 Q V^{0.15} N^{0.5}$$

Figure 12: Stinn-Allanore Equation; A cost model equation developed by Caspar Stinn and Antoine Allanore from the Massachusetts Institute of Technology (Stinn, & Allanore, 2020).

The Stinn-Allanore equation is broken down into three distinct categories of capital investments. The first category of capital investments is the front-end processing which is based on the production capacity and the electrolysis temperature (Stinn, & Allanore, 2020). The second category represents costs due to recovery process steps (Stinn, & Allanore, 2020). This is based on things such as the product molar mass and the current density. The role of the third category is to take into account the capital cost of the rectifier (Stinn, & Allanore, 2020). This third category takes into account variables such as the installed power capacity and the number of rectifier lines. All together, the sections total up to the direct capital cost. We must note though the equation does not include operating costs such as electricity, labor, chemicals, feedstocks, water, or maintenance. Additionally it does not include the amortization of the capital cost to determine a yearly payback, depreciation, or capital contribution to the overall product cost. Although the equation does not take these factors into consideration, we do include these

variables in our cost analysis. Operating cost calculations were based on percent values provided by the Department of Energy. For a complete list of the symbols, their descriptions, and values we used in the Stinn-Allanore equation, see Table 1.

Table 1: Variables within Stinn-Allanore Equation

Symbol	Meaning	Value
A	Electrode area (m ²)	120
ϵ	Current efficiency	0.9
F	Magnitude of electric charge per mole of electrons	96485
j	Current density (A/m ²)	2500
M	Electrolysis product molar mass (kg/mol)	0.02808
N	Number of rectifier lines	1
P	Installed yearly production capacity (metric ton)	160000
p	Installed yearly production rate (kg/s)	5.074
Q	Installed power capacity (MW)	236.7
T	Electrolysis Temperature (°C)	110
V	Cell operating voltage (V)	3.37
z	Moles of electrons reacting to produce a mole of product	4

Section 3.2: Modeling our Electrolysis System using COMSOL

The electrolysis system, shown in Figure 13, was modeled using COMSOL software in both 2D and 3D representations. The 2D model was created first in order to test the simulations for errors, since the run time for each simulation is shorter compared to running 3D model simulations.

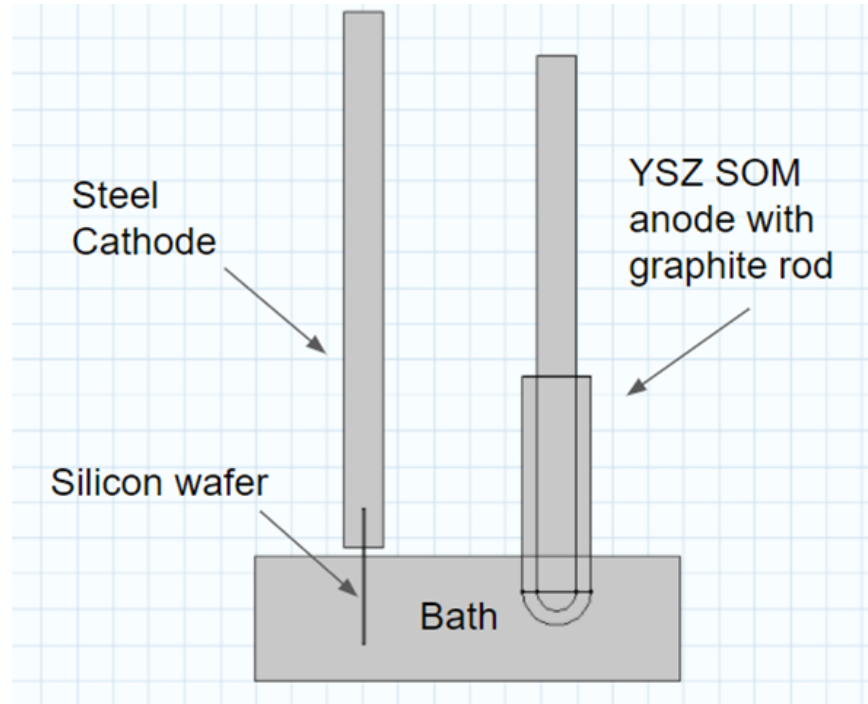


Figure 13: 2-Dimensional Schematic of Molten-Salt Electrolysis System

The first step in COMSOL is to create the geometry. In the 2D model, lines or basic shapes can be used to form different parts of the system. The line segments and segments of the shapes can be modified to the dimension of choice. The 3D model is similar in that 3-Dimensional shapes are placed in the system instead of lines. These shapes can then be modified to have the desired dimensions. The dimensions of each piece of equipment is Table 2 below.

Table 2: Dimensions of electrolysis equipment used in modeling the system in COMSOL.

Part	Dimensions (mm)	Material
Salt Bath	Radius 59.5 x 35	Custom
Silicon Wafer	25.4 x 0.55 x 38.1	Silicon [solid,bulk]
YSZ Tube	Radius 9.5 x 60	97 ZrO ₂ - 3 Y ₂ O ₃ (mol%) [solid]
Anode	Radius 5.5 x 15	Graphite 7087 [solid,across grain]
Cathode	Radius 5.5 x 15	310 [solid,unoxidized]

Once the geometry had been made, the next step was to define the material for each part, which are also defined in Table 2. All but one of the materials can be found in the material library in COMSOL. Since the salt bath is a custom mixture, COMSOL doesn't have the material in its database. Therefore, a custom one was created with the properties defined manually in Figure 14. These properties needed to be defined as they are required by the physics and multiphysics that will be used to simulate the model.

Property	Variable	Value	Unit	Property group
<input checked="" type="checkbox"/> Electrical conductivity	sigma_is...	438	S/m	Basic
<input checked="" type="checkbox"/> Thermal conductivity	k_iso ; ki...	2.33	W/(m·K)	Basic
<input checked="" type="checkbox"/> Dynamic viscosity	mu	.0078	Pa·s	Basic
<input checked="" type="checkbox"/> Density	rho	rho(T2)	kg/m ³	Basic
<input checked="" type="checkbox"/> Relative permittivity	epsilon_r...	1	1	Basic
<input checked="" type="checkbox"/> Heat capacity at constant pressure	Cp	928.5	J/(kg·K)	Basic
<input checked="" type="checkbox"/> Ratio of specific heats	gamma	1	1	Basic
<input type="checkbox"/> Coefficient of thermal expansion	alpha_is...	1	1/K	Basic

Figure 14: Salt Bath Material Properties

The density of the salt bath changes with temperature so an equation was needed instead of a constant value. An analytic function was added with the specifications below in figure 15. The T in rho(T2) needs to match the heat transfer physics number that is being used. This number is in the parentheses after the physics, ht1, ht2, etc.

Analytic

Plot Create Plot

Label:

Function name:

▼ Definition

Expression:

Arguments:

Derivatives:

▶ Periodic Extension

▼ Units

Arguments:

Function:

▶ Advanced

▼ Plot Parameters

Argument	Lower limit	Upper limit
T	293.15	1400

Figure 15: Salt Bath Density Analytic Function Input

After defining the materials and specifying property values, different physics was added to the model. In our case, the physics determined to be at play in our system were electric currents, heat transfer in solids, and laminar flow. For electric currents, 1.75 volts was supplied through the anode and 0 volts at the cathode. A temperature of 1373.15 K was specified for all exterior surfaces to simulate the heating of the furnace. To simulate laminar flow, gravity and no slip conditions were applied. However, the top of the salt bath had slip conditions and was modeled accordingly. A pressure point constraint of 0 Pa was added to a point in the salt bath and the model accounted for hydrostatic pressure.

With the physics in place, they were coupled together using multiphysics options built in COMSOL. Two multiphysics were chosen, electromagnetic heating and nonisothermal flow. Afterwards, a mesh of the system was created and a simulation is computed. Once the

computation is done, 2D plots and 3D plots with multi-slices are created to visualize the distribution of properties within the system.

Section 3.3: Experimentation

In this section we describe the equipment and connections needed to set up for the electrolysis experiments. We also describe the electrolysis steps, as well as preparing and analyzing the samples.

Equipment and Components

The equipment for our experiments include an 18-inch diameter Mellen furnace which is located in the Foundry laboratory in Washburn Hall at WPI. This furnace is illustrated in Figure 1. The supplemental furnace insulation has an opening that is able to fit a 6-inch pipe and approximately a 7-inch pipe for the tube bottom plate. The table has unistrut legs and spaces that provide support for the welded furnace tube assembly (Moudgal, Powell, 2019). The welded furnace tube assembly has a top flange and is made out of 310 stainless steel. The top plate has Kurt Lesker vacuum couplings which are $1 \times 1''$, $1 \times \frac{3}{4}''$, $2 \times \frac{1}{4}''$, and $2 \times \frac{1}{8}''$ for inner diameter dimensions. There are steel plugs to fill all the couplings besides the two $\frac{1}{4}''$ openings and the two $\frac{1}{8}''$ openings. To feed argon gas into the system there is a $\frac{1}{4}''$ outer diameter steel tube. Another $\frac{1}{4}''$ outer diameter steel tube is used for the argon outlet stream. To measure temperatures, there are two type K thermocouples. The cage has three $\frac{1}{4}''$ -20 threaded rods that hang from the top plate and a 316 stainless steel crucible support at the bottom plate (Moudgal, Powell, 2019). On the crucible, there are three 316 stainless steel sheet radiation baffles connected to the threaded rods. These three baffles are spaced approximately at the top, middle, and bottom of the supplemental furnace insulation. Included in the system is a fan to help cool the top plate and fittings (Moudgal, Powell, 2019).

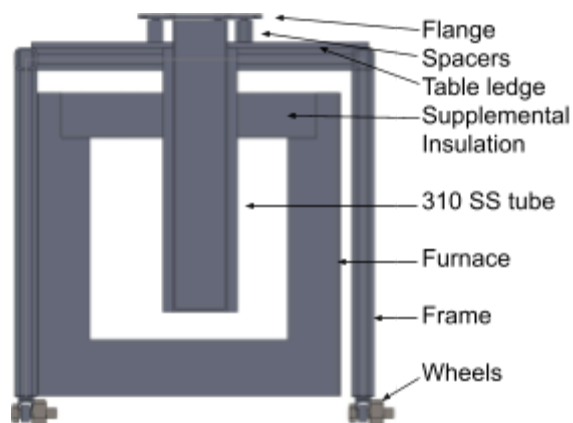


Figure 16: A schematic of the Mellen Furnace including the positions of the table ledge, supplemental insulation, 310 stainless steel tube, frame, and wheels. The supplemental insulation used was styrofoam (Moudgal, Powell, 2019).

Furnace Set-Up

1. Connect the heating elements, control and over-temp thermocouples to the power supply for the furnace.
2. Connect any extra components to the furnace in order to heat up and operate.
3. Program in low heat, around 200 °C, into the furnace to verify power is being received.
4. Turn the furnace off.
5. For the controlled atmosphere tube, put together the unistrut-table-spacer support.
6. Lower the stainless tube into the furnace through the opening on the top.
7. Confirm the tube is resting on the spacers.

(Moudgal, Powell, 2019)

Assemble the cage

1. Screw the threaded rods into from the bottom side of the plate, into the top side, using teflon tape.
2. Add a baffle, a washer and a nut in that order, to the threaded rods in a position that corresponds to the insulation position. Do this three times.
3. With the crucible support, washers and nuts, connect the bottom plate.

4. In the two $\frac{1}{8}$ " fittings on the top plate, insert the thermocouples so that one is sitting at the bottom of the crucible, and the other is outside at the same height
5. Insert the corresponding tubes into the $\frac{1}{4}$ " fittings where outlet tube is 2-3 cm below the top plate, while the inlet tube is 10-15 cm below the top plate.
6. Insert the cage into the stainless tube.

(Moudgal, Powell, 2019)

Gas Connection Set-Up

1. Connect a line between the regulator on the argon cylinder to the inlet of the rotameter as shown in Figure 17.
2. Connect a line from the outlet of the rotameter to the inlet of the 310 stainless steel tube high-temperature chamber.
3. Open an exhaust duct before proceeding to the next steps.
4. Connect a line from the high-temperature chamber to the exhaust duct. This should create negative pressure in the chamber. Insert a differential pressure sensor and an oxygen sensor to ensure that the chamber pressure is not below the room pressure.
5. Change the rotameter to a 200-300 SCCM flow rate and check the level of oxygen exiting the system. The volume of the chamber is 11 liters and the residence time is around 30-50 minutes.
6. If the level of oxygen does not fall after 10-20 minutes, then check the equipment for any leaks. Proceed to increase the flow rate to 500 SCCM.

(Moudgal, Powell, 2019)

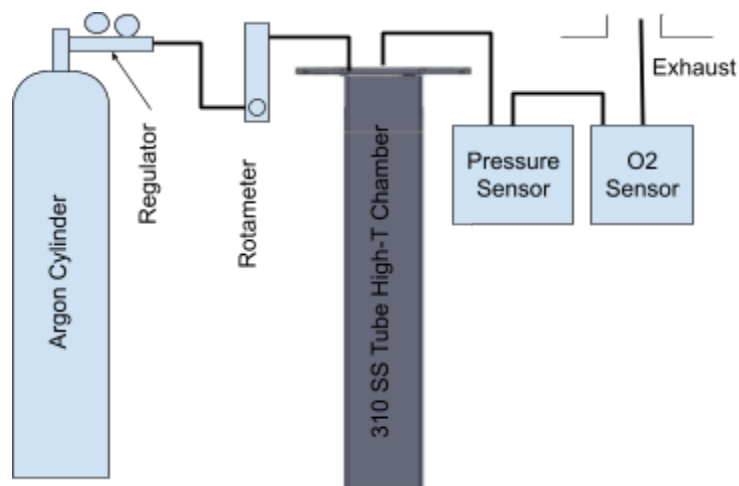


Figure 17: A schematic which shows the set-up of connecting the argon gas cylinder to the 310 stainless steel tube high-temperature chamber (Moudgal, Powell, 2019).

Set up data logging connections

1. Connect the data logger to the two type K thermocouples as well as the differential pressure sensor, oxygen sensor, and the furnace controller. To connect the data logger to the furnace controller, use the RS232 port (Moudgal, Powell, 2019).

Staged Furnace Heat-up

1. Make sure all safety signs are posted, visible and legible in the area of the furnace.
2. Oxygen pressure must reach 0.05 bar before starting the furnace or oxidation and burning could occur, this may take a long time.
3. Reduce the flow of the argon as low as possible while still having a low oxygen partial pressure, this flow should be around 100 SCCM.
4. Turn furnace heating on to 10 °C/min until reaching 500 °C and then hold for 10 minutes minimum.
5. Record the temperature at the start of heating up, every ten minutes during heating and at hold temperature.
6. If there is a data logger, temperature does not need to be manually recorded.
7. Measure the temperature at the top of the plate near the o-ring, the center, below the flange and at the fittings with a pyrometer.

8. If the temperature reading from the pyrometer reads at or above 200 °C, shut down the furnace as the atmosphere could become compromised.
9. If the temperature of the top plate is near the service temperature, turn on the fan and if temperature continues to increase, lower the furnace temperature slowly until it is off.
10. Use the thermocouples to get a temperature profile of the furnace by raising the thermocouples by 5 cm and waiting for the temperature to stabilize. Do this 3 times, up to 15 cm away, and once done lower the thermocouples back to the initial height.
11. Once temperature has stabilized in the furnace, increase temperature to 800 °C with 10 °C/minute and then hold for at least 10 minutes for temperature to stabilize.
12. Every 5 minutes while the temperature is increasing, record the temperature data.
13. As expressed above (step 30), get a temperature profile of the furnace.
14. Once the furnace temperature has stabilized, increase the temperature at 10 °C/min to 1000 °C and hold once that temperature has been reached for at least 10 minutes.
15. While the temperature is increasing, record the temperature data every 5 minutes.
16. As expressed above (step 30), get a temperature profile of the furnace.
17. Once the furnace temperature has stabilized, increase the temperature at 10 °C/min to 1150 °C and hold once that temperature has been reached for at least 10 minutes.
18. As expressed above (step 30), however the maximum height is now 30 cm instead of 15 cm, get a temperature profile of the furnace.
19. Lower temperature of furnace down to room temperature at a rate of 10 °C/minute.

(Moudgal, Powell, 2019)

Preparing Bath Salt Solution

1. Prepare the bath-in by using a scale to weigh out the proper amount of each salt.
2. Mixing all the salts (CaF_2 , MgF_2 , CaO , Al_2O_3 , & YF_3) together under a fume hood (See Table 3).
3. Once the salts have been mixed, place the canister in the paint mixing machine to fully homogenize the mixture.
4. Melt the salt mixture in the furnace.

5. Take crucible and mixture out. Let cool before handling.
6. Take the salt mixture solid and insert into plastic bags. Crush with a hammer until the solid breaks up into relatively smaller pieces. We do not need a super fine powder, and small chunks are okay to use. Add the crushed mixture back to the crucible.
7. Tare the crucible on a scale, then add the crushed mixture to take the weight of the salts.
8. Determine the amount of silica dioxide needed to add to the mixture. This is determined using defined weight percentages we would like to test. For example, if the crushed mixture weighs 0.48 grams, and our basis is 0.50 grams, we would add 0.02 grams. This is easily done by adding the silica dioxide straight to the crucible.
9. Once we have added the silica dioxide, transfer the crucible back to the heat furnace.
10. Allow the system to cool, before starting electrolysis.

Table 3: Weighted amount of compounds needed for each experimental run

Compound	Weighted Amount (g)
MgF ₂	364.1
CaF	488
CaO	66.9
YF ₃	31
Al ₂ O ₃	2
SiO ₂	50

Electrochemical Measurements & Electrolysis



Figure 18. Photograph of electrolysis cage set up (Espinosa, Rutherford, Wallace, Powell, 2020).

1. Screw the threaded rods into from the bottom side of the plate, into the top side, using teflon tape.
2. Add a baffle, a washer and a nut in that order, to the threaded rods in a position that corresponds to the insulation position. Do this three times.
3. With the crucible support, washers and nuts, connect the bottom plate.
4. In the two $\frac{1}{8}$ " fittings on the top plate, insert the thermocouples so that one is sitting at the bottom of the crucible, and the other is outside at the same height
5. Insert the corresponding tubes into the $\frac{1}{4}$ " fittings where outlet tube is 2-3 cm below the top plate, while the inlet tube is 10-15 cm below the top plate.

6. Insert the cage into the stainless tube.
7. Connect leads to the anode and the cathode, and lower both until they stop at the bottom of the crucible - they should both be immersed in the liquid tin.
8. Switch on power supply.
9. Run current and voltage sweep increasing voltage by 0.1V every 13 seconds.
10. Shut off the power supply.
11. Repeat step 9.
12. Hold at 1V for 1 hour.
13. Repeat steps 10 and 9.
14. Hold at 3V for 2.5 hour.
15. Repeat steps 10 and 9.
16. Hold at 2V for 1 hour.
17. Shut off the power supply.

(Moudgal, Powell, 2019)

Shut Down Procedure

1. Raise both the anode and cathode about 15 cm so their bottom points are completely out of the molten salt and roughly even with the top of the crucible.
2. Shut off the furnace at its power switch and the wall disconnect.
3. Shut off argon.
4. Turn off HP power supply.
5. Let the apparatus cool for at least 12 hours to room temperature

Sample Preparation and Polishing








Table 18.1: 5-Step Procedure for Preparing Silicon In Microelectronic Devices					
Sectioning	Precision Saw with blade recommended for microelectronic devices				
Mounting	Castable, typically EpoThin				
Surface	Abrasive / Size	Load - lbs [N] / Specimen	Base Speed [rpm]	Relative Rotation	Time [min:sec]
CarbiMet	600 [P1200] grit SiC water cooled	3 [13]	100		Until Plane
VerduTex	6µm MetaDi Supreme Diamond*	5 [22]	100		3:00
VerduTex	3µm MetaDi Supreme Diamond*	5 [22]	100		3:00
VerduTex	1µm MetaDi Supreme Diamond*	5 [22]	100		3:00
ChemoMet	0.06µm MasterMet Colloidal Silica	2 [9]	100		2:00
 - Platen  - Specimen Holder *Plus MetaDi Fluid Extender as desired					
Imaging & Analysis	Measurement & Analysis Applications, Manual Interactive Thickness				
Hardness Testing	N/A				

Figure 19: A table taken from Buehler’s Guide on how to mount and polish silicon using a 5-step procedure. Note that it is suggested to use EpoThin for mounting, but we used a similar epoxy called Epoxicure 2 for this process (Buehler SumMet, 2007).

1. After electrolysis, retrieve the silicon wafer to prepare for the sample analysis.
2. Silicon wafer should be weak enough to break into smaller pieces. Manually breaking the wafers will prevent the need to use the Precision Saw. Only one piece is required, other reminding bits can be stored and labeled in a bag. Make sure the sample fits inside the 1.5 inch diameter mold.
3. The sectioned sample is now casted in EpoxiCure 2. To prepare for the mount, mix the Epoxy Resin to Epoxy Hardener in a 4 to 1 ratio.
4. Coat the releasing agent on all surfaces within the mold.
5. The sample is stood up vertically within the mold by using a stand. The epoxy is then poured in, keeping in mind of maintaining the position of the sample.
6. A vacuum system is incorporated to extract all air pockets out of the resin. The samples can be left in the vacuum for approximately an hour.
7. Once the sample is sufficiently mounted, the samples are removed from the mold and polishing can take place. Using the Buehler polisher equipment, select the “5stepSilicon”

for the procedure on the display screen. This will automatically change the load weight, base speed, and timer on the equipment accordingly.

8. Use the CarbiMet surface with water as the abrasive.
9. Before changing to the next polishing surface, cleaning the equipment is required after each exchange.
10. The sample is rinsed and dried before viewing under a microscope.
11. All suspensions used will require proper chemical waste disposal.
12. Use the VerduTex surface with 6um diamond suspension.
13. Use the VerduTex surface with 3um diamond suspension. This suspension is in a small plastic spray bottle and must be sprayed on manually. To determine if enough has been added, the surface should be wet when touched.
14. Use the VerduTex surface with 1um diamond suspension.
15. Use the ChemoTex surface with 0.06um diamond suspension.
16. The abrasive used needs to be scraped off the ChemoTex surface or else the salt from the abrasive will crystallize on the surface.
17. Once the polishing process is completed, the Buehler polisher equipment can be turned off. Note that an example photograph of the mounted samples are shown in Figure 5.



Figure 20: A photograph of pieces of the silicon wafer mounted using Epoxicure 2 and a metal stand to hold the wafer upright.

Silicon Sample Analysis

Once the samples have been carefully polished, there are a few options available to analyze the samples. Scanning Electron Microscope (SEM) and Energy-Dispersive X-ray Spectroscopy (EDS) was used to detect the presence of silicon deposits on the wafer. To improve the performance of the equipment it is recommended to incorporate gold sputtering to the samples. To see more images taken from the SEM and EDS, refer to Appendix A and B below.

Chapter 4: Results and Discussion

This chapter presents our results from the techno-economic cost model, as well as our findings from COMSOL modeling, and from analyzing the samples from the electrolysis experiments.

Section 4.1: Techno-economic Cost Model

Before developing a cost model, it was also important to check the material balance created by last year's MQP team (Buasai, et al., 2020). In doing so, we made improvements to previous work completed and developed a more complete material balance. After a material balance was done on the molten-salt electrolysis system, our research team developed a techno-economic cost model of a start-up plant that produces solar-grade silicon using molten-salt electrolysis and the novel bath composition. Overall, a cost model that included raw material expenses, operating costs, total capital investments (TCI), etc., was developed by our research team during the summer. The previous cost model constructed by the previous MQP team was based on an interview with a senior process engineer who was working at an aluminum plant in South Carolina. On the other hand, our cost analysis was based on a cost model equation developed by researchers from the Massachusetts Institute of Technology.

Material Balance

To understand how much of each compound was needed in the bath composition, our research team performed a mass balance on the system. Last year's research team also performed an overall mass balance on the system and had identified 9 total streams in the process. For our own research, we considered only 5 of these 9 streams that were directly involved in ultimately producing the final silicon product. These 5 streams are shown in Figure 21.

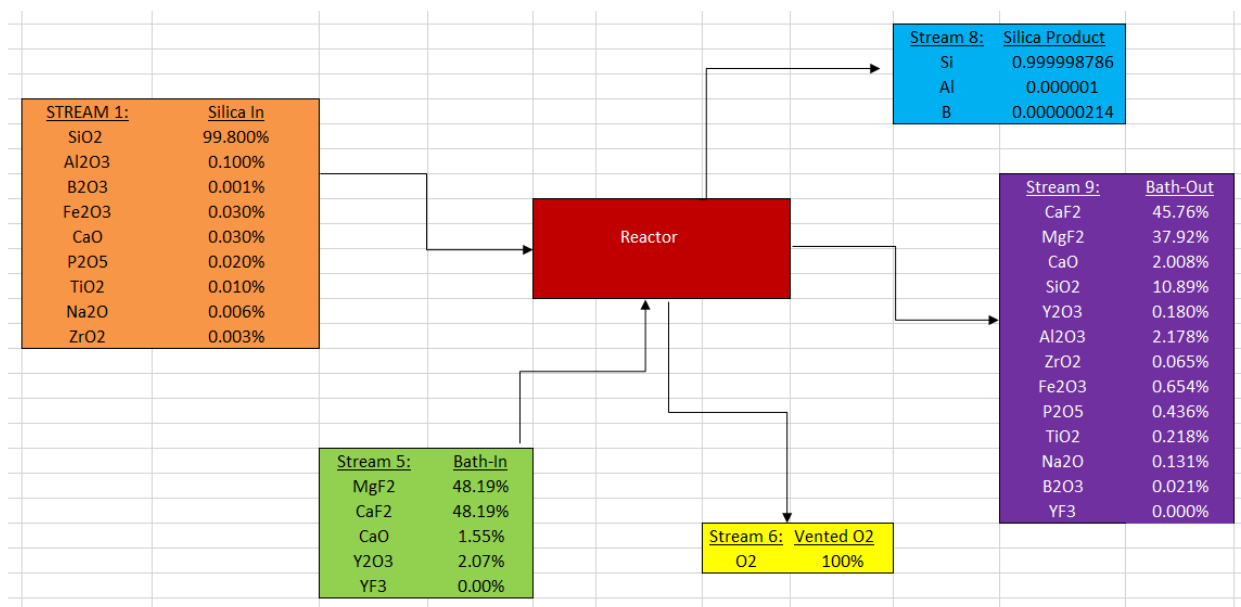


Figure 21: System Block Diagram; A simple block diagram to show what chemical compounds are directly involved to ultimately produce solar-grade silicon and their respective weight percentages. Note that this process uses yttrium oxide in the bath inlet composition, but we used yttrium (III) fluoride in our electrolysis experiments.

After the important chemical components and streams were identified, a mass balance was constructed knowing that what goes in must come out within the ARPA-E-METALS spreadsheet. Since we knew what silicon purity we wanted to achieve, we could figure out the amount needed of each compound in the bath composition, or in this case stream 5. Our research team found that we would need 48.19% of magnesium fluoride, 48.19% calcium fluoride, 1.55% calcium oxide, and 2.07% yttrium (III) fluoride. It is important to note that yttrium (III) fluoride is also listed under stream 5. If the user chooses to use yttrium (III) fluoride, the user can easily change this within the excel model we built and the percentages and the flow rates will automatically update. This gives the user the option to select between using yttrium oxide or yttrium (III) fluoride within the process.

Total Capital Investment Summary (CAPEX-Si)

To find out how much capital must be invested into a plant, the Stinn-Allanore equation was used. These values were obtained through the variables used in the experiments, such as temperature and voltage, while others are based off of the desired capacity, such as total installed

production rate and installed power capacity. For example, if the yearly production rate was 160,000 metric tons, the cost of one plant would be about \$1,682,450,000. A chart was created with different production capacities in order to determine the optimal plant capacity. For a more comprehensive look at the production capacity and corresponding cost of the plant please refer to Figure A.1 in Appendix A. Moreover, we compared the difference in cost between using one or two rectifiers. A second rectifier would allow for continual operation during maintenance if installed. To better visualize the data, charts were created to help determine the optimal number of cells for a single and double rectifier plant.

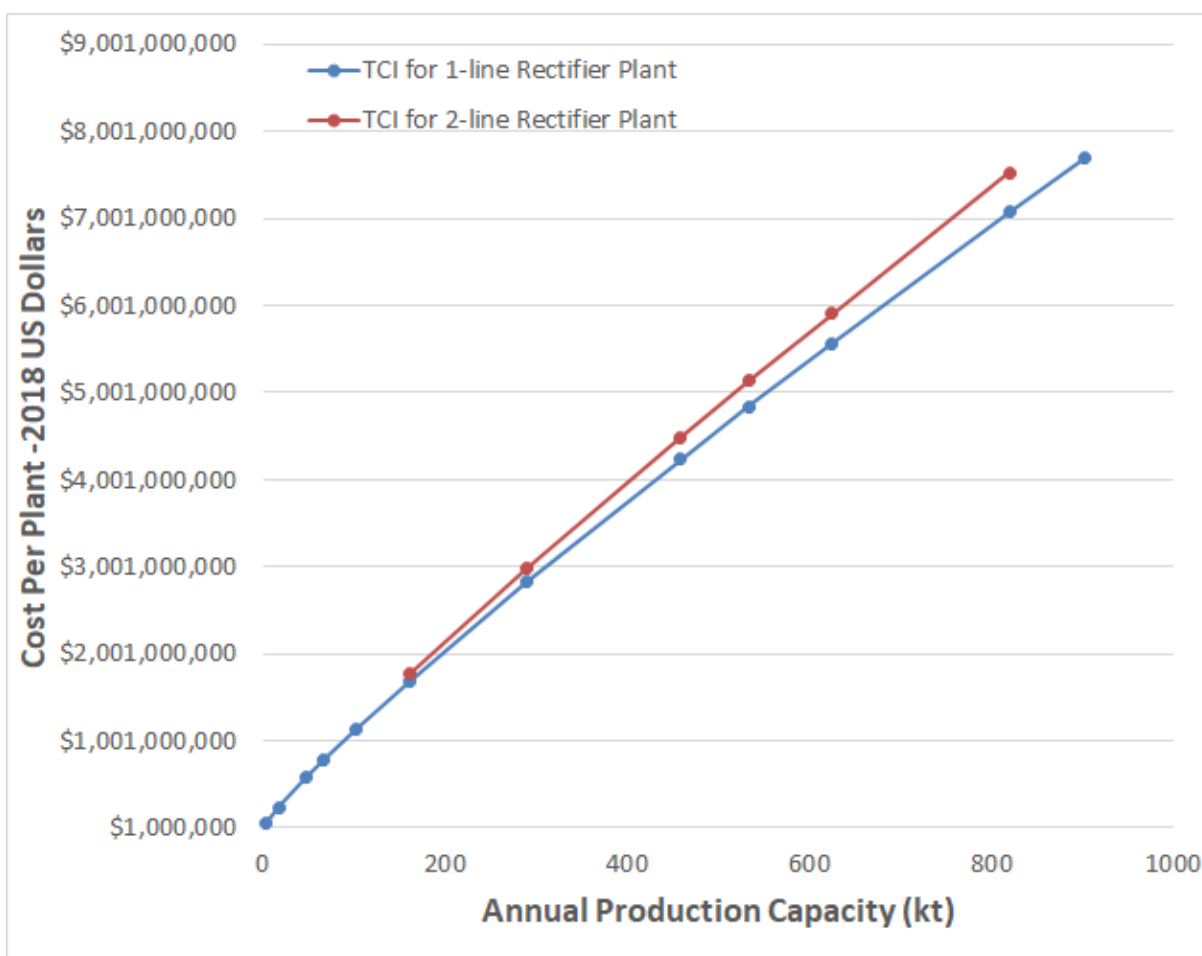


Figure 22: Cost per Plant vs Annual Production Capacity Graph

In Figure 22, the red line represents a plant with two rectifiers while the blue line represents a plant with one rectifier. As shown in the figure, a plant with two rectifiers at the

same production capacity is always more expensive than a plant with one rectifier. However, the costs between the two rectifiers are similar for smaller production capacities. The cost difference becomes more noticeable as the annual production capacities increase. If larger production capacities were added to the graph, the cost difference between the one and two rectifier plants would become exorbitant. Overall, this graph is useful for comparing and determining the costs of constructing a single or double rectifier plant.

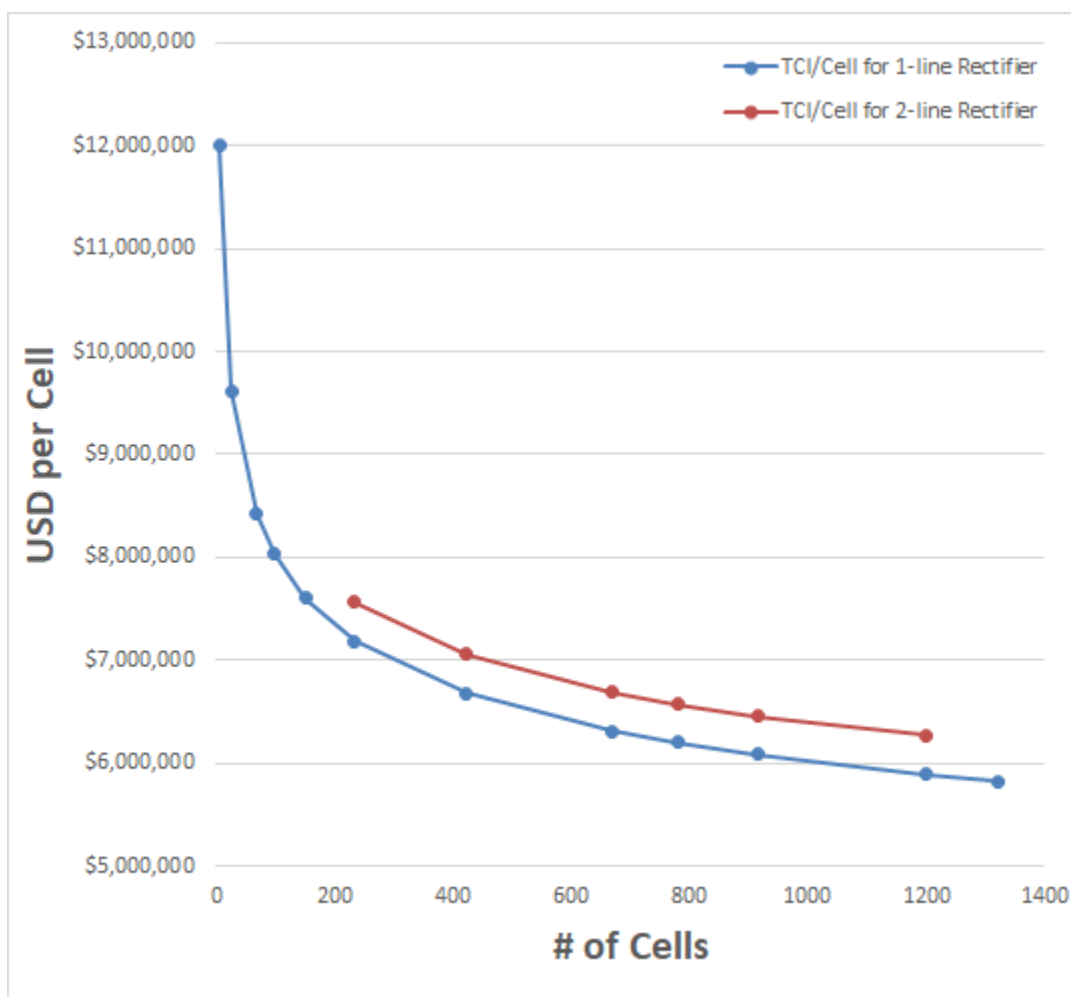


Figure 23: USD per Cell vs Number of Cells Graph

In Figure 23 the price of each cell is being compared to the number of cells for both single and double rectifier plants. According to the figure, incorporating a small number of cells in the plant proves to be incredibly cost-inefficient, as a small number of cells can cost up to \$12,000,000 per cell. The cost efficiency drastically improves as the cell count surpasses 200 as

the cost per cell starts to level off between \$7,000,000 to \$6,000,000. This plateauing effect is observed for both one and two rectifier plants, due to the marginal cost of production. As more products are produced, the cost for each cell is reduced. This is due to the fixed costs being spread out evenly for each cell, while only the variable costs are changing. This point is the most efficient number of cells, however it is not shown on the graph. The cost per cell for two rectifiers is more expensive compared to the cost per cell for one rectifier. The difference in costs is due to the installation expenses for a second rectifier.

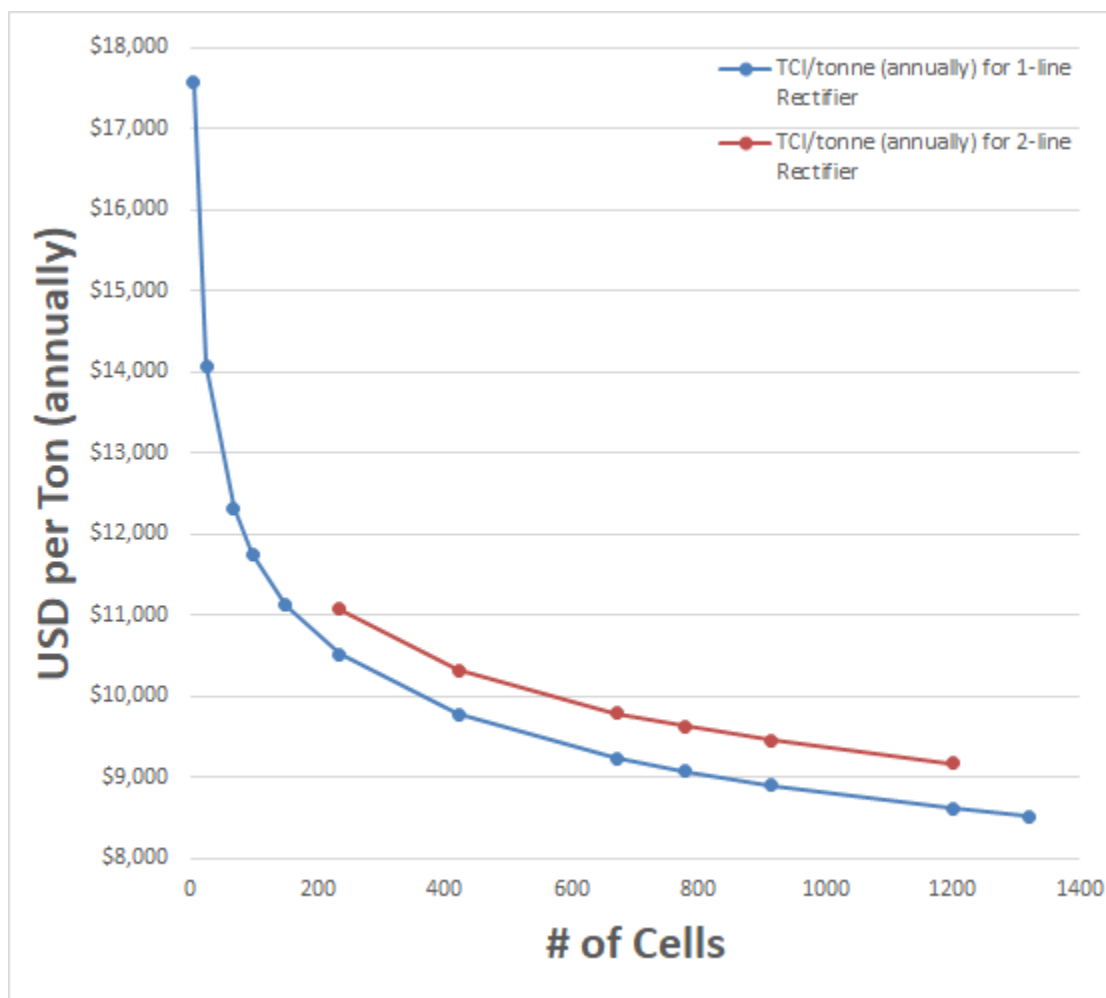


Figure 24: USD per Ton vs Number of Cells Graph

Figure 24 shows similar trends to Figure 23, except we are comparing the cost per ton against the number of cells. The cost per ton is just the cost of the plant divided by the production capacity. Note, the greater the production capacity, the more cells needed. In Figure

24 the two rectifier plants will be slightly more expensive largely due to installation costs when compared to the one rectifier plant. The most efficient number of cells is not depicted in the graph, however it can be determined by incorporating additional data points to show plants with higher cell counts.

Operating Expense/Income Summary

The total capital investment can be broken down into variable/operating cost and fixed cost. The fixed cost is going to be greater than the operating cost. To calculate the fixed cost of the project, the total capital investment was split into installation cost and fixed capital investment. For more information please refer to Figure A.2 in Appendix A. To calculate the installation cost and the fixed capital investment percentages were obtained from the Department of Energy. The install cost is broken down into auxiliaries (35.4%), buildings (21.4%), site development (5.3%), land (2.5%), and spare parts (0.5%). The fixed cost has two categories, working capital and start-up costs with a percentage of 19.2% and 9.0% respectively. Based on these calculations, our team determined the annual operation costs for plants with differing production capacities. These amounts can be seen in Figure A.3 in Appendix A.

The operating cost is split into three sections: fixed costs, variable costs, and indirect costs. The fixed cost includes the cost of maintenance and operating labor. The operating labor is further broken down into laboratory costs, supervision, plant overheads, insurance and royalties. The variable cost consists of raw materials, miscellaneous materials and utilities. The last category for the fixed capital investment is indirect costs, which is just 25% of the variable and fixed costs added up. The operating cost for a year was then determined by these values, and plotted in Figure 25 below.

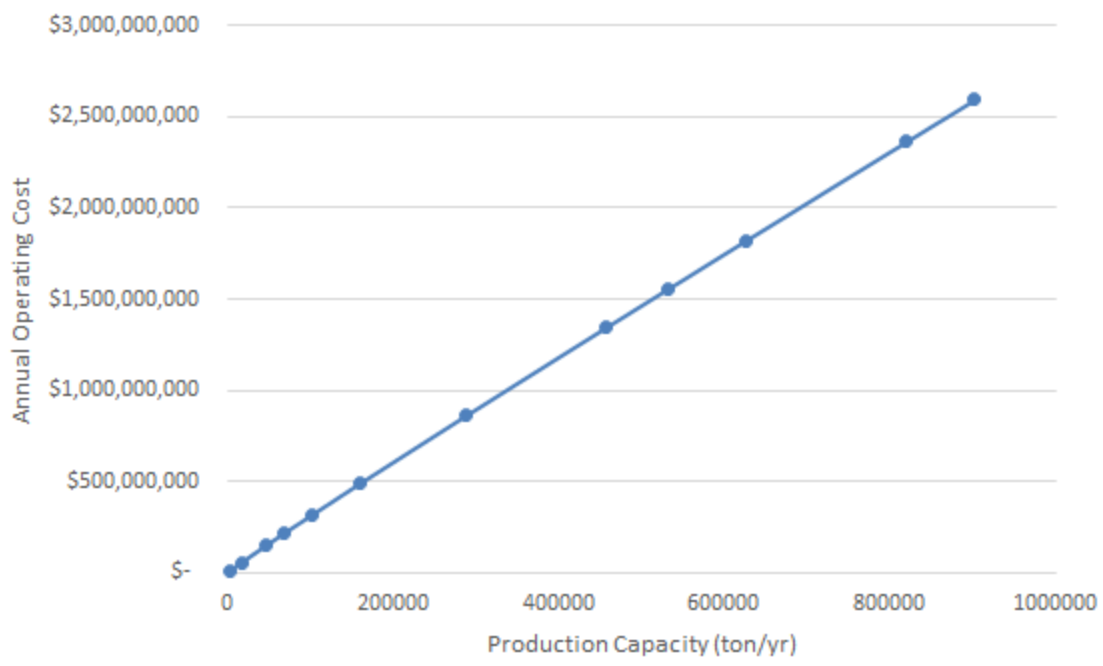


Figure 25: Annual Operating Cost vs Production Capacity Graph

As the production capacity increases, the annual operating cost increases linearly which is an expected result as more equipment, utilities and manpower are needed to operate larger plants at higher production capacities.

Overall Cost Analysis (Cost Analysis Ref. Model)

To best summarize and visualize the costs calculated, a few graphs were generated. Figure 26 evaluates the operating cost sensitivity, and compares the values obtained from the Stinn-Allanore cost model with the values obtained from last year’s interview model. The bars indicate the amount of money expenses due to different contributors of operating costs. The blue bars represent those figures obtained by last year’s cost model based on an interview. The red bars represent the figures obtained by our research team from using the Stinn-Allanore equation.

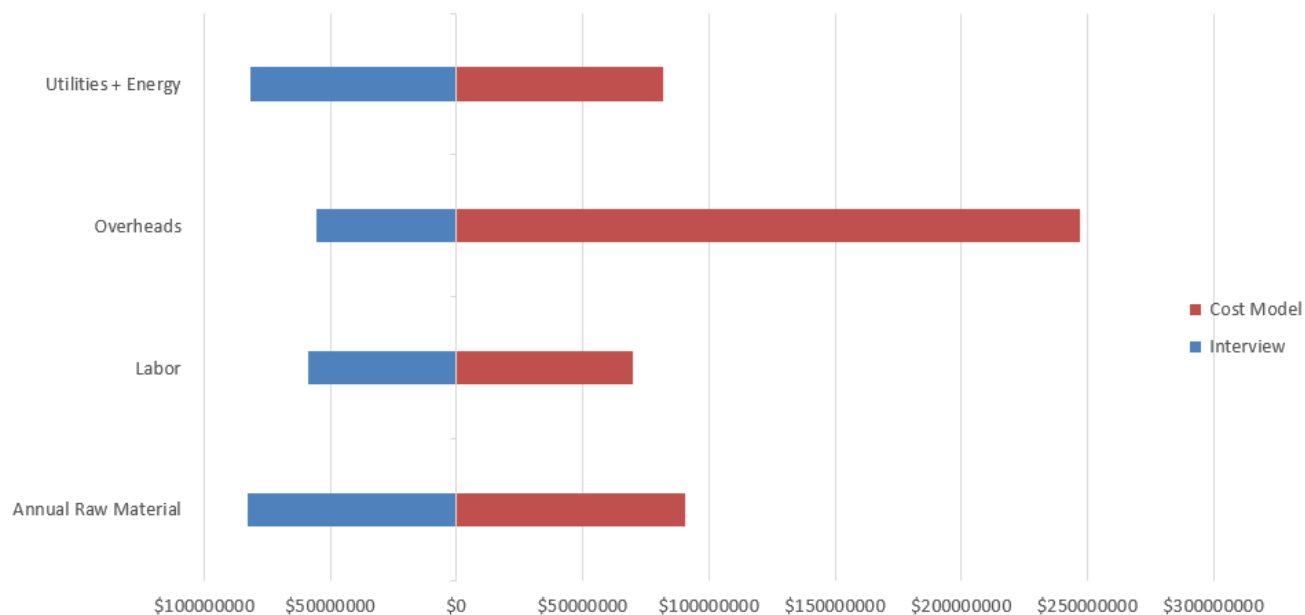


Figure 26: Operating Cost Sensitivity to Inputs Graph; Tornado graph comparing the cost model developed by our research team to last year's on different operating cost sensitivities to input.

According to our cost model, the cost of overheads (maintenance, plant overheads, insurance, royalties, and indirect fees) will have the biggest impact on operating cost. Besides this major difference, the costs calculated from the model for the other sectors such as labor, annual raw material, and utilities are similar to those reported from the interview.

To better categorize operating cost, Figure 27 divides the expenses into three costs. Of the three costs, the operating cost is most sensitive to fixed costs. This expense includes the cost of labor as well as overheads.

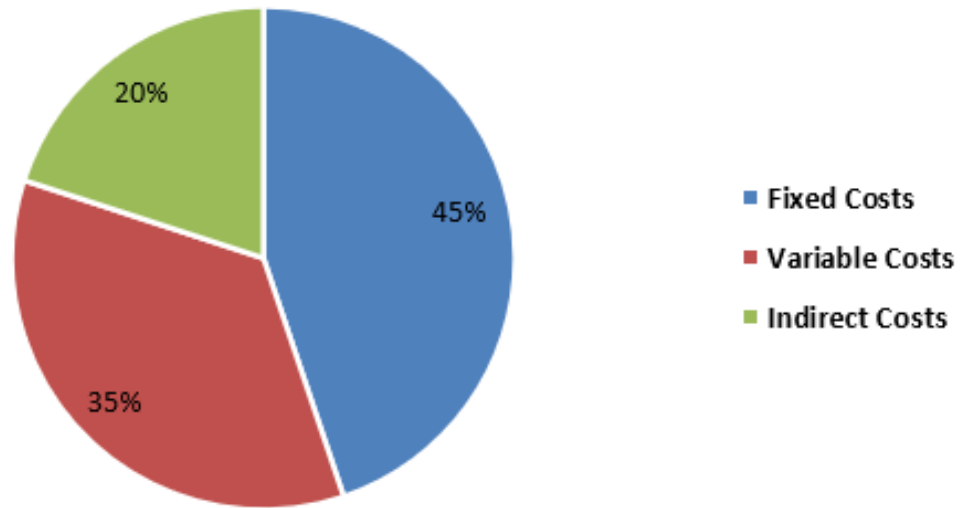


Figure 27: Annual Operating Costs Breakdown

For a more detailed look into the composition of the annual fixed cost, see Figure 28 above. The cost of maintenance and operating labor (OL) make up over 50% of the annual fixed cost.

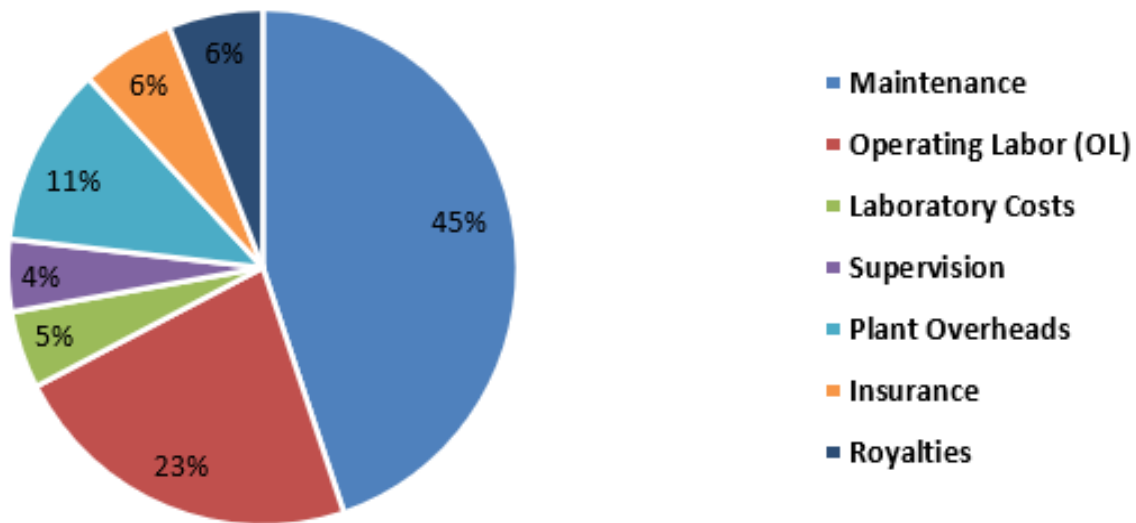


Figure 28: Annual Fixed Costs Breakdown

Variable costs make up 35% of the annual operating costs including the cost of raw materials, utilities, and miscellaneous materials. To investigate further into variable cost see Figure 29 below.

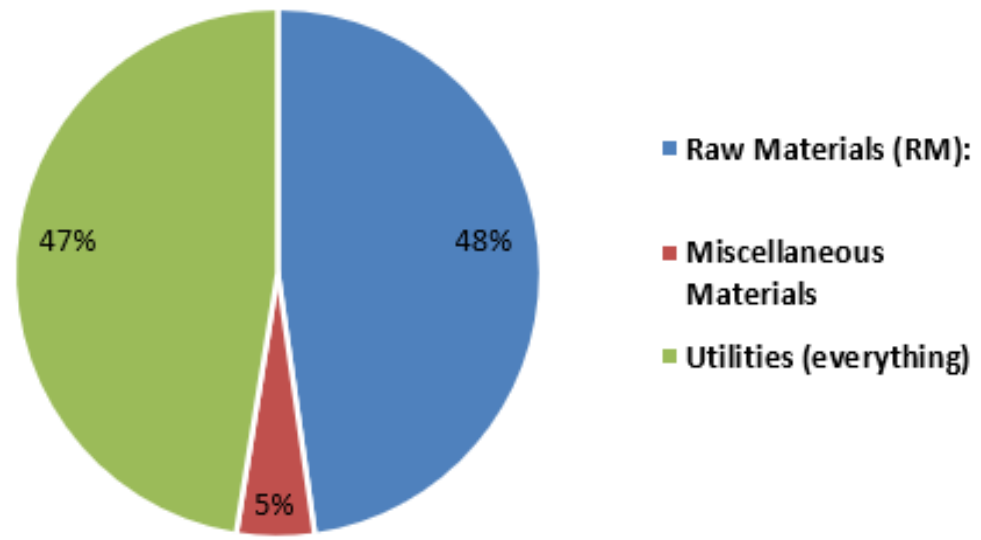


Figure 29: Annual Variable Costs Breakdown

According to Figure 30, the proposed plant will spend 63% of its annual raw material expenses on silica. As for indirect costs, this value is simply an estimate. According to the Department of Energy, the typical indirect costs would amount to something similar to a quarter of the sum of variable and fixed costs.

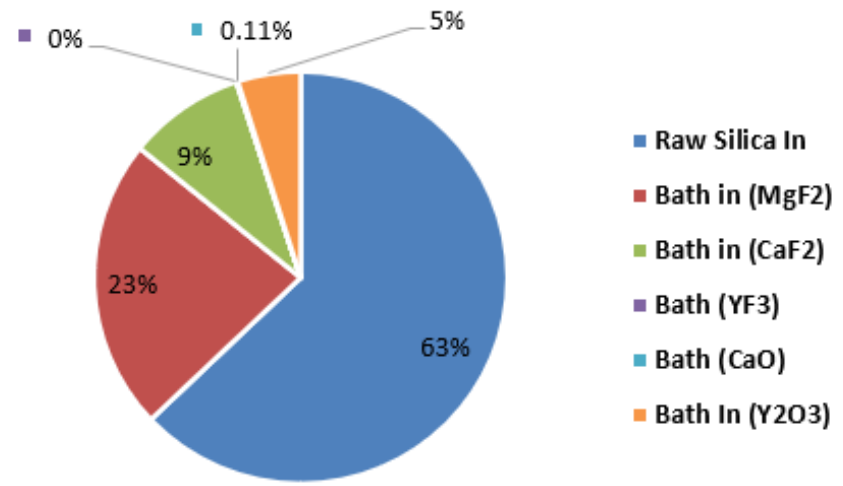


Figure 30: Annual Raw Material Costs Breakdown

User Friendly Interfaces within our Techno-economic Model

An important feature the research team incorporated into the model is the automation of the Excel file. The tab and overall cost model will fully update itself at the change of a value inputted by the user. Such a feature gives the users the ability to experiment with a few different options in terms of costs, production capacity, materials, etc, as well as specify the cost model to their own conditions and criterias. Besides constructing a fully functioning cost model, it's important that the information gathered is easily transferable to users with varied background knowledge on this topic. As a result, our research team incorporated a few user friendly interfaces that provide easy navigation as opposed to other tabs within the model where information may be more cluttered and disorganized. Some of the interfaces from the Excel can be found in Appendix A. Tab titled “Streams” as shown in Figure _Stream Summary_ in Appendix A, provides a compressed description of the individual streams within the system. The tab also includes an error checking service which looks over the overall mass balance of the system for mistakes. Such error checking section is depicted in Figure 31. The columns and rows regarding the mass fraction/balance are color coded. Red indicates that the value is greater than 10^{-15} , which suggests that the stream is not balanced. As indicated in Figure 31, all streams and components are green, thus suggesting that our system is balanced. All the information listed refers to the data found in the “Material Balance” tab.

Guide														
ERROR CHECKING: MASS BALANCES														
	Si	O	Mg	F	Ca	Y	B	Al	Fe	Zr	Na	Ti	P	
Mass Balance [kg/hr]	Element Bal. [kg/hr]	Element Bal. [kg/hr]	Element Bal. [kg/hr]	Element Bal. [kg/hr]	Element Bal. [kg/hr]	Element Bal. [kg/hr]	Element Bal. [kg/hr]	Element Bal. [kg/hr]	Element Bal. [kg/hr]	Element Bal. [kg/hr]	Element Bal. [kg/hr]	Element Bal. [kg/hr]	Element Bal. [kg/hr]	Element Bal. [kg/hr]
0	6.07153E-17	9.36751E-17	0	0	0	0	0	0	0	0	0	0	0	0
2.154404028	1.005029588	1.146852634	0	0	0.00946192	0	6.69095E-06	0.001140219	0.000452054	4.78483E-05	9.58956E-05	0.000129132	0.000188045	
0.244170906	0	0.002154146	0.045903508	0.129027151	0.063106114	0.003979987	0	0	0	0	0	0	0	0
-1.139335226	0	-1.139335226	0	0	0	0	0	0	0	0	0	0	0	0
-1	-0.999998786	0	0	0	0	0	-0.000000214	-0.000001	0	0	0	0	0	0
-0.259239708	-0.005030802	-0.009671555	-0.045903508	-0.129027151	-0.063568034	-0.003979987	-6.47695E-06	-0.001139219	-0.000452054	-4.78483E-05	-9.58956E-05	-0.000129132	-0.000188045	

Figure 31: Mass Balance Error Checker

For a more comprehensive look into stream composition, we constructed the tab titled “Composition”. Information regarding molecular weight, stream/species flow rate, molecular

formula, mass percent, and etc, can be located here. Although the information here like in “Streams” refers to the data calculated in other sheets, the information here is presented in a more organized and conceivable format as shown in Figure 32. The tab also incorporates an error checking service in which checks for the elemental balances within each stream as seen in Figure 33.

COMPOSITION OF EACH PROCESS STREAM										Stream	Species	Specific	Species							
line#	Stream #	Phase	Species Name	Mass Percent [wt/wt]	ENTER Molecular Formula (one species per line)										Flow [kg/hr]	Flow [kg/hr]	value [\$/kg]	value flow (absolute) [\$/h]		
					1	2	3	4	5	6	7	8	9	10	Formula	MW				
1	1	solid	Silica	99.85%	Si	1	O	2							SiO2	60.0843	2.154404	2.15009522	0.15	0.32
2	1	solid	Aluminum Oxide	0.1%	Al	2	O	3							Al2O3	101.9612	2.154404	0.002154404	#N/A	#N/A
3	1	solid	Iron Oxide	0.03%	Fe	2	O	3							Fe2O3	159.6882	2.154404	0.000646321	#N/A	#N/A
4	1	solid	Calcium Oxide	0.03%	Ca	1	O	1							CaO	56.0774	2.154404	0.000646321	0.15	0.00
5	1	solid	Phosphorus Pentaoxide	0.02%	P	2	O	5							P2O5	141.9446	2.154404	0.000430881	#N/A	#N/A
6	1	solid	Titanium Dioxide	0.01%	Ti	1	O	2							TiO2	79.8748	2.154404	0.00021544	#N/A	#N/A
7	1	solid	Sodium Oxide	0.000%	Na	2	O	1							Na2O	61.9788	2.154404	0.000129264	#N/A	#N/A
8	1	solid	Zirconium Dioxide	0.000%	Zr	1	O	2							ZrO2	123.2228	2.154404	6.46931E-05	#N/A	#N/A
9	1	solid	Boron Oxide	0.001%	B	2	O	3							B2O3	69.6202	2.154404	2.1544E-05	#N/A	#N/A
10	6	gas	Dioxygen	100%	O	2									O2	31.9988	1.139	1.13935226	#N/A	#N/A
11	9	liquid	Calcium Fluoride	43.367%	Ca	1	F	2							CaF2	78.0748	0.25924	0.112423281	0.40	0.04
12	9	liquid	Magnesium Fluoride	45.389%	Mg	1	F	2							MgF2	62.3018	0.25924	0.11766596	1.00	0.12
13	9	liquid	Calcium Oxide	3.162%	Ca	1	O	1							CaO	56.0774	0.25924	0.008196536	0.15	0.00
14	9	liquid	Silicon Dioxide	4.152%	Si	1	O	2							SiO2	60.0843	0.25924	0.010762573	0.15	0.00
15	9	liquid	Yttrium Fluoride	2.52%	Y	1	F	3							YF3	145.9011	0.25924	0.00653	1,000.00	6.53
16	9	liquid	Aluminum Oxide	0.830%	Al	2	O	3							Al2O3	101.9612	0.25924	0.002152515	#N/A	#N/A
17	9	liquid	Zirconium Dioxide	0.02493%	Zr	1	O	2							ZrO2	123.2228	0.25924	6.46931E-05	#N/A	#N/A
18	9	liquid	Iron Oxide	0.24931%	Fe	2	O	3							Fe2O3	159.6882	0.25924	0.000646321	#N/A	#N/A
19	9	liquid	Phosphorus Pentaoxide	0.16621%	P	2	O	5							P2O5	141.9446	0.25924	0.000430881	#N/A	#N/A
20	9	liquid	Titanium Dioxide	0.08310%	Ti	1	O	2							TiO2	79.8748	0.25924	0.00021544	#N/A	#N/A
21	9	liquid	Sodium Oxide	0.04986%	Na	2	O	1							Na2O	61.9788	0.25924	0.000129264	#N/A	#N/A
22	9	liquid	Yttrium Oxide	0.0000%	Y	2	O	3							Y2O3	225.81	0.25924	0	5.00	-
23	9	liquid	Boron Oxide	0.00804%	B	2	O	3							B2O3	69.6202	0.25924	2.0855E-05	#N/A	#N/A
24	8	solid	Silicon	99.9999%	Si	1									Si	28.0855	1	0.999998786	#N/A	#N/A
25	8	solid	Aluminum	0.00010%	Al	1									Al	26.9815	1	0.000001	#N/A	#N/A
26	8	solid	Boron	0.00002%	B	1									B	10.811	1	0.00000214	#N/A	#N/A
27	5	liquid	Yttrium Oxide	2.070%	Y	2	O	3							Y2O3	225.81	0.244171	0.005054338	5.00	0.03
28	5	liquid	Yttrium Fluoride	0.00%	Y	1	F	3							YF3	145.9011	0.244171	0.00000	1,000.00	-
29	5	liquid	Magnesium Fluoride	48.19%	Mg	1	F	2							MgF2	62.3018	0.244171	0.11766596	1.00	0.12
30	5	liquid	Calcium Fluoride	48.19%	Ca	1	F	2							CaF2	78.0748	0.244171	0.11766596	0.40	0.05
31	5	liquid	Calcium Oxide	1.55%	Ca	1	O	1							CaO	56.0774	0.244171	0.003784649	0.15	0.00

Figure 32: Composition Sheet

ERROR CHECKING: MASS BALANCES												
Si	O	Mg	F	Ca	Y	B	Al	Fe	Zr	Na	Ti	P
Element	Element	Element	Element	Element	Element	Element	Element	Element	Element	Element	Element	Element
Flow	Flow	Flow	Flow	Flow	Flow	Flow	Flow	Flow	Flow	Flow	Flow	Flow
[kg/hr]	[kg/hr]	[kg/hr]	[kg/hr]	[kg/hr]	[kg/hr]	[kg/hr]	[kg/hr]	[kg/hr]	[kg/hr]	[kg/hr]	[kg/hr]	[kg/hr]
1.00503	1.145066	0	0	0	0	0	0	0	0	0	0	0
0	0.001014	0	0	0	0	0	0.00114	0	0	0	0	0
0	0.000194	0	0	0	0	0	0	0.000452	0	0	0	0
0	0.000184	0	0	0.000462	0	0	0	0	0	0	0	0
0	0.000243	0	0	0	0	0	0	0	0	0	0	0.000188
0	8.63E-05	0	0	0	0	0	0	0	0	0	0.000129	0
0	3.34E-05	0	0	0	0	0	0	0	0	9.59E-05	0	0
0	1.68E-05	0	0	0	0	0	0	0	4.78E-05	0	0	0
0	1.49E-05	0	0	0	0	6.69E-06	0	0	0	0	0	0
0	1.139335	0	0	0	0	0	0	0	0	0	0	0
0	0	0	0.054713	0.05771	0	0	0	0	0	0	0	0
0	0	0.045904	0.071762	0	0	0	0	0	0	0	0	0
0	0.002339	0	0	0.005858	0	0	0	0	0	0	0	0
0.005031	0.005732	0	0	0	0	0	0	0	0	0	0	0
0	0	0	0.002551	0	0.00398	0	0	0	0	0	0	0
0	0.001013	0	0	0	0	0	0.001139	0	0	0	0	0
0	1.68E-05	0	0	0	0	0	0	0	4.78E-05	0	0	0
0	0.000194	0	0	0	0	0	0	0.000452	0	0	0	0
0	0.000243	0	0	0	0	0	0	0	0	0	0	0.000188
0	8.63E-05	0	0	0	0	0	0	0	0	0	0.000129	0
0	3.34E-05	0	0	0	0	0	0	0	0	9.59E-05	0	0
0	0	0	0	0	0	0	0	0	0	0	0	0
0	1.44E-05	0	0	0	0	6.48E-06	0	0	0	0	0	0
0.999999	0	0	0	0	0	0	0	0	0	0	0	0
0	0	0	0	0	0	0	0.000001	0	0	0	0	0
0	0	0	0	0	0	2.14E-07	0	0	0	0	0	0
0	0.001074	0	0	0	0.00398	0	0	0	0	0	0	0
0	0	0	0	0	0	0	0	0	0	0	0	0
0	0	0.045904	0.071762	0	0	0	0	0	0	0	0	0
0	0	0	0.057265	0.060401	0	0	0	0	0	0	0	0
0	0.00108	0	0	0.002705	0	0	0	0	0	0	0	0

Figure 33: Mass Balance Error Checker

Section 4.2: COMSOL Modeling

In this section, we discuss our results from COMSOL modeling and the distribution graphs generated to model properties such as current density, electric potential, temperature, and velocity in our electrolysis system.

Current Density

The 3D current density graph for the COMSOL simulation can be found in Figure 34. The 2D current density graph can be found in Appendix B. In the graph the electrode, anode and the silicon wafer are a deep red color which indicates that these locations have the highest current density.

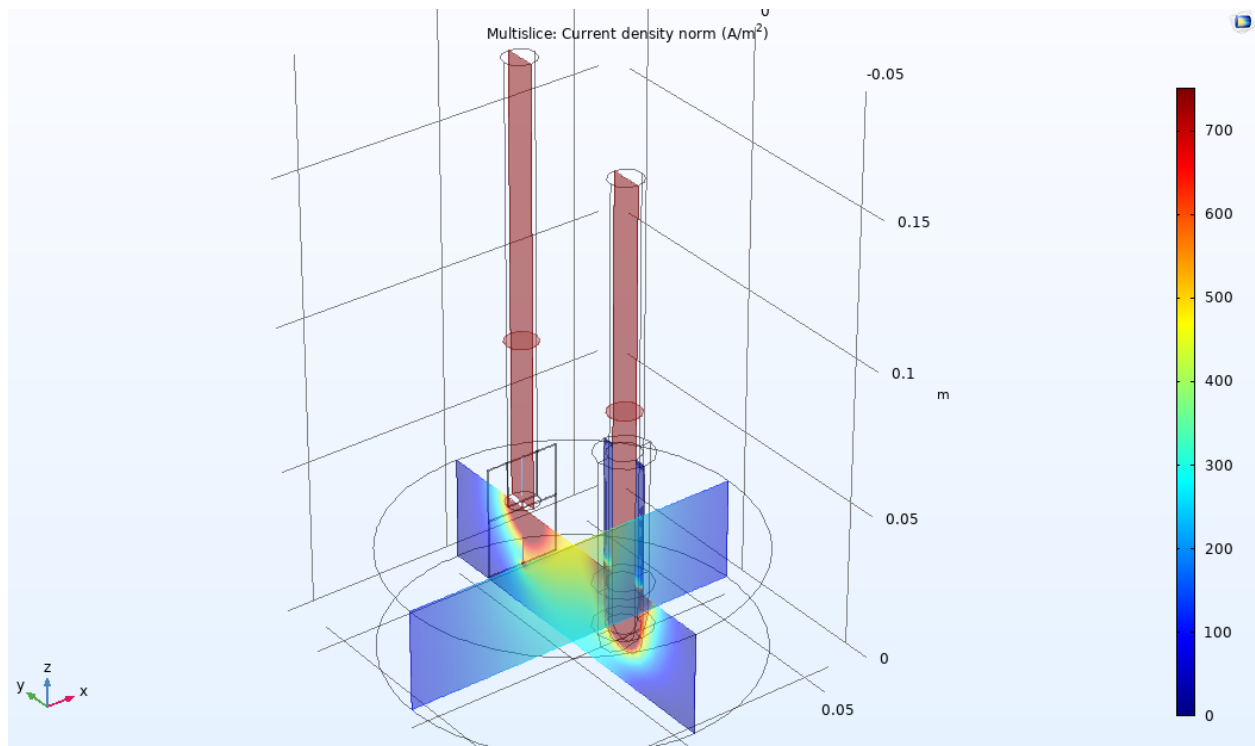


Figure 34: 3D Current Density COMSOL Graph

As indicated by the graph, the maximum current density value is 750 A/m^2 . However, the electrodes are both around $10,000 \text{ A/m}^2$ while the silicon wafer is around $80,000 \text{ A/m}^2$. The reason why the silicon wafer has such a high current density is due to the small area of the wafer relative to the size of the bath, and not high current. The same is true for both of the electrodes,

even though they have a larger area than the wafer. The current density distribution is lowest in the bath solution, as the bath has the largest area within the system. It is important to note the space between the electrodes and walls of the crucible have relatively low current density. As one moves farther away from the anode, the current density decreases as the current travels through the bath and spreads out. The current density is concentrated near and on the silicon wafer cathode. There are also higher current density spots near the top of the bath surface. This is because the current is supplied through the anode and reaches the surface of the bath first.

Electric Potential

The distribution of electric potential within the system is depicted in Figure 35. As indicated by the COMSOL graph, the maximum voltage is 1.75 V, which is supplied through the entire anode. For a 2D image of the electric potential see Appendix B.

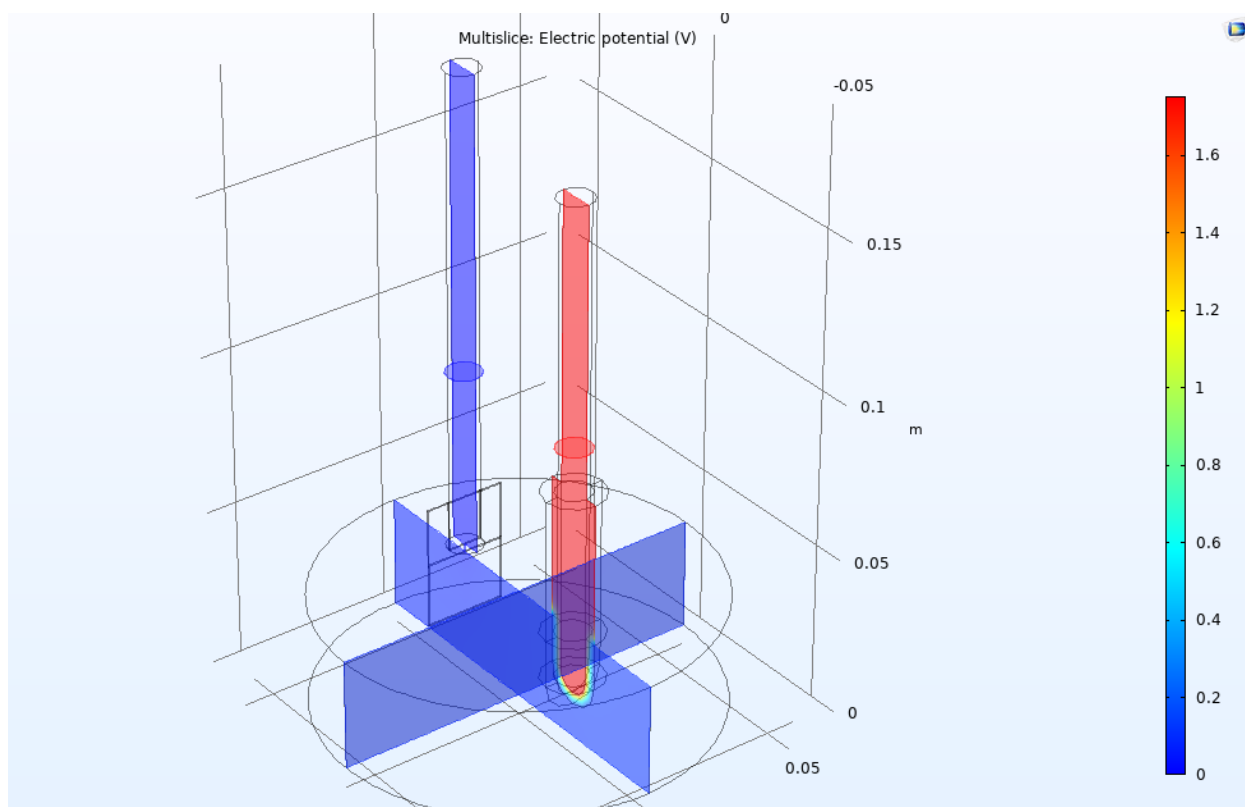


Figure 35: 3D Electric Potential COMSOL Graph

The YSZ SOM tube and graphite rod has the strongest gradient since it has the lowest conductivity in the system. The rest of the system has a much lower gradient, but it is not at zero potential. This is because the bath solution has a conductivity of 438 S/m, the steel cathode has a conductivity of 1,280,000 S/m, and the silicon wafer has a conductivity of 13,400 S/m. When comparing this to the conductivity of the YSZ SOM tube and graphite rod, which is 2 S/m, the YSZ SOM tube and graphite rod has a much lesser degree of electrical sensitivity.

Temperature

The temperature distribution of the system is depicted in Figure 36 and shows that our electrolysis system is at 1373 K. The temperature is highest (1374 K) in the areas immediately surrounding the YSZ tube within the bath.

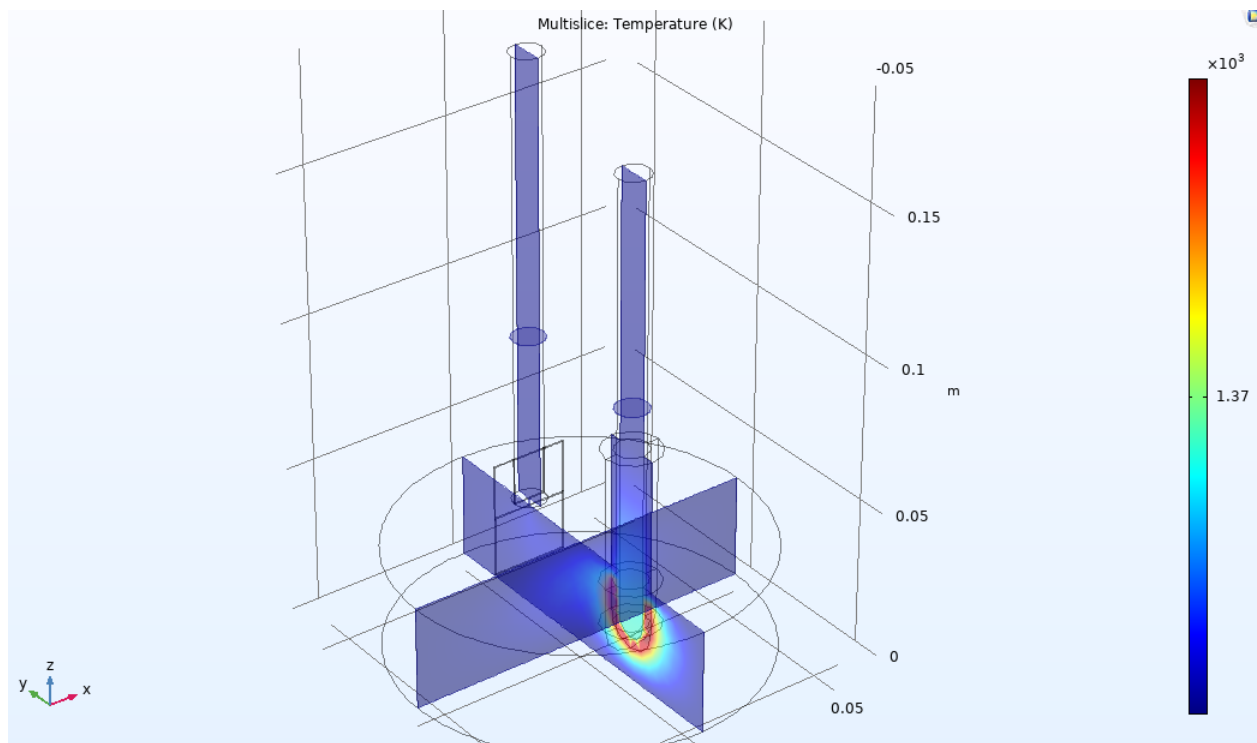


Figure 36: 3D Temperature COMSOL Graph

Here, a temperature gradient can be seen as the temperature decreases the further away from the tube. This is because the YSZ tube has a relatively high current density and low conductivity. The temperature between the cathode and anode is lower compared to areas closer

to the walls of the crucible. This is most likely due to our electrolysis system being heated inside of a furnace and insulated. Therefore the heat from the furnace reaches the walls of the crucible first, which is then transferred fastest to the bath solution near the walls. For a different view of the temperature distribution, see Figure B.5 in Appendix C for a 2D look at the system.

Velocity

The velocity graph indicates the flow rate of the bath is highest between the anode and cathode. A maximum velocity of 0.17 mm/s is met within the circular area between the two electrodes as seen in Figure 37. While Figure 37 shows the magnitude of the velocity, Figure 38 is included to show the direction of the fluid flow. Two-dimensional versions of both these figures can be found in Appendix B.

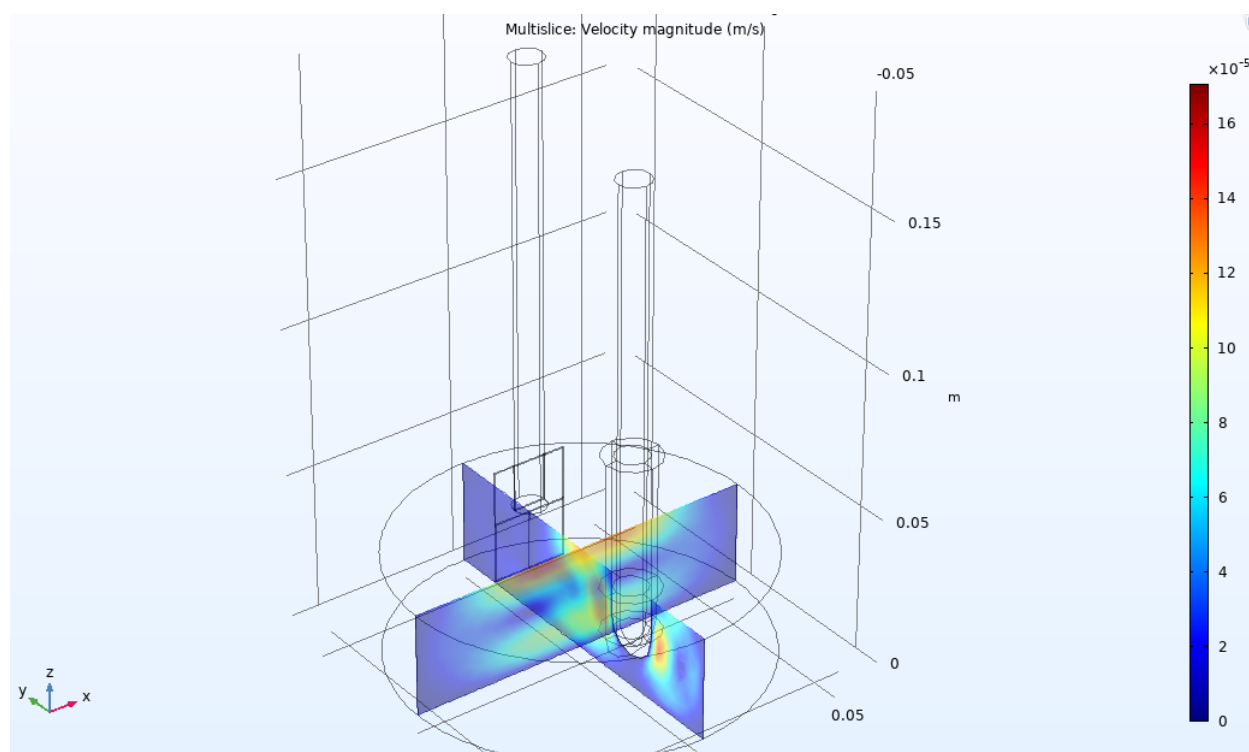


Figure 37: 3D Velocity COMSOL Graph

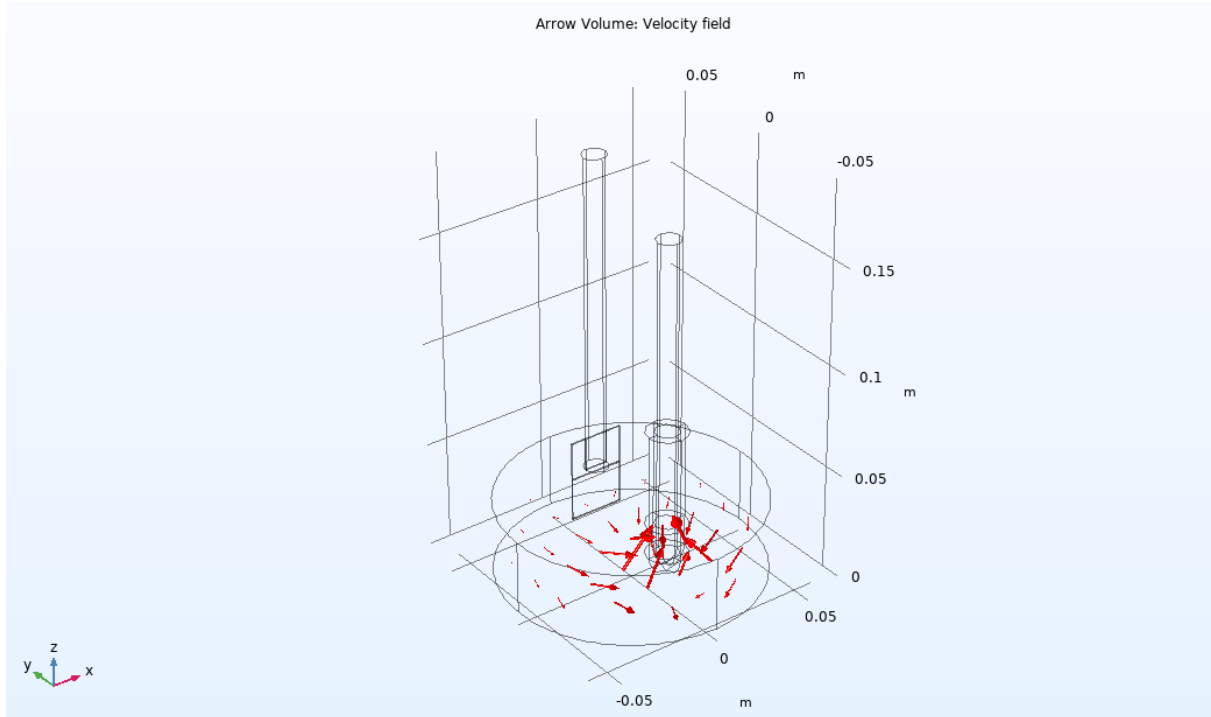


Figure 38: COMSOL graph with red arrows indicating the velocity field and direction.

As seen by the two figures, the velocity increases at the center of the bath and decreases away from the center. This is due to the slight changes in density caused by the temperature variance in the bath. However, if a stronger flow is needed, and an external magnetic field or internal current can be used to drive the velocity higher.

To determine the dominant transport mechanism, the diffusivity value of the system was calculated as well as the Peclet number. The diffusivity in our system was calculated to be $1.5 \times 10^{-8} \text{ m}^2/\text{s}$. Once we obtained the diffusivity, the Peclet number could easily be determined. Note that the Peclet number is dimensionless, and the Peclet number for our system was determined as 459. For detailed calculations of the diffusivity and Peclet number, see Appendix B. The Peclet number is a useful tool for determining the ratio between the heat transfer due to the velocity of the fluid and the heat transfer due to thermal conduction (Thermopedia, 2011). If the Peclet number is high, in which our case the Pe value is, this indicates the system has negligible diffusion outside the boundary layers and convection is dominating the system (Saldanha, 2019). This means that the temperature difference within our system is enough to drive heat transfer and a small flow rate. Furthermore, increasing the flow

rate in the electrolysis system will lead to a higher Reynold's number and thus drive the reaction faster.

Section 4.3: Electrolysis Experiments and Sample Analysis

The electrolysis experiments were led by Aditya Moudgal, a PhD student who also works with us on this research topic in the Energy Metals Research Group (Moudgal, 2019). Throughout the course of this project, a total of 9 electrolysis experiments were conducted. The results gathered from the first 6 experiments were rather inconclusive. In this section we discuss the results from these electrolysis experiments and what was learned from each.

Experiments 1-6

While running the first five electrolysis experiments, the team had been introduced to a number of unpredictable issues. When running the linear sweep voltammetry (LSV) for the first experiment, the current only read values between 0.01-0.02 A. Problems regarding a low ohmic current continued over to the next experiment. Also during this experiment the YSZ SOM tube surrounding the anode broke. Developing an efficient way to measure and record current was an ongoing difficulty and new issues involving the sealing of the furnace has caused the thinning of the cathode tube. By the time the 6th experiment was conducted, our team was finally able to mitigate most of these issues that have prevented the team from drawing any results. To avoid thermal stress and shock, the YSZ tube is positioned inside the furnace prior to electrolysis in order to keep the tube intact. To help with the results, the salt bath was baked at 350C prior to melting or electrolysis for 3 hours. While these changes helped improve the overall process, results could not be gathered as the voltage could not be measured after the first sweep.

Experiment 7

Experiment 7 showed promising results. With the integration of a new current measuring system, the experiments were able to progress. In addition to the new measuring system, the same procedural steps from experiment 6 were followed. While issues involving the detection of current still existed, silicon deposition could now be observed through analysis. Using SEM-EDS analysis shown in Figure 39 reveals potential signs of a 3-6 μm silicon deposit. Although deposition has been attained, the theoretical deposition calculated should be 108 μm .

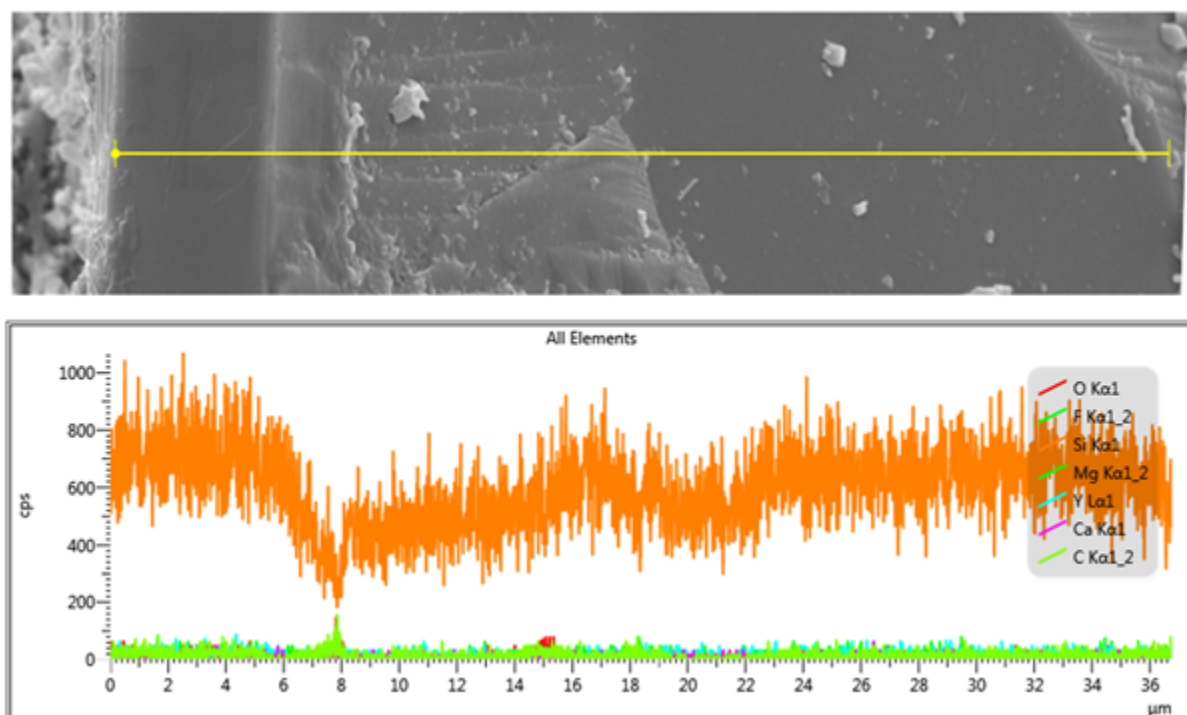


Figure 39: SEM-EDS Images From Experiment 7

The image was obtained through SEM analysis, which provides high resolution images revealing the microstructure as well as potential signs of silicon deposit on the sample. The graph on the bottom was obtained from EDS analysis, which reveals the elemental composition found on the silicon wafer. The orange shows the silicon composition found on the sample. Other elements listed in the legend existing in trace amounts are residual components from the salt bath. With the amount of deposition is not ideal, this experiment demonstrates signs of progress which has not been the case for the past experiments.

Experiment 8

Going forward, new challenges arose as the team experimented with running electrolysis at a higher voltage level. Theoretically, the higher the voltage applied, the greater the deposition occurs on the wafer. All other procedural steps remain unaltered as experiment 8 was conducted only this time for a longer duration. Analyzing the wafer post-electrolysis proved troubling. The silicon wafer itself had been thinned in arounds that were directly exposed to the electrolyte.

While greater deposition indeed occurs, the majority of deposits consist of what is believed to be silicon carbide rather than silicon. This deposit covered the surface of the wafer making it difficult to cut and section off the wafer sample. As a result, the sample is unable to position itself flat on the surface of the epoxy mold. Therefore upon polishing, only a small area was exposed making it difficult to analyze through SEM-EDS.

Experiment 9

To resolve issues like the formation of silicon carbide and the thinning of the wafer, the wafer was fully submerged into the flux during electrolysis. Electrolysis for experiment 9 was conducted in a new crucible made from stainless steel. Nevertheless the result from this experiment was inconclusive. The wafer had been embedded within the solid flux block and the team was unable to retrieve it. As a result, SEM-EDS analysis could not be done.

Chapter 5: Conclusions

The 2-D and 3-D COMSOL models we built are helpful tools for future research groups to understand the physics behind the electrolysis system. Researchers on this topic may also add and simulate additional studies in these models such as magnetohydrodynamics. Moreover, our research team has established the procedures for preparing and polishing samples for SEM and EDS analysis. While improvements have been made to the system and electrolysis procedure, more experiments need to be conducted to establish a baseline for producing solar-grade silicon via molten-salt electrolysis.

The cost model was created for its ability to be auto-updating when new inputs are used. The material balance was updated to use the latest compositions. The total capital investment equation allowed for a more accurate cost to be calculated. With this the operating and fixed cost were calculated. All these costs were then calculated for different production capacities to understand how bigger plants cost and cost per cell changes. As expected the cost per cell decreased as more cells were constructed in the plant. The operating cost also increases linearly as the production capacity increases. The silica is the raw material costing the most so maximizing the silicon purity that is produced is important. The cost model was made more user friendly to allow for future teams to quickly make changes and get new results for the cost without much work needed. This will allow for less time being spent updating the material balance and cost model, and more time being spent on experimentation.

The COMSOL results were very insightful into the physics of the electrolysis system. The temperature difference around the anode and YSZ tube caused by the low conductivity and the high current. This temperature difference causes a slight change in the density of the bath causing the bath to have a velocity. The small area of the silicon gives rise to it having a very high current density relative to the rest of the system. The silicon wafer is getting enough current to cause a reaction to get silicon deposition, however the slow velocity may be reducing the amount of silicon in the area of the wafer. With a higher velocity, there may be more silicon deposition with the increase in mixing. One way to determine if this is the case is to add a magnetic field pointing vertically in the bath to induce more movement from the bath. The results of the COMSOL model will allow for improvements in the equipment and process though changing the variable in COMSOL. This will allow for the changes to be tested without having to make drastic or expensive changes to the physical reactor.

Silicon deposition on the wafer was attained in the 7th experiment conducted. While the amount of deposition was not ideal, consistent experimentation will allow the project to progress. The team is currently focused on obtaining consistent results while troubleshooting problems that arise during the experiments. Throughout the duration of this project, several problems have appeared yet have also been sufficiently handled. Problems regarding the YSZ tube breaking, cathode thinning, furnace sealing, and more have impeded our progress but have all been resolved. While results are not obtained due to these hindrances, dealing with these issues now will allow for greater success in the next run. In this way, our contributions have played a part in the project's progression. Nevertheless, solar-grade silicon production through molten electrolysis shows promising results. To upscale this process will allow for increased production and holds the potential for replacing the Siemen's process which currently is the most common method practiced by the solar and integrated circuit industry. Molten salt electrolysis can significantly reduce the cost originally spent toward purifying silicon, thus reducing the cost of manufacturing. Such impact may even decrease the cost of solar panels, which also may entice those to consider renewable energy alternatives like solar energy.

Chapter 6: References

- Buasai, S., McMahon, A., Wu, Y. (2020, May 05). Solar Silicon Epitaxy by Molten Salt Electrolysis. Worcester Polytechnic Institute. Print.
- Buehler SumMet. "A Guide to Material Preparation and Analysis." 2007.
- Colpan, C. O., Nalbant, Y., & Ercelik, M. (2018). 4.28 Fundamentals of Fuel Cell Technologies. <https://doi.org/10.1016/B978-0-12-809597-3.00446-6>
- Corbari, L., Cambon-Bonavita, M. A., Long, G. J., Grandjean, F., Zbinden, M., Gaill, F., & Compère, P. (2008). Iron oxide deposits associated with the ectosymbiotic bacteria in the hydrothermal vent shrimp *Rimicaris exoculata*. *Biogeosciences*, 5(5), 1295-1310.
- Encyclopaedia Britannica. (2020, February 06). Electrolysis. Retrieved from <https://www.britannica.com/science/electrolysis>
- Energy-Dispersive X-ray Spectroscopy (EDS). (2020, May 6). Retrieved May 5, 2021, from <https://chem.libretexts.org/@go/page/148440>
- Espinosa, G., Rutherford, M., Wallace, L., Powell, A. "Experiment 1." 23 November, 2020.
- G. Fisher, M. R. Seacrist and R. W. Standley, "Silicon Crystal Growth and Wafer Technologies," in *Proceedings of the IEEE*, vol. 100, no. Special Centennial Issue, pp. 1454-1474, 13 May 2012, doi: 10.1109/JPROC.2012.2189786.
- Guan, X., Pal, U.B., Jiang, Y. et al. Clean Metals Production by Solid Oxide Membrane Electrolysis Process. *J. Sustain. Metall.* 2, 152–166 (2016). <https://doi.org/10.1007/s40831-016-0044-x>
- Hasannezhad, Hossein, and Amirhossein Meysami. "Effects of Porosity and Electrical Resistance of Metallurgical Coke and Semicoke on Silicon Recovery in an Electric Arc Furnace." *JOM* 71.1 (2019): 336-341.

- I. M. Kirpichnikova and V. Shestakova, "Problems of Using Solar Photovoltaic Panels and Ways to Increase their Efficiency," *2020 International Conference on Industrial Engineering, Applications and Manufacturing (ICIEAM)*, Sochi, Russia, 2020, pp. 1-7,
- Laubach, Tracy. "How Solar Works." *Pinterest*, Solarcraft, 2018,
www.pinterest.com/pin/383298618268842055/.
- Moudgal, A., Powell, A. "Heat Up and Characterize Furnace." 25 September, 2019.
- Müller, G., and J. Friedrich. "Crystal Growth, Bulk: Method." *Encyclopedia of Condensed Matter Physics*. By Franco Bassani. Amsterdam: Elsevier/Acad., 2005. Print.
- NanoScience. (2020, August 19). Scanning electron microscopy. Retrieved May 06, 2021, from
<https://www.nanoscience.com/techniques/scanning-electron-microscopy/>
- Ngo, P. D. (1999). Energy dispersive spectroscopy. In *Failure Analysis of Integrated Circuits* (pp. 205-215). Springer, Boston, MA.
- OpenEI. (2010, July 13). Electrolysis. Retrieved from <https://openei.org/wiki/Electrolysis>
- Pal, U., (2019). *Method and Apparatus for Producing Solar Grade Silicon Using a SOM Electrolysis Process*. US 10,266,951 B2. Retrieved from
<https://patentimages.storage.googleapis.com/cd/07/46/bc5d5c7846b403/US10266951.pdf>
- Ramos, A et al. "Deposition Reactors for Solar Grade Silicon: A Comparative Thermal Analysis of a Siemens Reactor and a Fluidized Bed Reactor." *Journal of crystal growth* 431.C (2015): 1–9. Web.
- Richardson, L. (2020, September 25). How Do Solar Panels Work? Step by Step Guide: EnergySage.
- Residential and Commercial ITC Factsheets*, Energy Department, Office of Energy Efficiency & Renewable Energy, January 2020.

"SILICON INGOT PRODUCTION PROCESS FOR WAFERS." *Basics of Microstructuring*. MicroChemicals. Web. 6 May 2021.

Saldanha, N. (2019, January 21). Péclet number. Retrieved from [https://openwetware.org/wiki/P%C3%A9clet_number_\(Pe\)_-_Nishanth_Saldanha#:~:text=In%20diffusion%20dominated%20regimes%2C%20the,number%20is%20greater%20than%20one.](https://openwetware.org/wiki/P%C3%A9clet_number_(Pe)_-_Nishanth_Saldanha#:~:text=In%20diffusion%20dominated%20regimes%2C%20the,number%20is%20greater%20than%20one.)

Sokolich, Mark. "Silicon Purification from Silicon Dioxide." *Quora*, 2019, qph.fs.quoracdn.net/main-qimg-a766c122edf8675ee2f7d2519a3c8592

"Solar Industry Research Data." SEIA, 2020, <https://www.seia.org/solar-industry-research-data>

Stinn, C., & Allanore, A. (2020, June 01). Iopscience. Retrieved from <https://iopscience.iop.org/article/10.1149/2.F06202IF/meta>

Thermopedia. (2011, February 4). PECLLET number. Retrieved from <https://www.thermopedia.com/content/1014/>

Appendix A: Techno-Economic Cost Model

Note, the excel sheet we developed using a spreadsheet created with built-in functions from the ARPA-E-METALS programs is submitted along with our report. We hope this file will be helpful for future students/researchers working on these problems.

Production Capacity (Tonne per year)	Production Capacity (kt per year)	C Per Plant (calculated from equation)	USD/tonne	USD/cell	Q (Installed power capacity per Rectifier line, MW)	p (Total installed production rate, kg/s)	# of cells	# of Rectifiers (N)
3416	3	\$6,015,941	\$17,567	\$32,000.69	5.055	0.108333333	5	1
17082	17	\$30,276,710	\$14,066	\$9,611.069	25.275	0.541666667	25	1
46463	46	\$572,286,459	\$12,317	\$8,415.977	68.748	1.473333333	68	1
66961	67	\$786,557,911	\$11,746	\$8,026.101	99.078	2.123333333	98	1
102492	102	\$1,140,036,382	\$11,123	\$7,600.243	151.65	3.25	150	1
159888	160	\$1,681,418,285	\$10,516	\$7,185.548	236.574	5.07	234	1
288344	288	\$2,818,674,565	\$9,775	\$6,679.324	426.642	9.143333333	422	1
457798	458	\$4,230,648,560	\$9,241	\$6,314.401	677.37	14.516666667	670	1
532958	533	\$4,836,087,098	\$9,074	\$6,200.112	788.58	16.9	780	1
625201	625	\$5,565,852,817	\$8,903	\$6,083.009	925.065	19.825	915	1
819936	820	\$7,088,842,113	\$8,621	\$5,890.702	1213.2	26	1200	1
901930	902	\$7,689,030,341	\$8,525	\$5,825.023	1334.52	28.6	1320	1
159888	160	\$1,709,603,764	\$11,068	\$7,562.409	236.574	5.07	234	2
288344	288	\$2,927,709,915	\$10,327	\$7,056.185	426.642	9.143333333	422	2
457798	458	\$4,483,145,443	\$9,793	\$6,691.262	677.37	14.516666667	670	2
532958	533	\$5,130,038,693	\$9,626	\$6,576.973	788.58	16.9	780	2
625201	625	\$5,910,780,650	\$9,454	\$6,459.870	925.065	19.825	915	2
819936	820	\$7,521,075,337	\$9,173	\$6,267.563	1213.2	26	1200	2

Figure A.1: Production Capacity & Cost of Plant Chart

		from interview										from cost model																
		Production Capacity (tonnes/year)										Production Capacity (tonnes/year)																
For \$I		160000	5416	17082	46463	66961	102492	159888	288344	457798	532958	625201	819936	901930														
Installed Costs (ISBL) per capacity		\$ 807,042,843	\$ 28,345,715	\$ 113,483,618	\$ 270,293,105	\$ 371,494,340	\$ 538,443,587	\$ 794,140,351	\$ 1,331,270,884	\$ 1,998,151,656	\$ 2,284,102,616	\$ 2,628,821,014	\$ 3,338,641,434	\$ 3,631,558,729														
Auxiliaries	35.4% of ISBL	\$ 285,620,101	\$ 10,031,817	\$ 40,162,927	\$ 95,659,288	\$ 131,475,363	\$ 190,560,282	\$ 281,053,787	\$ 471,149,366	\$ 707,164,784	\$ 808,365,535	\$ 930,364,639	\$ 1,181,576,804	\$ 1,285,243,007														
Buildings	21.4% of ISBL	\$ 172,700,532	\$ 6,065,750	\$ 24,284,561	\$ 57,840,502	\$ 79,496,734	\$ 115,222,500	\$ 169,939,505	\$ 284,881,022	\$ 427,588,023	\$ 488,779,177	\$ 562,546,080	\$ 714,441,812	\$ 777,123,705														
Site development	5.3% of ISBL	\$ 43,175,132	\$ 1,516,437	\$ 6,071,140	\$ 14,460,125	\$ 19,874,183	\$ 28,805,624	\$ 42,484,875	\$ 71,220,253	\$ 106,897,002	\$ 122,194,790	\$ 140,638,515	\$ 178,610,447	\$ 194,290,920														
Land	2.5% of ISBL	\$ 19,926,878	\$ 699,894	\$ 2,802,064	\$ 6,673,902	\$ 9,172,897	\$ 13,294,900	\$ 19,608,898	\$ 32,870,877	\$ 49,337,064	\$ 56,897,579	\$ 64,909,142	\$ 82,435,567	\$ 89,688,091														
Spare parts	0.5% of ISBL	\$ 4,035,214	\$ 141,729	\$ 567,418	\$ 1,351,466	\$ 1,857,472	\$ 2,692,218	\$ 3,970,702	\$ 6,656,354	\$ 9,990,758	\$ 11,420,513	\$ 13,144,105	\$ 16,693,207	\$ 18,157,794														
Fixed Capital Investment (FCI) per capacity		\$ 1,332,500,610	\$ 46,801,341	\$ 187,371,728	\$ 446,278,388	\$ 613,370,788	\$ 889,019,109	\$ 1,311,197,617	\$ 2,198,048,757	\$ 3,299,129,286	\$ 3,771,260,210	\$ 4,340,421,495	\$ 5,512,399,271	\$ 5,996,032,245														
Working Capital	19.2% of FCI	\$ 256,310,616	\$ 9,002,382	\$ 36,041,527	\$ 85,843,017	\$ 117,983,752	\$ 171,005,552	\$ 252,212,883	\$ 422,801,420	\$ 634,597,637	\$ 725,413,469	\$ 834,893,388	\$ 1,060,326,908	\$ 1,153,355,193														
Start-up Costs	9.0% of FCI	\$ 119,925,072	\$ 4,212,121	\$ 16,863,456	\$ 40,165,055	\$ 55,203,371	\$ 80,011,720	\$ 118,007,785	\$ 197,824,388	\$ 296,921,636	\$ 339,413,419	\$ 390,637,935	\$ 496,115,934	\$ 539,642,902														
Total Capital Investment (TCI) per capacity		\$ 1,708,736,488	\$ 60,015,843	\$ 240,276,710	\$ 572,286,459	\$ 786,557,911	\$ 1,140,058,382	\$ 1,681,418,285	\$ 2,818,674,565	\$ 4,230,648,560	\$ 4,836,087,098	\$ 5,565,957,817	\$ 7,088,842,113	\$ 7,689,030,341														

Figure A.2: Fixed Cost Calculation Chart

Capacity (tonne/year)		3416	17082	46463	66961	102492	159888	288344	457798	532958	625201	819936	901930
FCI based on the yearly capacity		\$ 46,801,341	\$ 187,371,728	\$ 446,278,388	\$ 613,370,788	\$ 889,019,109	\$ 1,311,197,617	\$ 2,198,048,757	\$ 3,299,129,286	\$ 3,771,260,210	\$ 4,340,421,495	\$ 5,512,399,271	\$ 5,996,032,245
Fixed Costs		\$ 6,469,595	\$ 27,917,654	\$ 69,915,612	\$ 97,930,198	\$ 145,160,857	\$ 219,262,078	\$ 379,595,334	\$ 584,562,000	\$ 673,930,734	\$ 782,634,693	\$ 1,009,310,260	\$ 1,103,818,626
Maintenance	7.5% of FCI	\$ 3,510,101	\$ 14,052,880	\$ 33,470,879	\$ 46,002,809	\$ 66,676,433	\$ 98,339,821	\$ 164,853,657	\$ 247,434,696	\$ 282,844,516	\$ 325,531,612	\$ 413,429,945	\$ 449,702,418
Operating Labor (OL)		\$ 1,056,641	\$ 5,283,206	\$ 14,370,321	\$ 20,710,169	\$ 31,699,238	\$ 49,450,812	\$ 89,180,524	\$ 141,589,931	\$ 164,836,039	\$ 193,365,353	\$ 253,593,906	\$ 278,953,296
Laboratory Costs	21.5% of OL	\$ 227,178	\$ 1,135,809	\$ 3,089,619	\$ 4,452,686	\$ 6,815,336	\$ 10,631,924	\$ 19,173,813	\$ 30,441,835	\$ 35,439,748	\$ 41,573,551	\$ 54,522,690	\$ 59,794,959
Supervision	20.0% of OL	\$ 211,328	\$ 1,056,641	\$ 2,874,064	\$ 4,142,034	\$ 6,339,848	\$ 9,890,162	\$ 17,836,105	\$ 28,317,886	\$ 32,967,208	\$ 38,673,071	\$ 50,718,781	\$ 55,790,659
Plant Overheads	50.0% of OL	\$ 528,321	\$ 2,641,603	\$ 7,185,161	\$ 10,355,084	\$ 15,849,619	\$ 24,725,406	\$ 44,590,262	\$ 70,794,965	\$ 82,418,019	\$ 96,682,677	\$ 126,796,953	\$ 139,476,648
Insurance	1.0% of FCI	\$ 468,013	\$ 1,873,717	\$ 4,462,784	\$ 6,133,708	\$ 8,890,191	\$ 13,111,976	\$ 21,980,488	\$ 32,991,293	\$ 37,712,602	\$ 43,404,215	\$ 55,123,993	\$ 59,960,322
Royalties	1.0% of FCI	\$ 468,013	\$ 1,873,717	\$ 4,462,784	\$ 6,133,708	\$ 8,890,191	\$ 13,111,976	\$ 21,980,488	\$ 32,991,293	\$ 37,712,602	\$ 43,404,215	\$ 55,123,993	\$ 59,960,322
Variable Costs		\$ 3,675,328	\$ 18,376,619	\$ 49,984,395	\$ 72,036,320	\$ 110,259,690	\$ 172,005,120	\$ 310,197,236	\$ 492,493,257	\$ 573,350,355	\$ 672,584,083	\$ 882,077,480	\$ 970,285,201
Raw Materials (RM)		\$ 1,755,120	\$ 8,775,580	\$ 23,869,570	\$ 34,400,250	\$ 52,653,460	\$ 82,139,400	\$ 148,131,710	\$ 235,185,430	\$ 273,797,960	\$ 321,186,080	\$ 423,227,640	\$ 463,350,380
Raw Silica In		\$ 1,104,050	\$ 5,520,230	\$ 15,015,020	\$ 21,639,300	\$ 33,121,380	\$ 51,669,350	\$ 93,181,470	\$ 147,942,150	\$ 172,231,160	\$ 202,040,400	\$ 264,971,010	\$ 291,468,110
Bath In (MgF2)		\$ 401,990	\$ 2,009,970	\$ 5,467,120	\$ 7,879,080	\$ 12,059,800	\$ 18,613,320	\$ 33,526,250	\$ 53,867,190	\$ 62,711,000	\$ 73,964,900	\$ 96,478,560	\$ 106,126,410
Bath In (CaF2)		\$ 160,800	\$ 803,990	\$ 2,186,850	\$ 3,151,630	\$ 4,823,930	\$ 7,525,330	\$ 13,571,320	\$ 21,546,880	\$ 25,084,420	\$ 29,425,960	\$ 38,591,420	\$ 42,450,560
Bath (YF3)		\$ -	\$ -	\$ -	\$ -	\$ -	\$ -	\$ -	\$ -	\$ -	\$ -	\$ -	\$ -
Bath (CaO)		\$ 1,940	\$ 9,700	\$ 26,380	\$ 38,010	\$ 58,180	\$ 90,770	\$ 163,690	\$ 259,890	\$ 302,560	\$ 354,930	\$ 465,480	\$ 512,020
Bath In (Y2O3)		\$ 86,340	\$ 431,690	\$ 1,174,200	\$ 1,692,230	\$ 2,590,150	\$ 4,040,630	\$ 7,286,940	\$ 11,569,320	\$ 13,468,760	\$ 15,799,890	\$ 20,721,170	\$ 22,793,280
Miscellaneous Materials	10.0% of RM	\$ 175,512.0	\$ 877,558.0	\$ 2,386,957.0	\$ 3,440,025.0	\$ 5,265,346.0	\$ 8,213,940.0	\$ 14,813,171.0	\$ 23,518,543.0	\$ 27,379,796.0	\$ 32,118,608.0	\$ 42,122,764.0	\$ 46,335,038.0
Utilities (everything)		\$ 1,744,696.15	\$ 8,723,480.74	\$ 23,727,867.62	\$ 34,196,044.52	\$ 52,340,884.47	\$ 81,651,779.77	\$ 147,252,354.96	\$ 233,789,283.94	\$ 272,172,599.22	\$ 319,279,395.24	\$ 418,727,075.72	\$ 460,599,783.29
Indirect Costs	25.0% of Costs	\$ 2,536,231	\$ 11,573,568	\$ 29,975,002	\$ 42,491,629	\$ 63,855,137	\$ 97,616,799	\$ 172,448,143	\$ 269,263,814	\$ 311,820,272	\$ 363,804,694	\$ 472,846,935	\$ 518,525,957
Annual Operating Costs		\$ 12,681,154	\$ 57,867,841	\$ 148,875,009	\$ 212,458,147	\$ 319,776,694	\$ 489,083,997	\$ 862,240,713	\$ 1,346,319,071	\$ 1,559,101,362	\$ 1,819,023,471	\$ 2,364,234,675	\$ 2,592,829,784

Figure A.3: Operating Cost Calculation Chart

PROCESS STREAMS						
Enter process streams only on this sheet. (Do not enter utilities such as cooling water, compressed gas, etc.)						
Inputs and outputs must be at 25C and 1bar. Include compressors on the 'Equipment' sheet if gas feeds must be pressurized.						
Silicon	Primary product					
8	Primary product Stream #					
1.00	[kg/hr] Rate of production (@ full capacity)					
18,264.84	[kg/hr] Targeted Production (@ full capacity)					
18,263.84	[kg/hr] Departure from Target					
						Guide
21						
Stream Summary at 100% Plant Capacity						
Stream #	Description	Phase	Input/Output [select]	Mass Flow [kg/hr]	Sum of stream's mass fractions	
1	Silica Raw Material	solid	in	2.154	1	
5	Bath In	liquid	in	0.244	1	
6	Vented Oxygen	gas	out	1.139	1	
8	Silicon Product	solid	out	1.000	1	
9	Bath Out	liquid	out	0.259	1	

Figure A.4: Stream Summary

FINAL	kg/hr														Mass Fraction													
Streams + Substreams	Si	Al	B	O	Mg	Ca	F	Y	Fe	Zr	Na	Ti	P	Total	Si	Al	B	O	Mg	Ca	F	Y	Fe	Zr	Na	Ti	P	Total
1 Raw Silica In	1.0050	0.0011	0.0000	1.9653	0.0004	0.0000	0.0000	0.0000	0.0000	0.0000	0.0000	0.0001	0.0001	2.54	0.4665	0.0005	0.0000	0.7723	0.0002	0.0000	0.0000	0.0000	0.0000	0.0000	0.0000	0.0000	1.0000	
5 Bath In				1.133	0.0453	0.0631	0.0000	0.0000	0.0000	0.0000	0.0000	0.0000	0.0000	0.0000	0.0442	0.0254	0.0000	0.9442	0.1800	0.2568	0.5351	0.0174	0.0002	0.0002	0.0004	0.0000	1.0000	
6 Vented O2	0.0050	0.0000	0.0000	0.0000	0.0000	0.0000	0.0000	0.0000	0.0000	0.0000	0.0000	0.0000	0.0000	0.0000	0.0050	0.0000	0.0000	0.0000	0.0000	0.0000	0.0000	0.0000	0.0000	0.0000	0.0000	0.0000	1.0000	
8 Silicon Product	1.0000	0.0000	0.0000	0.0000	0.0000	0.0000	0.0000	0.0000	0.0000	0.0000	0.0000	0.0000	0.0000	1.0000	0.999998	0.000001	0.000000	0.000000	0.000000	0.000000	0.000000	0.000000	0.000000	0.000000	0.000000	0.000000	1.0000	
Check Bal	0.000000	0.000000	0.000000	0.000000	0.000000	0.000000	0.000000	0.000000	0.000000	0.000000	0.000000	0.000000	0.000000	0.00													0.00	

Figure A-5: Stream Composition in Kg/hr Calculations

FINAL	kg/hr														Mass Fraction													
Combined Streams	Si	Al	B	O	Mg	Ca	F	Y	Fe	Zr	Na	Ti	P	Total	Si	Al	B	O	Mg	Ca	F	Y	Fe	Zr	Na	Ti	P	Total
1 Raw Silica In	1.0050	0.0011	0.0000	1.9653	0.0004	0.0000	0.0000	0.0000	0.0000	0.0000	0.0000	0.0001	0.0001	2.54	0.465500	0.000529	0.000000	0.772298	0.000214	0.000000	0.000000	0.000000	0.000000	0.000000	0.000000	0.000000	0.000000	1.0000
5 Bath In				1.133	0.0453	0.0631	0.0000	0.0000	0.0000	0.0000	0.0000	0.0000	0.0000	0.0000	0.044221	0.025400	0.000000	0.944221	0.180000	0.256800	0.535100	0.017400	0.000200	0.000200	0.000400	0.000000	1.0000	
6 Vented O2	0.0050	0.0000	0.0000	0.0000	0.0000	0.0000	0.0000	0.0000	0.0000	0.0000	0.0000	0.0000	0.0000	0.0000	0.005000	0.000000	0.000000	0.000000	0.000000	0.000000	0.000000	0.000000	0.000000	0.000000	0.000000	0.000000	1.0000	
8 Silicon Product	1.0000	0.0000	0.0000	0.0000	0.0000	0.0000	0.0000	0.0000	0.0000	0.0000	0.0000	0.0000	0.0000	1.0000	0.999947	0.000053	0.000000	0.000000	0.000000	0.000000	0.000000	0.000000	0.000000	0.000000	0.000000	0.000000	1.0000	
Check Bal	0.000000	0.000000	0.000000	0.000000	0.000000	0.000000	0.000000	0.000000	0.000000	0.000000	0.000000	0.000000	0.000000	0.00													0.00	

Figure A-6: Combined Stream Compositions in Kg/hr Calculations

COMPOSITION OF EACH PROCESS STREAM										Stream		Species		Specific						
line#	Stream #	Phase	Species Name	Mass Percent [wt/wt]	ENTER Molecular Formula (one species per line)										Flow [kg/hr]	Flow [kg/hr]	value [\$/kg]	flow (absolute) [\$/h]		
					1	2	3	4	5	6	7	8	9	10	Formula	MW				
1	1	solid	Silica	99.8%	Si	1	O	2							SiO2	60.0843	2.1544	2.15009522	0.15	0.32
2	1	solid	Aluminum Oxide	0.1%	Al	2	O	3							Al2O3	101.961	2.1544	0.002154404	#N/A	#N/A
3	1	solid	Iron Oxide	0.03%	Fe	2	O	3							Fe2O3	159.688	2.1544	0.000646321	#N/A	#N/A
4	1	solid	Calcium Oxide	0.03%	Ca	1	O	1							CaO	56.0774	2.1544	0.000646321	0.15	0.00
5	1	solid	Phosphorus Pentaoxide	0.02%	P	2	O	5							P2O5	141.945	2.1544	0.000430881	#N/A	#N/A
6	1	solid	Titanium Dioxide	0.01%	Ti	1	O	2							TiO2	79.8748	2.1544	0.00021544	#N/A	#N/A
7	1	solid	Sodium Oxide	0.006%	Na	2	O	1							Na2O	61.9788	2.1544	0.000219264	#N/A	#N/A
8	1	solid	Zirconium Dioxide	0.003%	Zr	1	O	2							ZrO2	123.223	2.1544	6.46321E-05	#N/A	#N/A
9	1	solid	Boron Oxide	0.001%	B	2	O	3							B2O3	69.6202	2.1544	2.1544E-05	#N/A	#N/A
10	6	gas	Dioxygen	100%	O	2									O2	31.9988	1.139	1.139335226	#N/A	#N/A
11	9	liquid	Calcium Fluoride	45.389%	Ca	1	F	2							CaF2	78.0748	0.25924	0.11766596	0.40	0.05
12	9	liquid	Magnesium Fluoride	45.389%	Mg	1	F	2							MgF2	62.3018	0.25924	0.11766596	1.00	0.12
13	9	liquid	Calcium Oxide	1.709%	Ca	1	O	1							CaO	56.0774	0.25924	0.00443097	0.15	0.00
14	9	liquid	Silicon Dioxide	4.152%	Si	1	O	2							SiO2	60.0843	0.25924	0.010762573	0.15	0.00
15	9	liquid	Yttrium Fluoride	1.95%	Y	1	F	3							YF3	145.901	0.25924	0.00505	1,000.00	5.05
16	9	liquid	Aluminum Oxide	0.830%	Al	2	O	3							Al2O3	101.961	0.25924	0.002152515	#N/A	#N/A
17	9	liquid	Zirconium Dioxide	0.02493%	Zr	1	O	2							ZrO2	123.223	0.25924	6.46321E-05	#N/A	#N/A
18	9	liquid	Iron Oxide	0.24931%	Fe	2	O	3							Fe2O3	159.688	0.25924	0.000646321	#N/A	#N/A
19	9	liquid	Phosphorus Pentaoxide	0.16621%	P	2	O	5							P2O5	141.945	0.25924	0.000430881	#N/A	#N/A
20	9	liquid	Titanium Dioxide	0.08310%	Ti	1	O	2							TiO2	79.8748	0.25924	0.00021544	#N/A	#N/A
21	9	liquid	Sodium Oxide	0.04986%	Na	2	O	1							Na2O	61.9788	0.25924	0.000219264	#N/A	#N/A
22	9	liquid	Yttrium Oxide	0.0000%	Y	2	O	3							Y2O3	225.81	0.25924	0	5.00	-
23	9	liquid	Boron Oxide	0.00804%	B	2	O	3							B2O3	69.6202	0.25924	2.0855E-05	#N/A	#N/A
24	8	solid	Silicon	99.999%	Si	1									Si	28.0855	1	0.999998786	#N/A	#N/A
25	8	solid	Aluminum	0.00010%	Al	1									Al	26.9815	1	0.000001	#N/A	#N/A
26	8	solid	Boron	0.00002%	B	1									B	10.811	1	0.000000214	#N/A	#N/A
27	5	liquid	Yttrium Oxide	0.000%	Y	2	O	3							Y2O3	225.81	0.24417	0	5.00	-
28	5	liquid	Yttrium Fluoride	2.07%	Y	1	F	3							YF3	145.901	0.24417	0.00505	1,000.00	5.05
29	5	liquid	Magnesium Fluoride	48.19%	Mg	1	F	2							MgF2	62.3018	0.24417	0.11766596	1.00	0.12
30	5	liquid	Calcium Fluoride	48.19%	Ca	1	F	2							CaF2	78.0748	0.24417	0.11766596	0.40	0.05
31	5	liquid	Calcium Oxide	1.55%	Ca	1	O	1							CaO	56.0774	0.24417	0.003784649	0.15	0.00

Figure A-7: Composition of Process Stream Breakdown

Appendix B: COMSOL Simulation Results

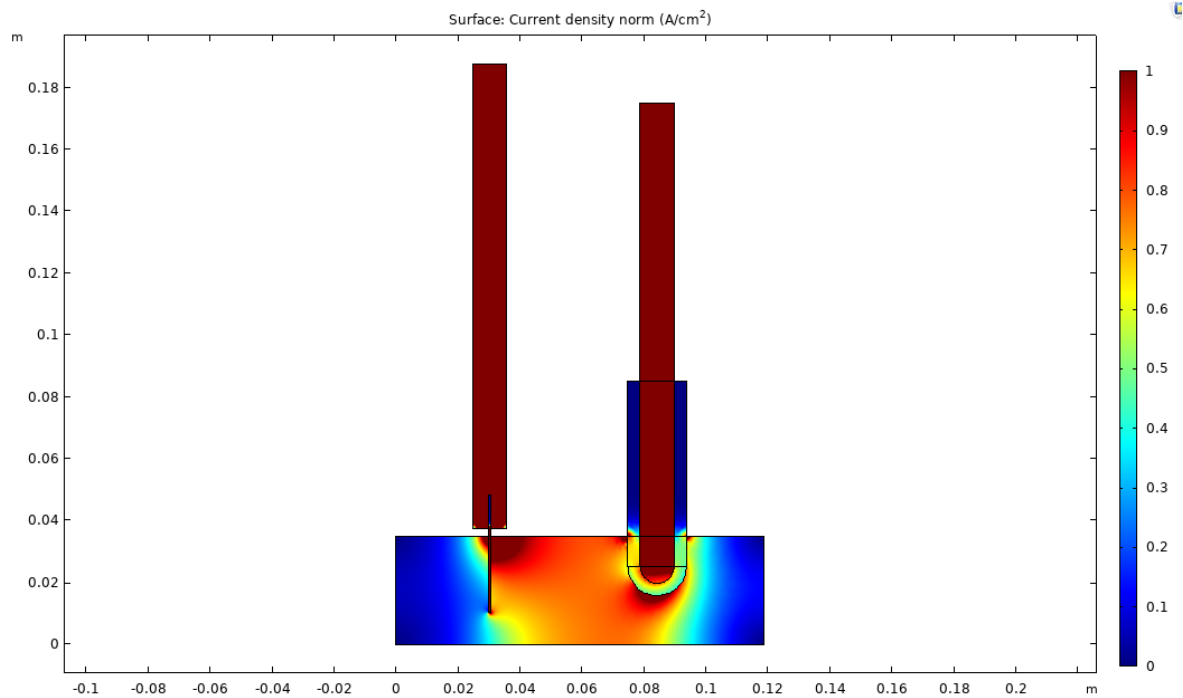


Figure B.1: 2D Current Density COMSOL Graph

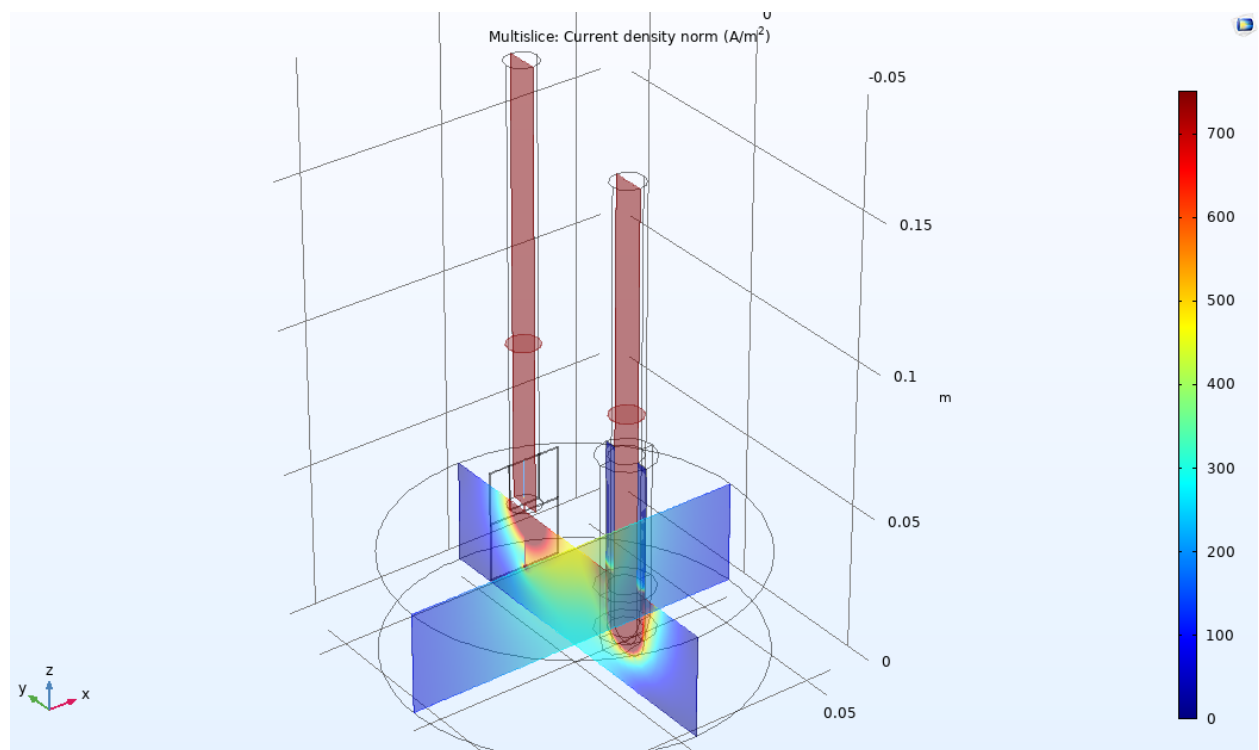


Figure B.2: 3D Current Density COMSOL Graph

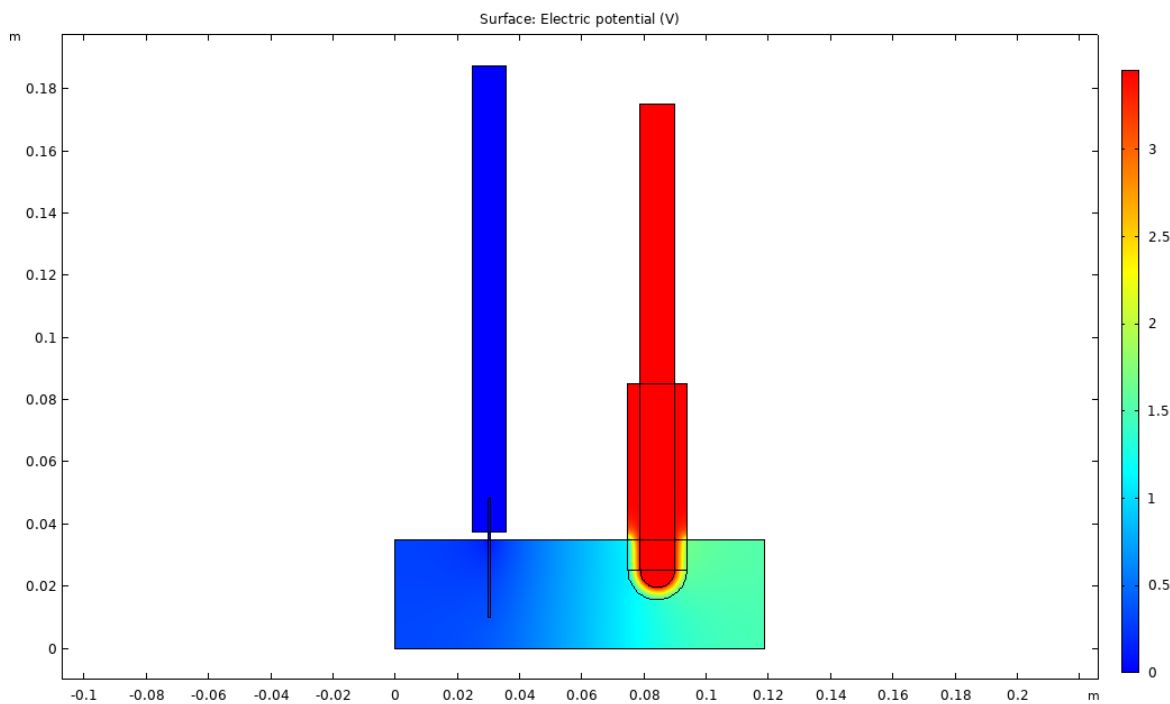


Figure B.3: 2D Electric Potential COMSOL Graph

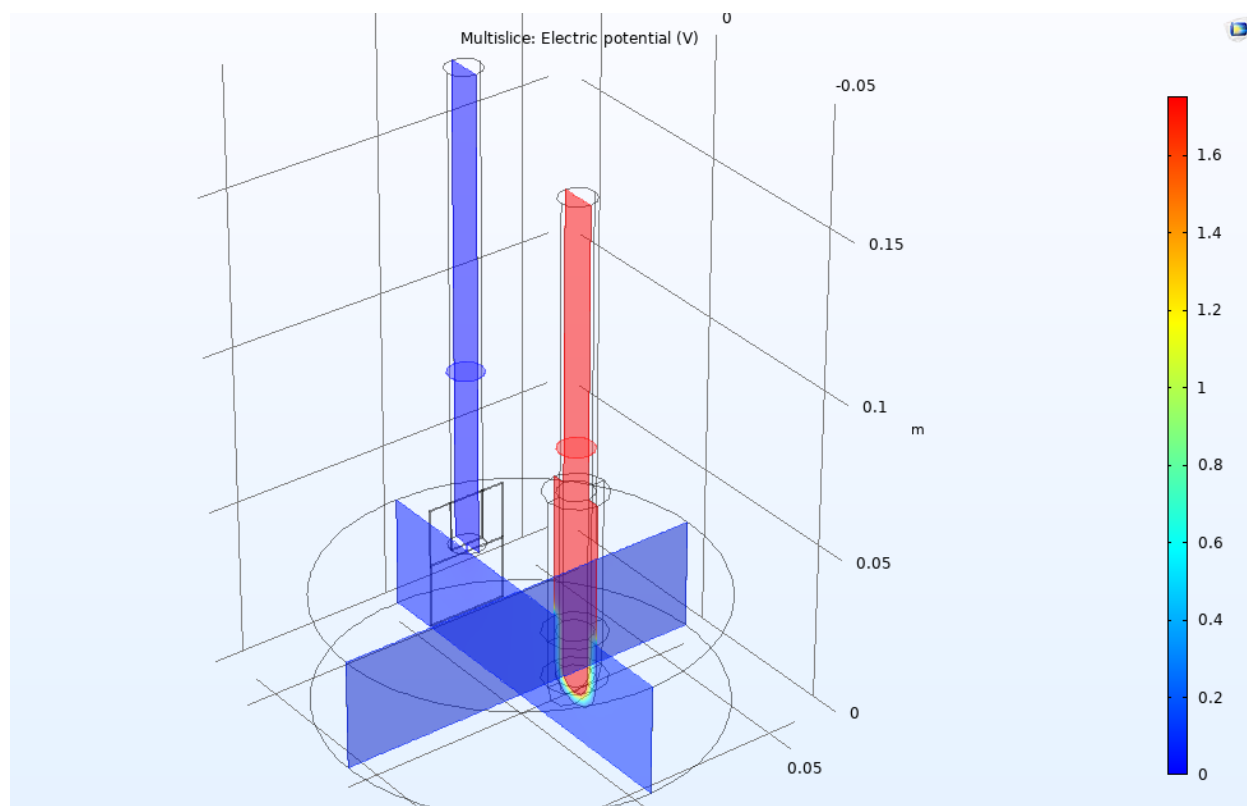


Figure B.4: 3D Electric Potential COMSOL Graph

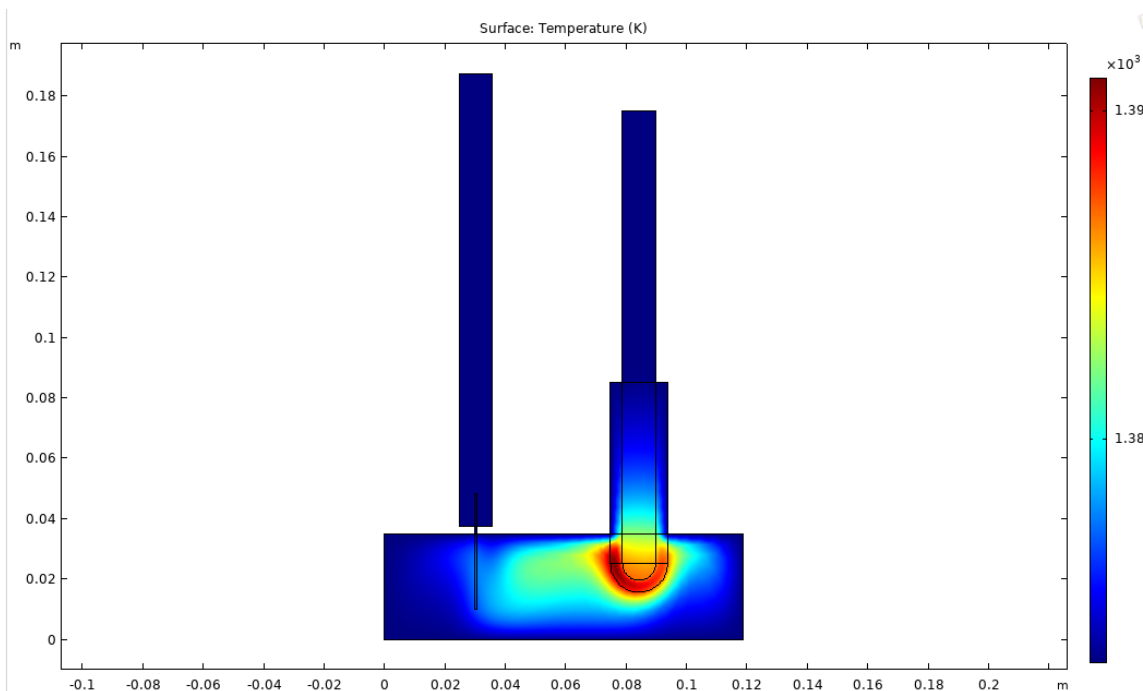


Figure B.5: 2D Temperature COMSOL Graph

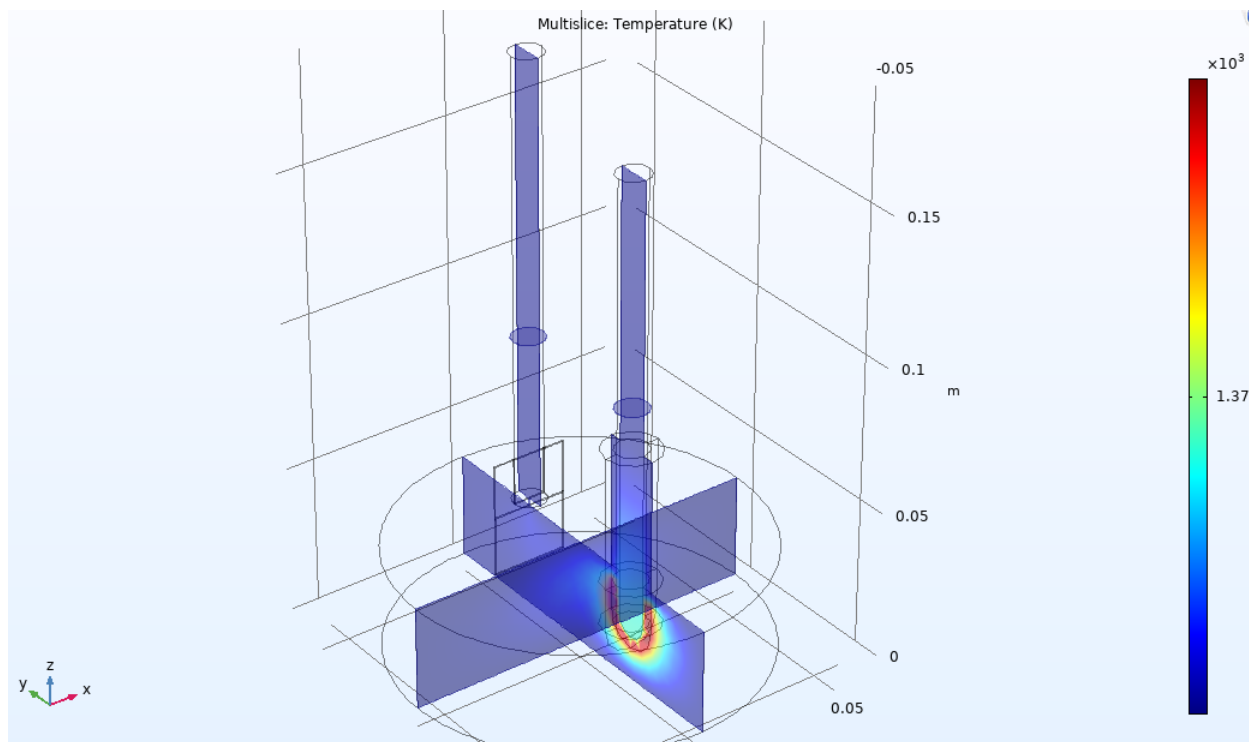


Figure B.6: 3D Temperature Graph COMSOL Graph

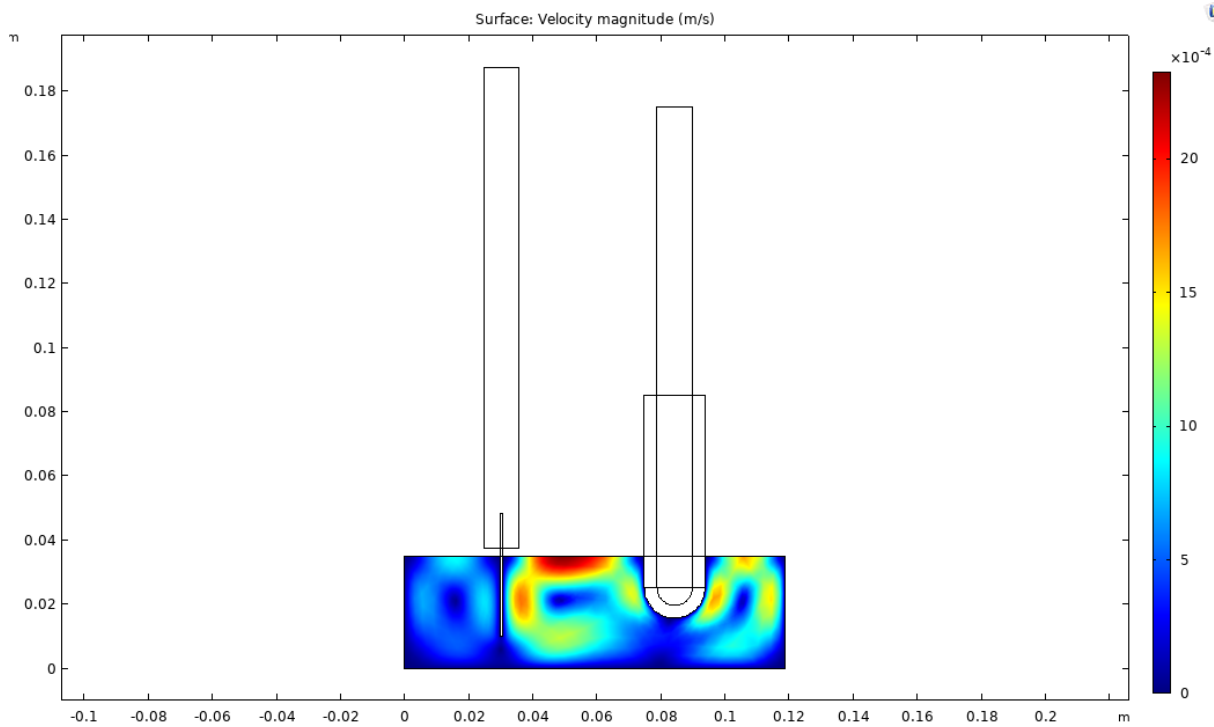


Figure B.7: 2D Velocity COMSOL Graph

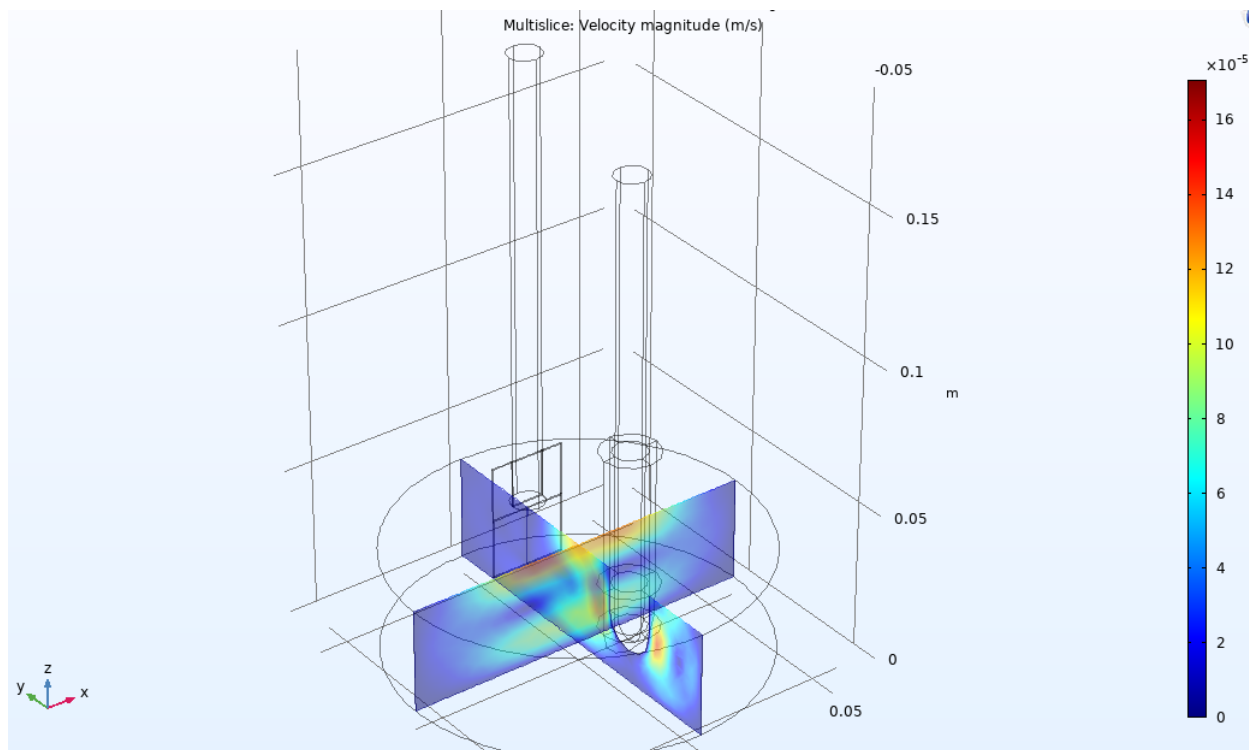


Figure B.8: 3D Velocity COMSOL Graph

Calculating Diffusivity and the Peclet Number

$$D = \frac{RT\sigma}{n^2 F^2 C}$$

R= ideal gas constant ($8.314 \frac{kg m^2}{K mol s^2}$)

T= Temperature (1373 K)

σ = Conductivity ($438/\Omega m$ or $438 \frac{s^3 A^2}{kg m^3}$)

n= Number of electrons. For silicon it is 4.

F= Faraday constant ($96500 C/mol = 96500 \frac{A s}{mol}$)

C= concentration ($2166.667 \frac{mol SiO_2}{m^3}$)

$$D = \frac{8.314 (kg m^2 / K mol s^2) * (1373 K) * (438 s^3 A^2 / kg m^3)}{(4)^2 * (96500 A s / mol)^2 * (2166.667 mol SiO_2 / m^3)}$$

$$D = 0.000000015 m^2 / s$$

$$D = 1.5 \times 10^{-8} m^2 / s$$

$$\text{Peclet Number} = \frac{uL}{D}$$

U = Velocity ($1.7 \times 10^{-4} m/s$)

L = Length between Cathode and Anode (0.0405 m)

$$Pe = \frac{(1.7 \times 10^{-4} m/s) * (0.0405 m)}{1.5 \times 10^{-8} m^2 / s}$$

$$Pe = 459$$

Appendix C: Electrolysis Experiments and Analysis

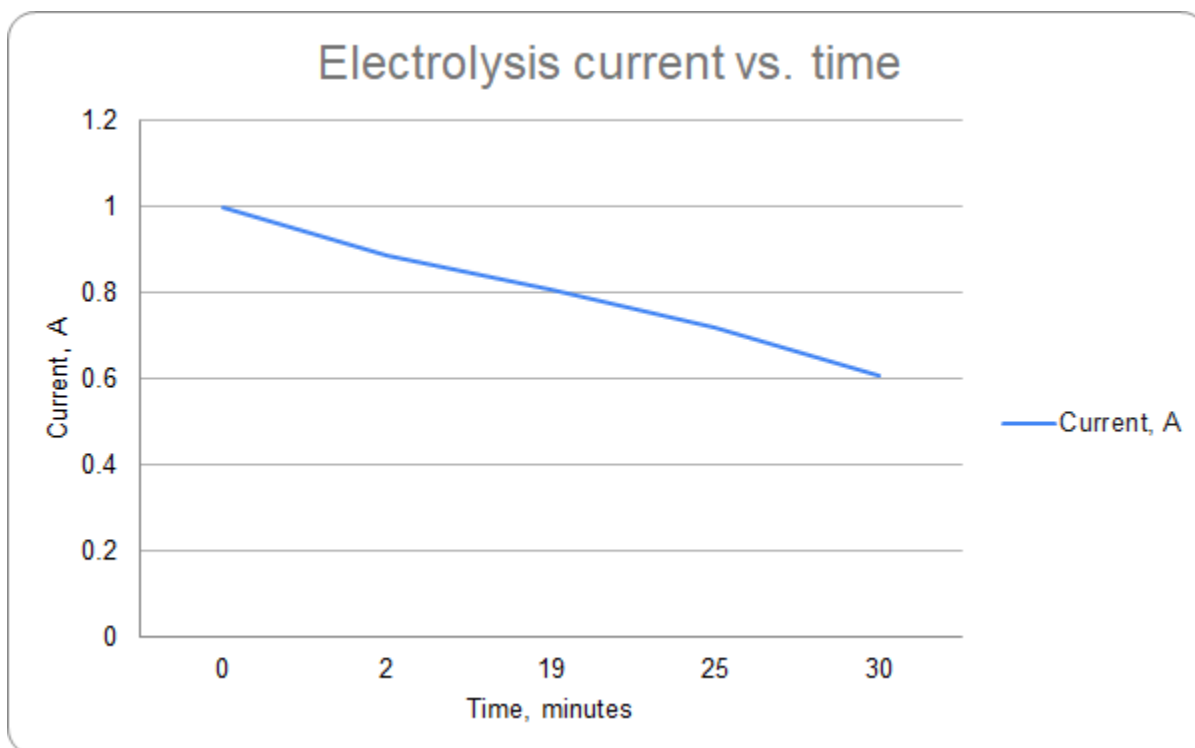


Figure C.1: Experiment 7 Electrolysis 1 Current vs Time

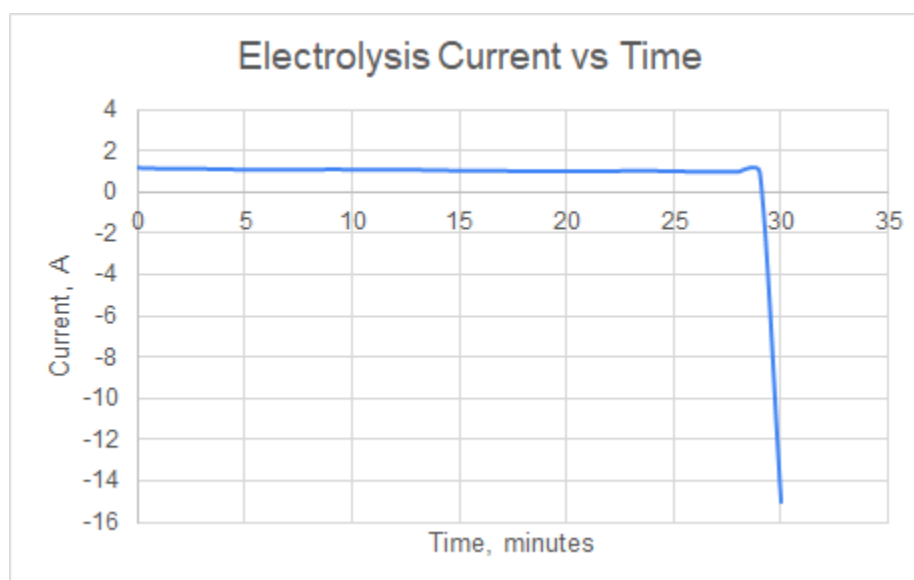


Figure C.2: Experiment 7 Electrolysis 3 Current vs Time

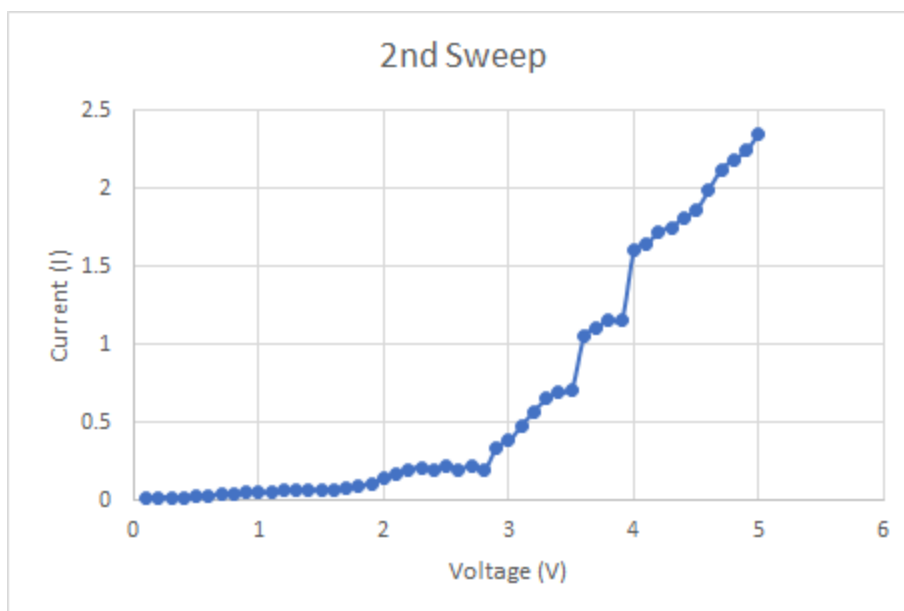


Figure C.3: Experiment 7 Sweep 2 Current vs Voltage

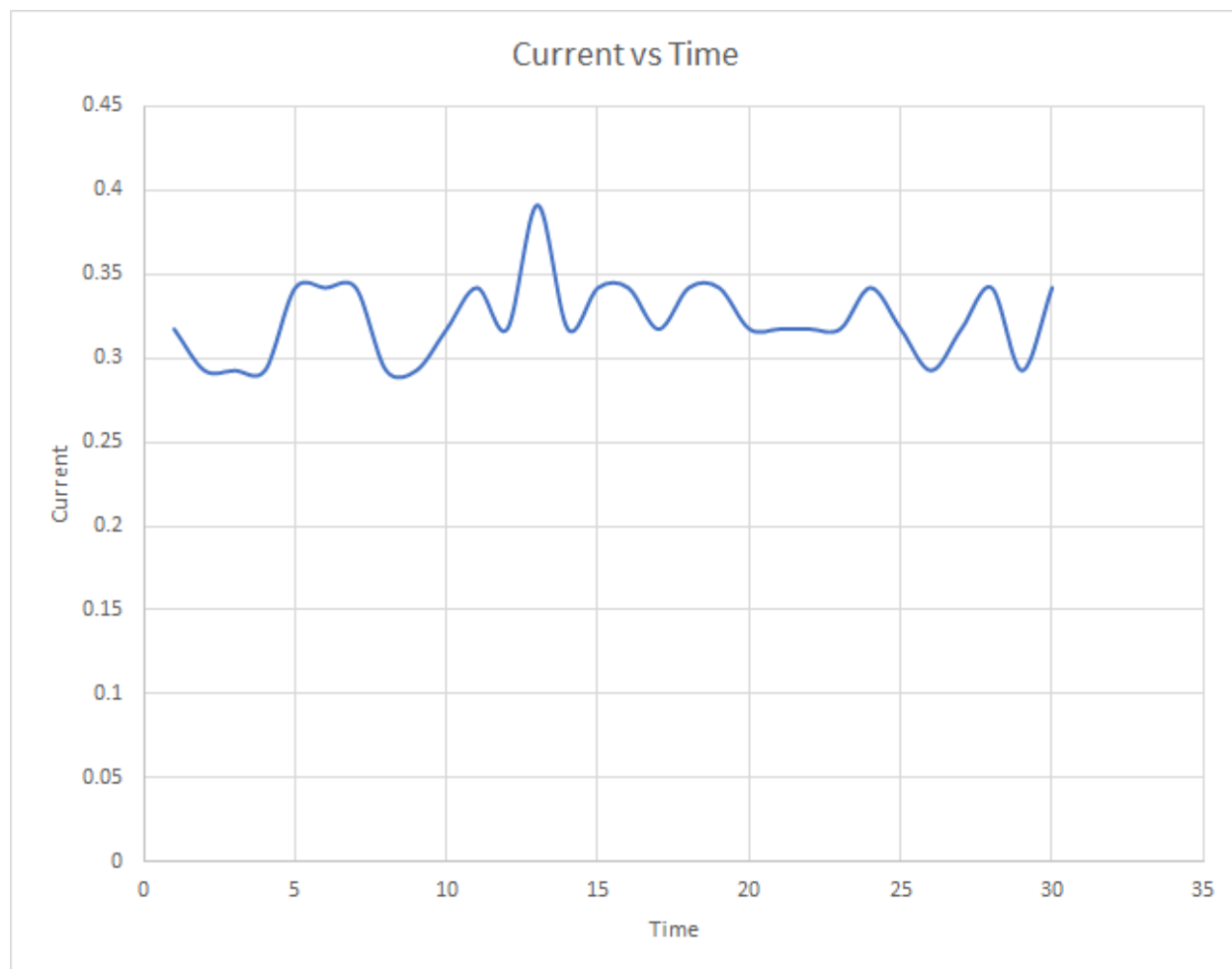


Figure C.4: Experiment 8 Hold 1 Current vs Time (min)

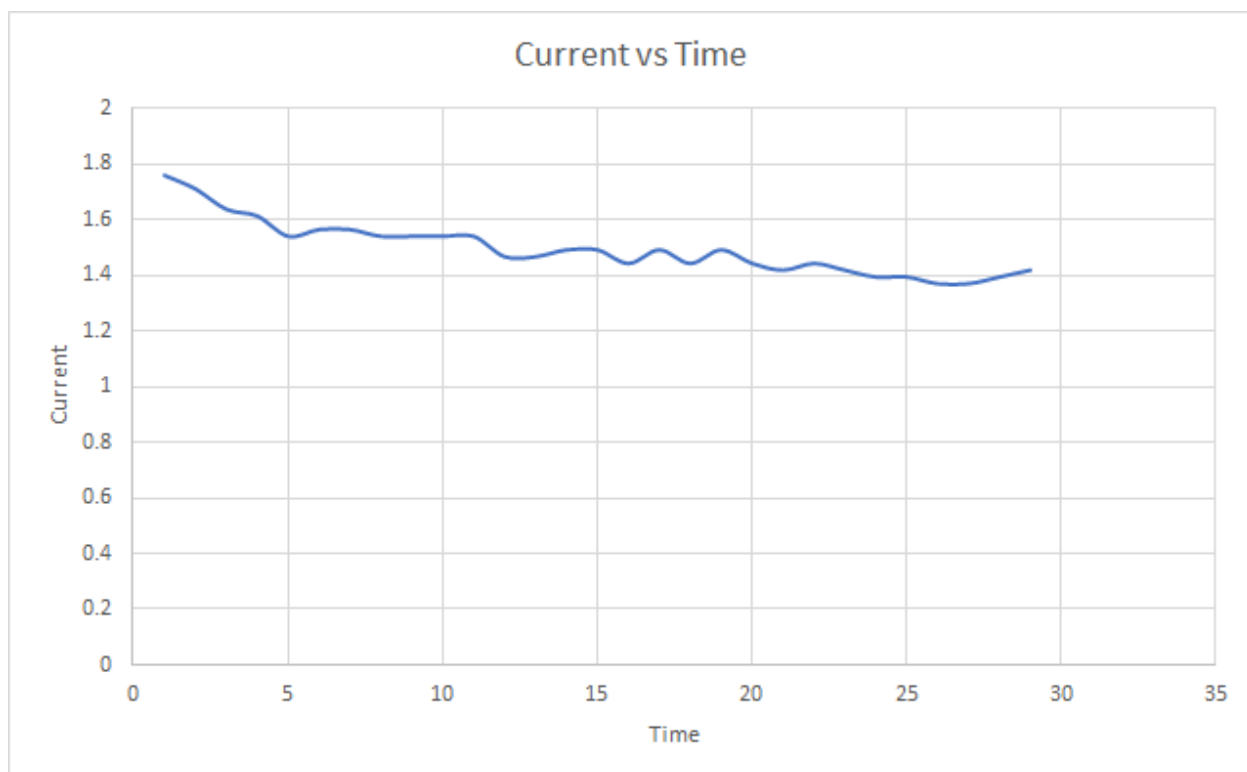


Figure C.5: Experiment 8 Hold 2 Current vs Time (min)

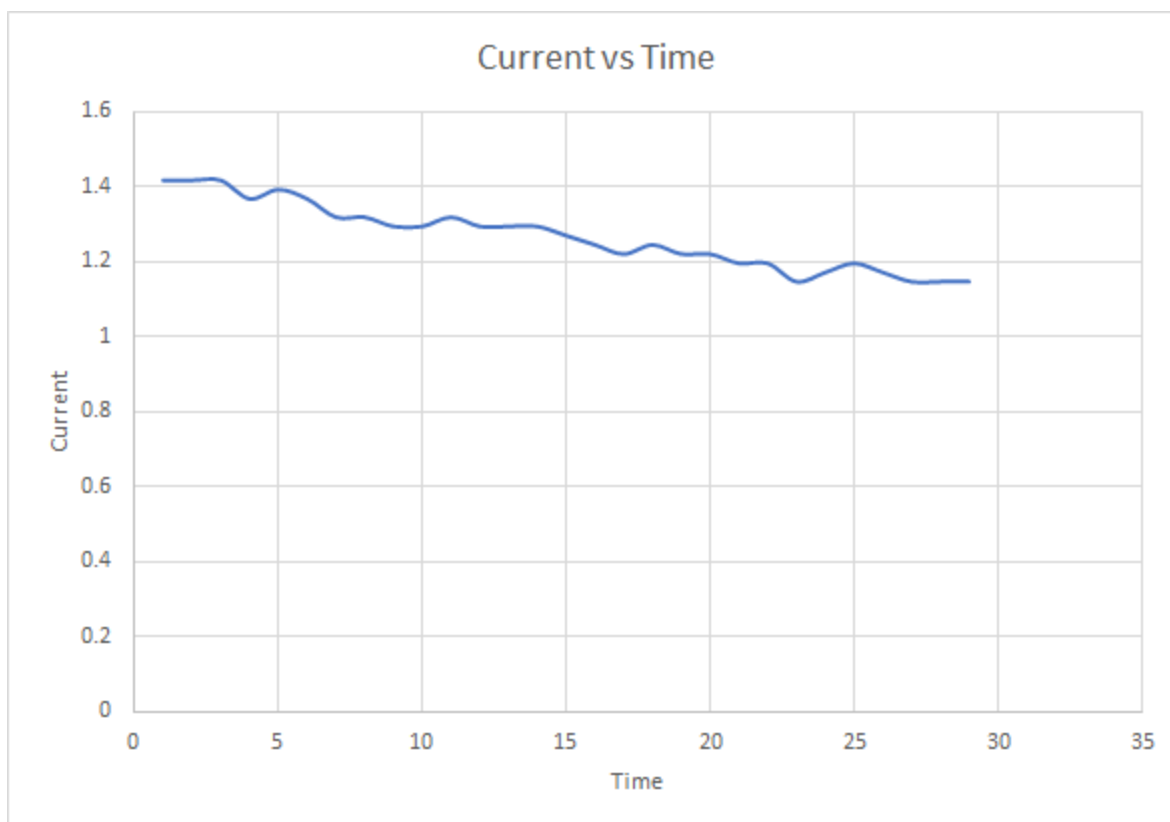


Figure C.6: Experiment 8 Hold 3 Current vs Time (min)

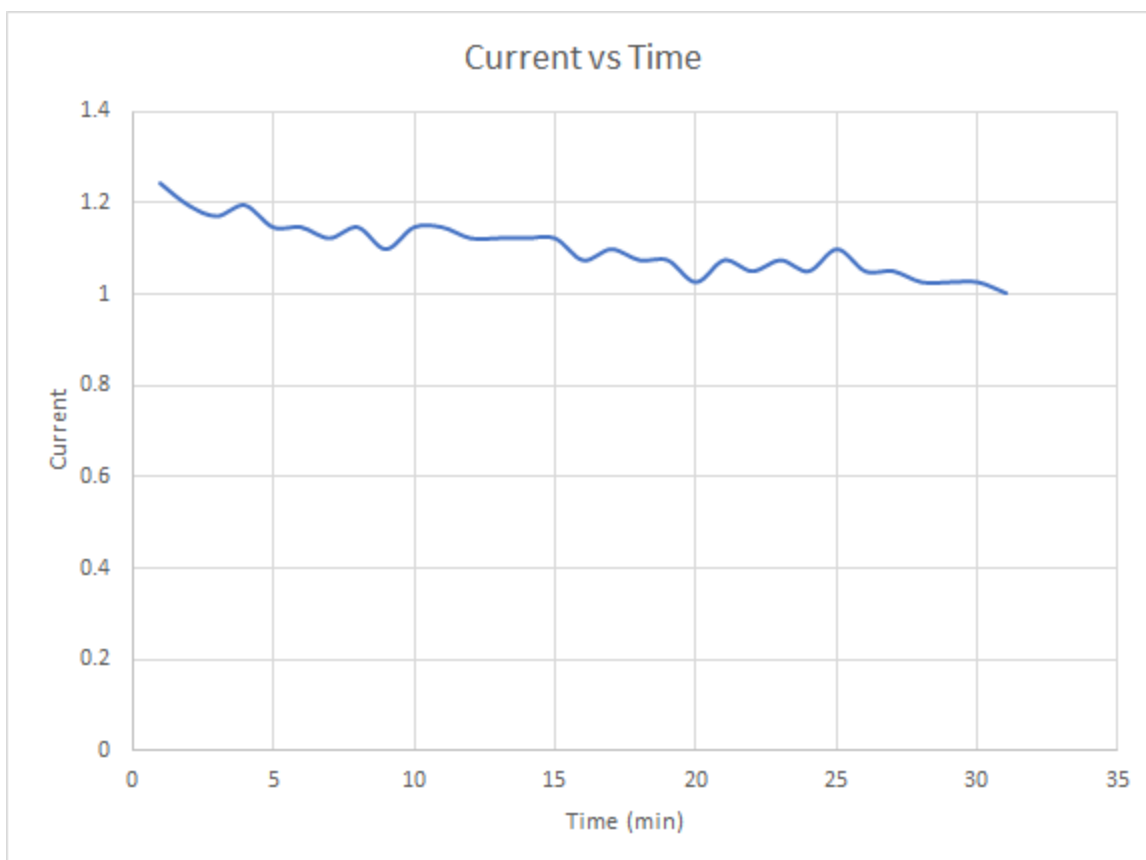


Figure C.7: Experiment 8 Hold 4 Current vs Time

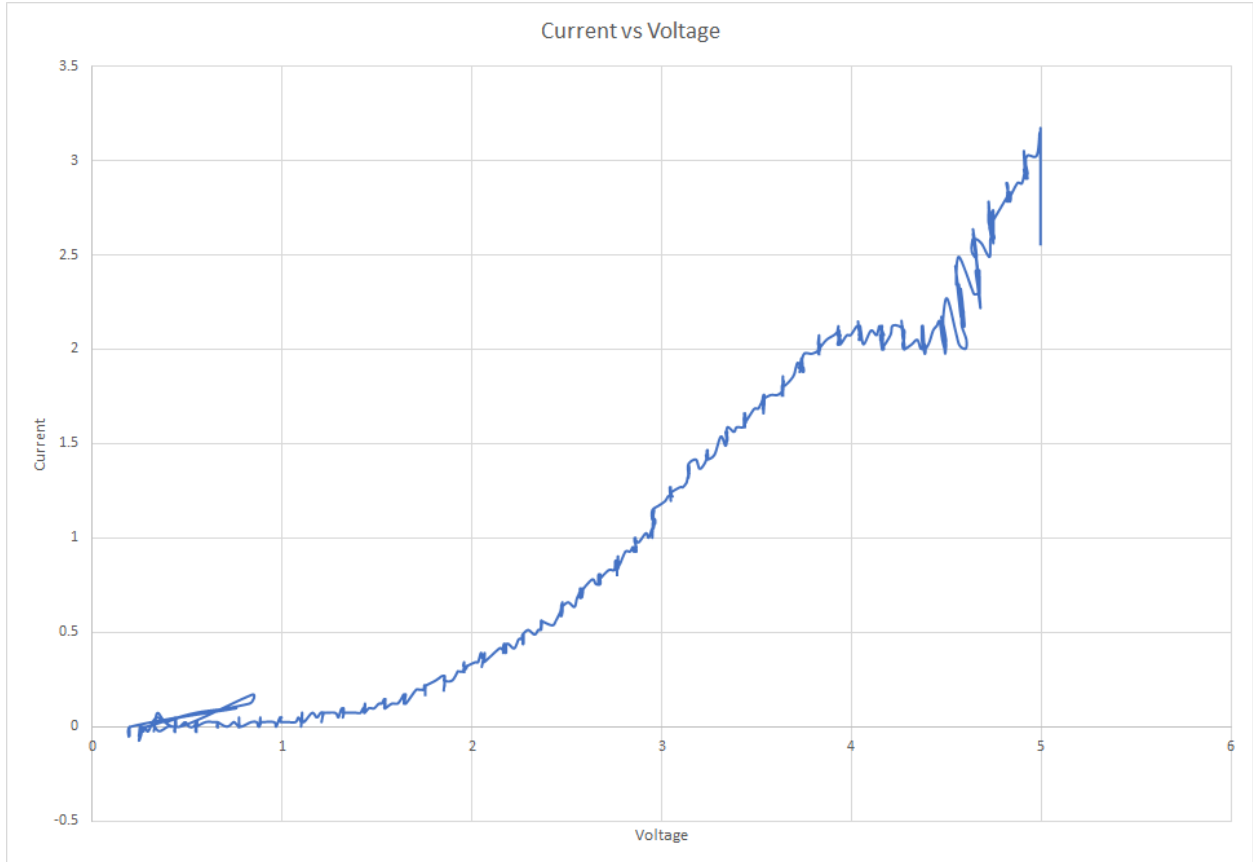


Figure C.8: Experiment 8 Sweep 1 Current vs Voltage

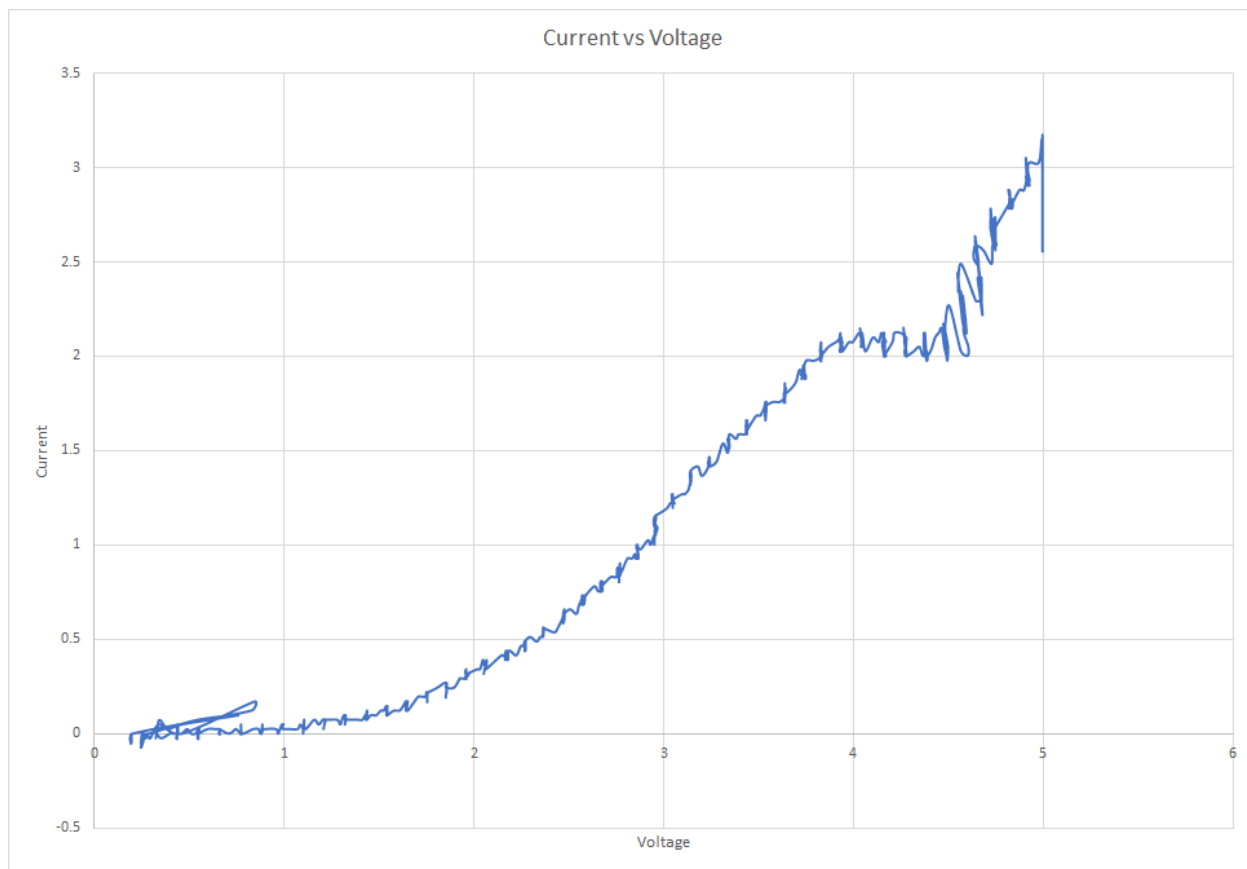


Figure C.9: Experiment 8 Sweep 2 Current vs Voltage

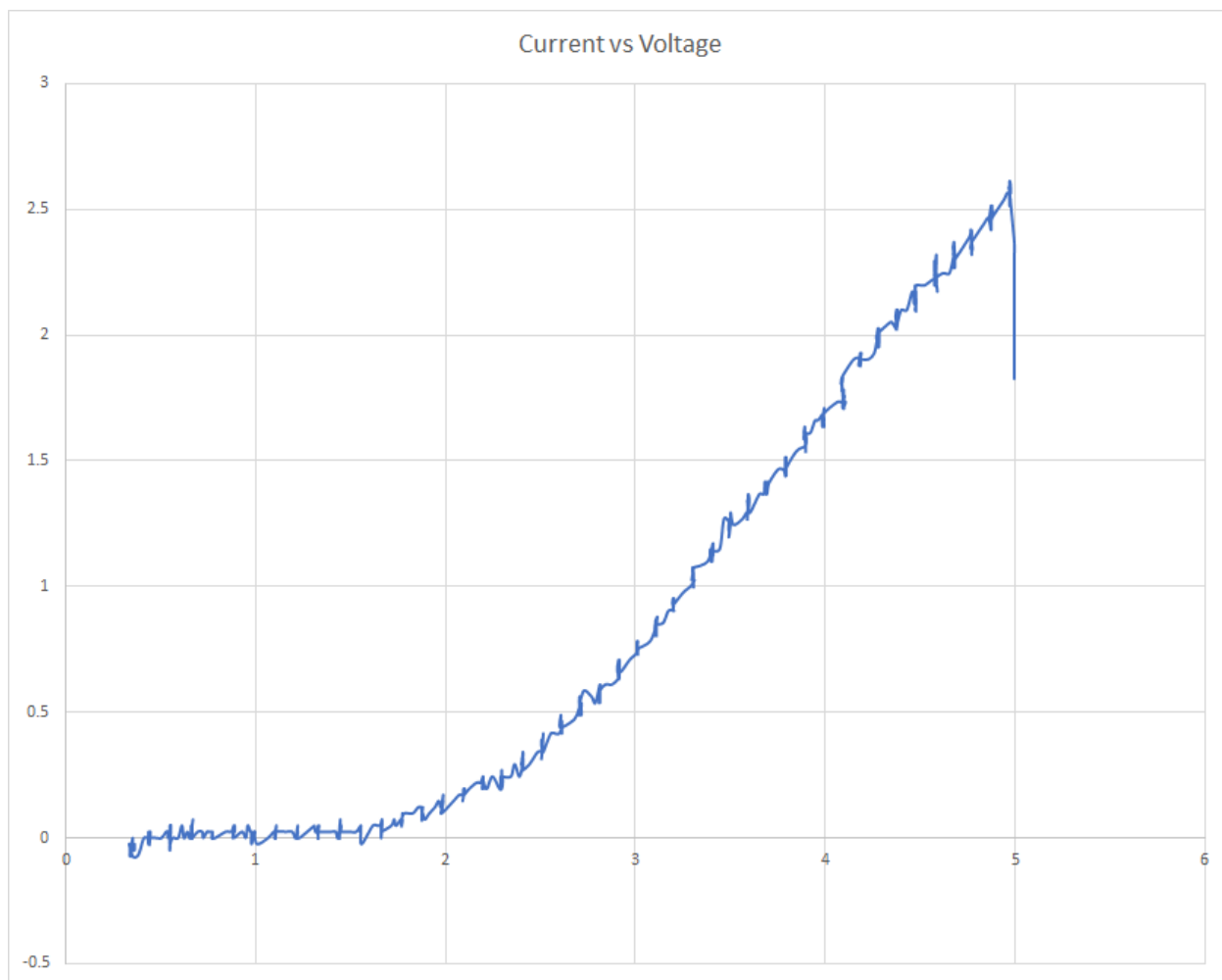


Figure C.10: Experiment 8 Sweep 3 Current vs Voltage

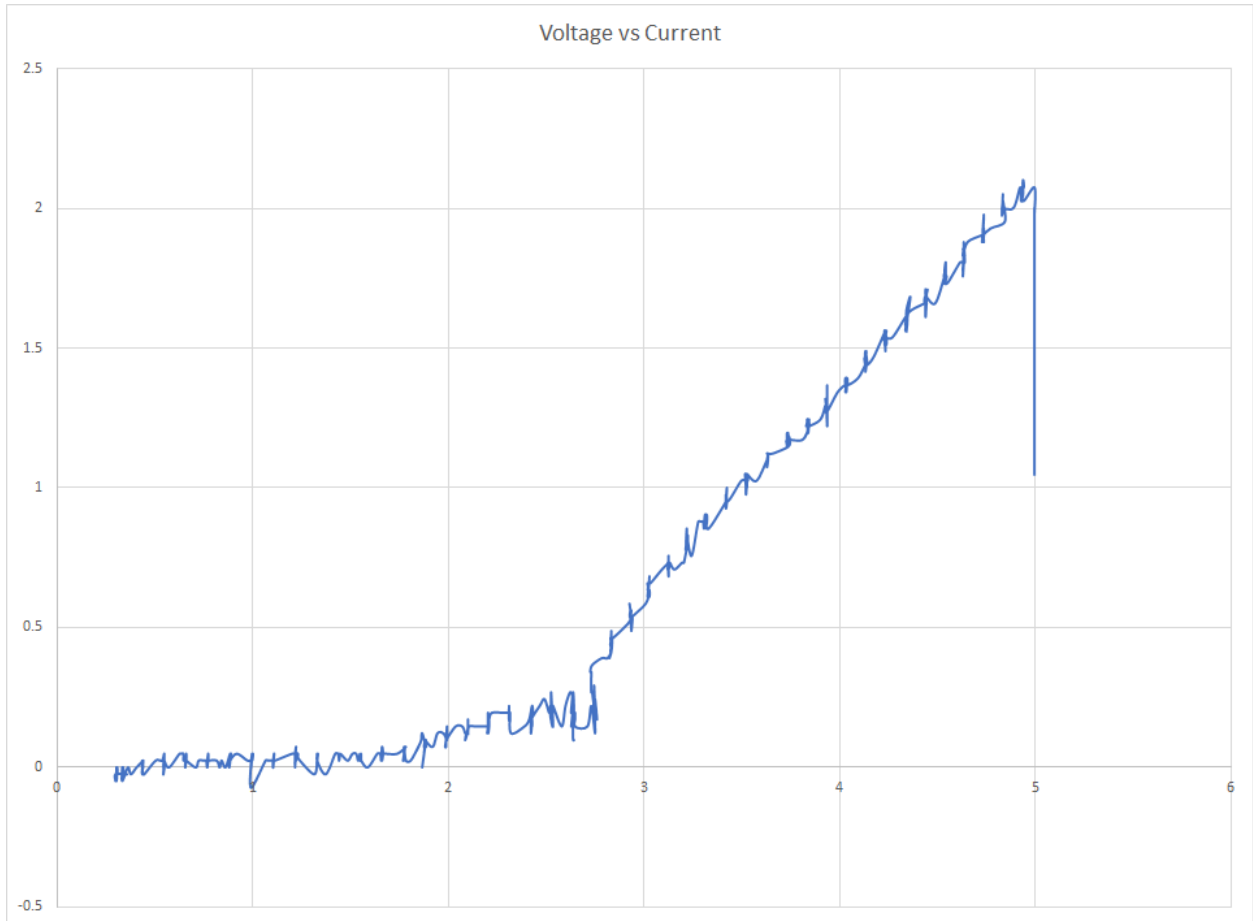


Figure C.11: Experiment 8 Sweep 4 Current vs Voltage